KIET IJCE

KIET International Journal of Communications & Electronics

VOLUME 1, FIRST ISSUE, JAN - FEB 2013, ISSN: 2320 - 8996

Department of Electronics and Communication Engineering
KIET GROUP OF INSTITUTIONS
(An Integrated Campus approved by AICTE)
Accredited by NAACeith Grade 'A', NBA Accredited and ISO 9001-2000
13-Km Stone, Ghaziabad-Meerut Road,
Ghaziabad-201206, UP, INDIA
Ph: 0120-2675314/315, Tele- 01232-227978
www.kiet.edu

Editorial Board

Editorial

Interference from other stations is the main reason behind scaling of packed radio networks in transmission. Interference is caused due to nearby stations as well as from distant stations because the signals received from those stations could be strong or week. Thus the overall noise level and interference caused due to the transmission of signal to a particular station are analyzed and found to remain manageable even as the system scales to billions of nodes. Thus to avoid collision in the packet data transmission new concepts are developed. Telecommunication can be achieved by either sending signals through cables or by letting generated signals propagate naturally through space as electromagnetic radiation. Cables can provide unlimited bandwidth, but require a lot of capital investment. The cable costing becomes expensive due to labour costing and installation charges.

Nowadays, a high performance analog circuit using low voltage becomes essential mainly due to the advance of the large scale integration with complicated circuit systems and the demand for battery-operated portable equipments. However, supply voltage reduction in analog circuit causes several performance degradations and, therefore, new approaches in the design are needed to obtain analog circuits with enough bandwidth, gain and linearity. Operational transconductance amplifier (OTA) is one of the most basic cells as OTA finds many applications in many analog circuits such as operational amplifier, voltage comparators, A-D and D-A converters and high frequency filters.

The edition of KIET IJCE contains articles on Communications through Pseudo Random Scheduling for Packed Radio Networks via Channel Division, Development of Data Acquistion and Analysis System for HF/DF Chemical Lasers, Comparative Analysis of CMOS based Pseudo Differential Amplifiers, Metamaterial based Optical Suface Plasmon Resonance Sensor and Optical Detection of Chlorine for Chemical Oxygen Iodine Laser areas.

We take this opportunity to thank all those contributors, reviewers in making this issue a memorable one. Suggestions and feedback from our readers are welcome for the overall improvement of quality of the Journal.

KIET IJCE KIET International Journal of Communications & Electronics
Volume. No. 1, Issue No. 1, Jan – Feb 2013, ISSN: 2320 - 8996.

Preface

Dear Researchers,

We take this opportunity to welcome you all to the first issue of International Journal of Communications & Electronics (KIET - IJCE). This journal will provide a forum for in depth and substantial discussions on the theory, design and implementation of the emerging technologies in Communications, Networking, Microwave and Electronics techniques, thus providing solutions and strategies for business resilience.

It gives us an immense pleasure to have an amalgam of researchers from the fields of Communication Engineering, Electronics, and related technologies. The purpose of the Journal is to provide a platform to foster interdisciplinary communication among the delegates and to support the sharing process of diverse fields in various concepts and principles related to these domains.

Our appreciation also goes to entire team whose dedication and timeless efforts have gone for number of days for the first issue of the Journal.

Editors

Message

I am delighted to note that the Department of Electronics and Communication Engineering, KIET Group of Institutions, Ghaziabad is introducing First issue of International Journal of Communications and Electronics (KIET - IJCE).

I appreciate the efforts on the part of the Editorial Committee in bringing out an issue on Communications, Networking, Microwave and Electronics techniques.

I understand that the papers contributed for publication in the first issue are on almost all the current aspects of Communication Systems, Electronics systems, Microwave Engineering, Signal Processing & Applications, Networking Technologies and several others.

I have great pleasure in congratulating the Editors of this issue of KIET - IJCE for their untiring efforts in bringing out this first issue which will be a valued treasure for all who pursue research in Communications, Networking, Microwave and Electronics Engineering areas.

Let me close with warmest regards.

Dr. Narendra Kumar
President
KIET – IJCE

Message

It gives me immense pleasure in writing this foreword for the first issue of the KIET International Journal on Communications and Electronics (KIET - IJCE) being started by the Department of Electronics and Communication Engineering, KIET Group of Institutions, Ghaziabad. This journal is targeted towards researchers, professionals, educators and students to share innovative ideas, issues, recent trends and future directions in the fields of software and network technologies.

The journal KIET - IJCE is targeted towards researchers, professionals, educators and students and industrial papers on the theory, design and implementation of the emerging technologies as well as share innovative ideas, issues, recent trends and future directions in the fields of Communications, Networking, Microwave and Electronics techniques. Furthermore, it will enable the researchers in the various domains to foster the exchange of concepts, prototypes, research ideas and the results of research work which could contribute to the academic arena and also benefit business and industrial community.

I am sure that this issue would greatly benefit researchers, students and faculty. Young scientists and researchers will find the contents of the issue helpful to set roadmaps for their future endeavors.

Dr. Sanjay Sharma
Editor – in - chief
KIET - IJCE

ABOUT THE KIET - IJCE

International Journal of Communications and Electronics solicits original research papers addressing theoretical and practical implementations in Electronics and Communication system applications for the Upcoming Edition of IJCE. It is the vision of IJCE to publish research articles in all areas of human study without financial restriction to readers using the open access model of publication. We strongly believe that the open access model will spur research across the world especially as researchers gain unrestricted access to high quality research articles. IJCE is a bi - monthly journal and if the manuscript does not suit in the current issue then it can be considered for the next upcoming issue. Authors are invited to submit their original manuscripts.

ABOUT THE DEPARTMENT

Department of ECE grooms the students to excel in the field of technology. Our students are trained in both software and hardware skills and basic inputs are provided to make them self-confident to work in industry and get encouragement for higher studies & research. The department also contributes to the society by accomplishing technical projects that caters to the various requirements of the present day world. The students are also encouraged to participate in various technical and extra-curricular events. The department has qualified and dedicated faculty members to provide good technical support to all the students. The department of ECE has a vision to become a centre of excellence in the field of Electronics and Communication Engineering. All our faculty and students are dedicated to achieve this goal with full vigor, enthusiasm and good ethical values. Department is running B.Tech. (ECE), M.Tech. (ECE). Department is involved in high quality research on several domains like Optical Integrated Circuits, Signal Processing and Communication, Semiconductor Device Characterization and Integration, Advanced Microwave Techniques, and other emerging fields under *AICTE Modrobs Projects*.

KIET IJCE
KIET International Journal of Communications & Electronics
Volume. No. 1, Issue No. 1, Jan - Feb 2013, ISSN: 2320 - 8996

Communication through Psuedo Random Scheduling for Packed Radio Networks via Channel Division

Sweta Srivastav[1], **Gaurav Srivastava**[2], **Ramesh Mishra**[3]
[1]*Lecturer IET Dr R.M.L.Avadh University Faizabad*
[2]*College of engineering Sciences and Technology Lucknow*
[3]*Lecturer IET Dr R.M.L.Avadh University Faizabad*
[1]*swetadeep07@gmail.com*, [2]*deepa_4852@yahoo.co.in*, [3]*heybabyaryan@gmail.com*

Abstract: *The paper presents the principal difficulty in scaling a system of packet radio stations where interference from other stations in the system interference comes both from nearby stations and from distant stations Each nearby interfering station is a particular problem, because a signal received from it may be as strong as or stronger then the desired signal from some other station. Far off interfering stations are not individually a problem, since each of their signals will be weaker, but the combined effect may be he dominant source of interference, the paper is superior to ideal time division multiplexing of a clear channel.*

1. INTRODUCTION

Interference from other station is the main reason behind scaling of packed radio networks in transmission. Interference is caused due to nearby stations as well as from distant stations because the signals received from those stations could be strong or week. Thus the overall noise level and interference caused due to the transmission of signal to a particular station are analyzed and found to remain manageable even as the system scales to billions of nodes. Thus to avoid collision in the packet data transmission new concepts are developed in this paper. Telecommunication can be achieved by either sending signals through cables or by letting generated signals propagate naturally through space as electromagnetic radiation cables can provide unlimited bandwidth, but require a lot of capital investment. the cable costing becomes expensive due to labour costing and installation charges.

2. PACKED DATA NETWORKS MODELLING

A signal either transmitted or received is most completely as a real valued function of time. Signal transmitted by source is denoted as $S_i(t)$,and the received signal at the station is denoted as $y_i(t)$.the parameter that are to be considered for the system performance are its power level and bandwidth and both are regulated by government regulation and limitations. Noise and propagation determine the received signals as a function of the transmitted signal assuming linearity and time invariance a general model is

$$yi(t) = ni(t) + \sum_{j=1}^{M} hij(t) * sj(t)$$

Where M=no of stations
H_{ij} = response at station i to an impulse in time transmitted by station j
Where H_{ij} =signal due to thermal noise at station i
*= convolution symbol

3. SOURCES OF INTERFERENCE IN PACKED DATA TRANSMISSION

Interference can come from various sources which include thermal noise, atmospheric effects, extraterritorial effects. Along with all those interference from other source interference create a lot of problem. Thus impulse response hij(t) is a general model for propogation in that can represent the strength of the propogation, the propogation delay and any multipath propogation. So hij(t) will be assumed to be just a scalar multiple of unit impulse hij(t) and the equation above can be simplified to

$$yi(t) = ni(t) + \sum hijSj(t)$$

Where $h_{ij}(t)$ are now scalars and the propogation model is not complete until $h_{ij}(t)$ are specified. The signal will be received successfully at a station i from k if, while ratio is at least small factor >1 and probably around 3. The required signal to noise ratio is

$$\frac{S}{N} \gtrsim \propto (2^{C}/_{w} - 1)$$

Where C = capacity, S=Power of the signal received at station i from sending station K. The power contained is the sum of the interfering signals.

$$N = ni(t) + \sum \sum_{j=1, j=k}^{M} hij(t) * Sj(t)$$

4. SPREAD SPECTRUM

Spread spectrum is the term used to describe techniques for practically achieving communication by radio when the signal to noise ratio is less than 1 that is within the used bandwidth spread spectrum is used to get multiple access over a single channel or single bandwidth. Most widely used technique in spread spectrum is direct sequence spread spectrum (DSSS)which is followed by a modulator and a demodulator, but as soon as the modulator signal transmitted a pseudo random code is generated. The receiver then uses a narrow filter and detector to isolate the signal and demodulate it to get the transferred bits. Spread spectrum radio techniques can be used to build systems that are capable of communication at the rates with in the Shannon bounds in channels where the interference has lowered the signal to noise ratio to well below one, but their are some practical limits. Some additional signal levels. or headroom will be needed over the minimum implied by the Shannon bound. It is found that around 5 db of headroom after propagating gain is needed to achieve a 10^{-6} bit error probability using a DS/BPSK radio link with viterbi decoding in a spread spectrum multiple access application. (For example the processing gain of around 30 db would handle a few hundred $100\sqrt{10} \fallingdotseq 316$ interfering signals each with a error correcting codes.

5. CHALLENGES IN INTERFERENCE SIGNALS

Interference is limited to try to schedule transmission so that each packet can be transferred without experiencing any interference from any other transmissions. For completely filled in propagation matrix, this approach would require co ordination between all stations participating in the system and exclusive one at a time use of channel. The co ordination would be challenging if there are many millions of stations

6. NOISE LEVEL IN LARGE SYSTEM

In presence of high level of interference signal to noise rates are bounded by the Shannon limit and hence rate of communication reduces. Relationship between signals to noise ratio is significantly less than one.

7. MULTIPLE ACESS COMMUNICATION THEORY

FDM is the most straight forward method of managing the separation of users. Different users of the spectrum are isolated from each other in frequency and the receiver can use a band pass filter to separate the desired signal. Same ways TDM can allow for statistical multiplexing of the traffic and eliminates the problem of transient channel assignment, but introduces the problem of resolving contention for the channel. Random aces schemes and explicitly scheduled schemes can nicely solve the problem in situations where all the stations or when all the station can hear each other equally well in case of non uniform propagation and non centralized traffic, the potential performance of random access scheme is less understood. Coode division multiplexing is the term used to denote spread spectrum technique of multiplexing, where the signals are allowed to overlap in time and frequency

8. PACKET RADIO NETWORKS

Packet radio networks comes from work in multiple access communication theory by the use of propagation models that do not have all the receivers receiving the same signal Interference is a quantifiable phenomenon and is measured by the resulting signal to noise ratio a which packets are receive.

9. NOISE LEVELS IN LARGE SYSTEMS

In presence of high levels of interference signal to noise ratio will be reduced and hence the communication rate will reduce. The relationship between signal to noise ratio is significantly less than one. If we consider that stations are distributed at some average density ρ throughout the infinite plane, and that each station is operating its transmitter at unit power output and at duty cycle η. Now power radiated per unit area in the plane is an average $\eta\rho$. For a receiver located in the plane, the power level received from a station a distance of one characteristics length $R_o = {}^{-1/2}$ can be computed. If the growth in the overall level of interference then assume that M interfering stations are distributed randomly within a circle of radius R, then stations outside the circle can be ignored Average density ρ is then $M/\Pi R^2$ if M increase the distance to the nearest neighbours also decreases remaining proportional to the distance. The distance to nearest neighbour also decreases, remaining proportional to the distance $R_o = {}^{-1/2}$

The signal level s from such a nearest neighbour transmitting with unit power would be

$$S = \propto / R_o^2$$

$$= \propto / (1/\sqrt{\rho})^2$$

$$= \propto \rho$$

Where depends on the antennas and wavelength used. The total power of interfering signals N, ignoring the contribution from local interference inside the circle of radius $R_o = {}^{-1/2}$ can be calculated as

$$N = \int_{Ro}^{R} \propto \left(\frac{1}{r^2\eta} 2\Pi r dr\right)$$
$$= \propto \eta 2\Pi$$
$$= \propto \eta 2\Pi (lnR - lnRo$$
$$= \propto \eta 2\Pi (R/Ro)$$
$$= \propto \eta 2\Pi ln\sqrt{M}/\Pi$$
$$= \propto \eta \Pi lnM/\Pi$$

So the signal to noise ratio (SNR) is

$$\frac{S}{N} = \frac{\propto}{\propto \eta\, ln \frac{M}{\Pi}}$$
$$= \frac{1}{\eta \Pi ln \frac{M}{\Pi}}$$

The expected signal to noise ratio of a signal from one of the nearest neighbours depends only on the M and η(the duty cycle).The signal to noise ratio falls very slowly approaching –db for η=1 as the number of stations approaches $10^{12.}$ This observation is encouraging The signal to noise ratio of a neighbours transmission falls slowly even as the number of stations grows exponentially

10. WORK PERFORMED THROUGH PSUEDO RANDOM SCHEDULING FOR PACKED RADIO NETWORKS VIA CHANNEL DIVISION

Interference from a nearby station transmitter may be a problem if it is used to transmit at high power. It could be problematic if the nearby station transmitter delivers and interfering signal with power sufficient to significantly lower the signal to noise ratio of packet receptions. Whether the effect is significant or not will depend on how much processing gain the stations are using. The power levels are usually discussed in decibels algorithm. But the effect of an additional interfering signal on overall interference level which is already quite high. The power level adds but the logarithmic levels do not increase. Say if two signals one at a power level of 20 db and other the other at a power level of 10 db are added the power level of the resulting signal is 20.4db. which is barely a significant change. In order for the addition of a week signal to increase the overall level of interference by more than 1 db its power level must be at least one fourth the power level of the overall interference One decibel which is about a 25 percent change is a reasonable threshold for significance. While we can strictly budget the additional level of interference we may tolerate from each nearby neighbour independently, as two additional sources of interference can combine to produce an even greater level of extra interference, we can hold each such potential additional sources of interference to a maximum increase of 1 db in total interference and budget a few decibels of addition headroom. It would then take more than four simultaneous high power transmissions each contributing just under1 db threshold from nearby neighbours to have more than a 3db effect on the overall level of interference only in frequent circumstances. And neighbour 's transmission increase the level of interference by more than 1 db. In order for an interfering station to significantly increase by more than 1 db the total amount of interference, it would have to deliver more than 20 times or 13 db more the amount of power that it is delivering to the intended recipient. If the noise level is 20 db or the target receive power. Choosing 13 db here is 1 decibel more conservative. Assuming $1/r^2$ propogation, this threshold will be exceeded only when station is more than five times as far away as the interference from the transmitter. If the distant stations we are communicating with are at a distance of $2\rho^{-1/2}$ then the expected no of stations inside a circle with a radius of one fifth this distance only $\Pi(2/5)^2 \approx 0.5$. This no is well under the interference threshold of four nearby transmitter. If when high power must be used, an additional constraints can be placed on the scheduling to avoid interfering with and neighbours reception. Those packet transmission that will require high power must not be scheduled at a time that overlaps with a receive window at a neighbour who is too close.

11. CONCLUSION

This paper presents a pseudo random scheduling method that can be used to ensure that packets are not received at times when the signal to noise ratio would be unacceptably lowered due to nearby near by sources of interference. The method requires neither global synchronization or global coordination. Each station can arrange independently with its immediate neighbours to ensure that its transmission do not mask the reception of packets either by itself or by any particularly close neighbours. The maximum total throughput or fraction of time spent sending out of a station is around 0.21 for a single neighbour and can be increased as more neighbours are added. A station can even spend more than half of the time sending if it has a sufficient number of neighbours. The expected delay per hop due to the scheduling method is a few scheduling slots which, with four sub slots is around two dozen packets. The design strategy introduced above yield a design for an effective packet radio network that can scale to seemingly arbitrary density and requires no centralized centralized co ordination of channel use above paper shows how to ensure that packets are sent only at times at which they will not be dropped due to collisions, but we do not require any global synchronization or co ordination.

12. REFERENCES

[1] Rodger E. Ziemer, Rodger L. Peterson, Digital Communications and Spread Spectrum Systems, (New York, Macmillan Publishing Company, 1985)

[2] Ferrel G. Stremler, Communications Systems, (Addison-Wesley Publishing Company, 1990.

[3] Taub, Herbert and Donald L. Schilling. *Principles of Communication Systems* (Second Edition). McGraw-Hill, 1986. Sklar, Bernard. *Digital Communications Fundamentals and Applications.* Prentice Hall, 1988.

[4] Golub, G. H. and C. F. VanLoan. *Matrix Computations* (2 Edition). Baltimore, MD: Johns Hopkins, 1989. Robert K. Morrow and James S. Lehnert. Packet throughput in slot-ted ALOHA DS/SSMA radio systems with random signature sequences. IEEE Transactions on Communications, 40(7):1223{1230, July 1992.

[5] IEEE. Proceedings of the IEEE, volume 75, number 1, January 1987. Special Issue on Packet Radio Networks

[6] Dimitri Bertsekas and Robert Gallager. Data Networks. Prentice-Hall, 1987.

[7] David L. Nicholson. Spread Spectrum Signal Design. Computer Science Press, 1988.

[8] Hideaki Takagi and Leonard Kleinrock. Optimal transmission ranges for randomly distributed packet radio terminals. IEEE Transactions on Communications, COM-32(3):246{257, March 1984.

[9] Claude E. Shannon and Warren Weaver. The mathematical theory of communication. University of Illinois Press, 1996.

KIET IJCE KIET International Journal of Communications & Electronics
Volume. No. 1, Issue No. 1, Jan - Feb 2013, ISSN: 2320 - 8996

Development of Data Acquisition and Analysis System for HF/DF Chemical Lasers

Vidya Sagar[1], Chhaya Ravikant[2], Mainuddin[3], Manish Borkar[4], Alok P Mittal[5]

[1,3,4]Laser Science & Technology Centre, Metcalfe House, Delhi -110054, India
[2]Department of Applied Sciences, GGS IP University, Kashmere Gate, Delhi-6, India
[5]Instrumentation & Control Engineering, NSIT, Dwarka, New Delhi, India
[2]Corresponding author: chhaya_rkant@yahoo.co.in

Abstract: *The paper reports the development of data acquisition and analysis system (DAS) for a noisy and hostile environment for arc operated hydrogen fluoride/ deuterium fluoride (HF/ DF) chemical lasers. HF/ DF is a high power chemical laser based on vibrational transition. The typical lasing wavelength of HF is 2.7 μm and that of DF is 3.8 μm. The plasma arc discharge in an arc heater/ generator is essentially employed for inducing thermal dissociation of SF_6 for production of fluorine atoms. The dissociation of SF_6 is a much safer alternative than other options of combustion of F_2/ NF_3 in an environment of H_2/D_2. Another accrued advantage is that the composition of the lasing mixture to an extent may be varied independently of the pressure and temperature of its constituents. But the arc load is complex load and involved high voltage transients and electromagnetic noise. The development of suitable DAS for monitoring and performance evaluation of parameters for 50 kW arc tunnel is implemented with proper protection devices. Since each designed plasma arc tunnel is unique in itself and specific to the application, DAS would enable altering arc discharge for optimization of the intended laser.*

Keywords: *HF/DF Laser, Arc tunnel, DAS, Optical fibre*

1. INTRODUCTION

Gas lasers have wide range of applications in various defense and industrial scenarios [1]. HF/DF gas lasers fall in class of high power chemical lasers based on vibrational transition. These lasers have proved their mettle in various defense applications. However, one of their limitations is the toxicity of its constituent elements. Hence, production of lasing species through combustion forms a safety concern. In this context, the use of arc plasma generator [2, 3, 4] is beneficial as it offers safe decomposition of SF_6 for generation of fluorine atoms to be used subsequently for lasing action.

Arc plasma heater or generator is a versatile tool for optimizing lasers parameters [5] such as gas flow rate, pressure, temperature and Mach no. etc. These parameters are to be acquired and monitored in real time. So a compatible Data Acquisition and analysis System (DAS) is essential for monitoring and control the operation of arc driven HF/ DF tunnel. A DAS consists of individual sensors with necessary signal conditioning, multiplexing, data conversion, data processing, data handling & associated transmission storage & display systems. Any DAS can be divided into two types on the basis of environment in which the system works. These are defined as a system which is suitable for less noisy environment or for the favorable conditions and the other one which is working in hostile environment like arc tunnel [6, 7]. The precise control of flow of gases (i.e. Nitrogen, Sulphur Hexafluoride, Hydrogen & Oxygen) with proper time sequencing, need to change the flow parameters during operation and handling of various sub systems are some of the important features of arc driven HF/ DF tunnel. Also safety considerations demand operation from remote control console. Keeping these features in mind, it is important that arc driven HF/ DF tunnel should be operated with a dedicated DAS, where all the controls are in the hands of a single operator. We have operated arc driven HF/ DF laser system that was developed in-house. Using DAS, the basic arc behavior is studied and lasing experiments are reported on 50 kW arc tunnel.

2. SYSTEM DESCRIPSTION

The goal of all chemical lasers is efficient conversion of chemical energy into coherent radiations of high power beam. Most of the recent developments in high power HF/ DF chemical lasers are based on combustion of Fluorine/ NF_3 gas with Helium and H_2 / D_2 to have lasing compositions. These types of lasers are difficult to use in normal laboratory environment because of toxic & hazardous gases. In order to overcome this drawback and to have laboratory useable HF/ DF Laser, arc tunnel is used for optimization of various laser parameters. The arc heater is used to create fluorine atoms by thermal dissociation of SF_6, which is very safe gas as compared to other fluorine based gases in laboratory environment. The arc heater has the advantage that it allows independent variation of gas composition with respect to temperature & pressure and thereby permitting ideal gas mixture ratio at required temperature & pressure conditions for longer run times. Arc heater is neat & clean and best laboratory apparatus for optimizing laser parameters. The presented work in this paper discusses the development of DAS for a kW level HF chemical Laser facility using arc discharge method.

The Data Acquisition and Analysis System (DAS) for arc driven hydrogen fluoride chemical laser system was realized with ADAM 5000 series cards of Advantech make (schematics shown in fig 1). This system consists of system Kernel with plug in modules. The system Kernel handles all software functions between the field devices and the host computer, including signal conditioning, data conversion, calibration, alarm monitoring, internal diagnosis and communication. As the arc plasma is a complex load involving high voltage transients and electromagnetic interference (EMI), so the system has been developed to cater for EMI induced environment with fiber optic cable as the communication link between the DAS and the PC. The DAS initiates the operation of various subsystems such as power, gas, water etc. It also switches 'off ' these subsystems after the defined run time. Various experimental parameters such as gas flow, pressure, temperature, voltage, current, power etc. are being acquired, displayed on the screen & stored in the PC. In case of any parameter going out of set range or in case of gas leakage an alarm is sounded and the system is switched off. The DAS has been designed for 24 analog inputs channels, 16 digital outputs, sampling rate of 10samples/sec with distributed I/ O features and RS 485 as serial communication interface with PC. It is capable of communicating up to 1200 metres with a speed of 9.6KBPS. Thus the cards for arc heater driven system are chosen for 2.5kV dc opto-isolation in communication lines and 3kV dc isolation in the power lines & I/O lines. Also to reduce EMI optical fiber communication link has been used. The 820nm wavelength is used as a carrier wave with fiber core/clad diameter 62.5/125μm and typical attenuation at this wavelength is 12.5 dB.

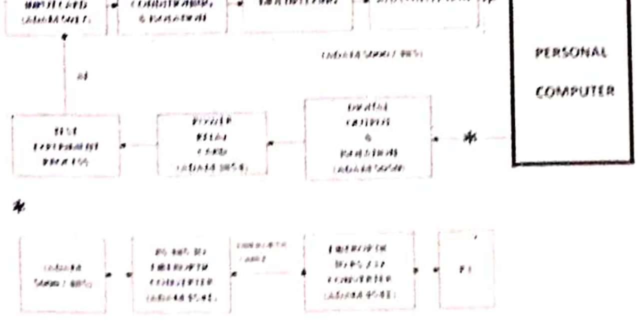

Fig 1 BLOCK DIAGRAM OF DACS FOR ARC DRIVEN HF CHEMICAL LASER

The dedicated DAS is utilized to control and monitor the safe functioning of arc test bed facility (schematics shown in fig 2) comprising of arc heater, cooling water system, gas supply system and power supply system along with smooth operation of arc tunnel for lasing experiments. The details of various sub systems developed for safe operation of 50 kW arc tunnel are as:

A. Arc Heater: The arc heater was designed to provide a highly energized, continuous plasma source, composed of free electrons, positively charged ions and neutral atoms [8, 9, 10]. The system is capable of operating with gases such as argon, nitrogen, helium, and mixture of such gases. The plasma is formed in a direct current electric arc and discharged in to a plenum chamber for mixing of other gases (such as N_2, SF_6) for achieving desired lasing composition temperature close to 2000 K. The DAS ensures the safe operation at such a high temperatures by incorporating the proper sequence of operation and interlocks.

B. Direct Current Power Source: The power for the arc heater is obtained from combination of industrial welding machines (i.e. rectifiers and generators) of Miraj Electronics make rectifiers for dc Output: open circuit voltage (OCV) of 80V, 600 Amp, input: 45KVA, 415V, 3Ph, 50 Hz and Advani Orlikon make generators for OCV 60V, 450 Amp dc max, Input: 26kW, 3ph, Induction motor, 2850rpm, with a total rating of 780 V OCV and 600 Amp current capacities for operating arc heaters up to 200kW ratings. These are connected to the arc heater with cables of 1000 A rating through a control panel and monitored from DAS.

C. Cooling system: De-ionized water supplied by a de-ionized water plant is utilized for arc heater cooling. The water is supplied from a storage tank filled with ionized water, which is pumped employing a 20 HP multistage centrifugal pump at a pressure of 10 Kg/cm^2 with a flow rate of 300 lpm. The flow through the arc heater system, mainly the manifold and the electrodes, is monitored online by the DAS through thermal flow meter. The coolant stream from arc heater system is then supplied back to a second manifold and to another tank for water disposal.

D. Gas Supply System: The gas supply systems for arc heater and plenum comprise of a cylinder bank to feed the high pressure gas manifolds and dome regulators for the desired high mass flow rates and pressures. Dome regulators are employed for flow regulation and strain gauge (IRA make with accuracy ±0.5 torr) and peizo-resistive (Yokogawa make with accuracy of ±0.25 torr) type pressure transducers are used for pressure measurements and control by the DAS in cavity and plenum respectively. Thermal mass flow meter (Bronkhorst make with accuracy of ±1%) for SF_6 and coriolis mass flow meters (with accuracy of ±0.5%) for N_2 & H_2 are placed for mass flow measurements through DAS.

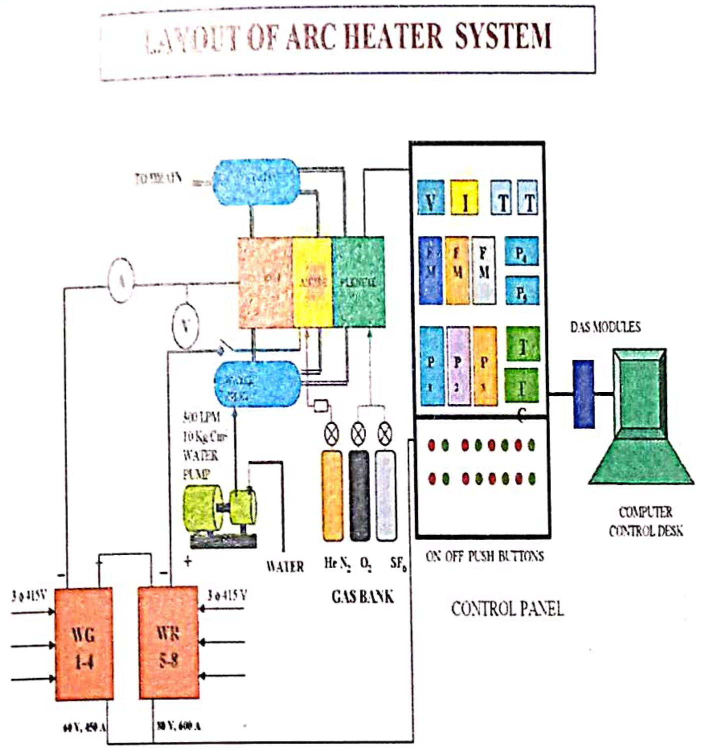
LAYOUT OF ARC HEATER SYSTEM

Fig. 2: Arrangement of various sub systems of arc plasma generator

E. D.M. Plant: A de-mineralized water plant was installed for this purpose supplying 600 liters per hour of water with less than 1 siemens conductivity.

F. Control Panels: Control panels were designed & developed for measurement and control of different arc related parameters such as voltage, current, flow, pressure & temperature etc from single control console at DAS station. The control panels were made operational for safe working of 50 kW arc tunnel. Instrumentation was directed towards the two-fold purpose of arc operation and performance evaluation. Primary instrumentation is directed towards the determination of arc performance and is basically necessary for an energy analysis to evaluate performance of arc heater. Pt-100 RTDs (with accuracy of ±1%) and R-type thermocouple (with accuracy of ±0.5%) were used for water and plenum temperature measurements respectively.

G. Development of 50 kW arc tunnel: The 50 kW arc tunnel consisting of arc heater, plenum, supersonic nozzle, cavity, diffuser and dump was integrated for lasing experiments (schematics shown in fig 3). In a chemical Laser, the population inversion is by the chemical reaction, where reaction mostly involves free atoms since the fuels involved do not react rapidly in their molecular form [11, 12, 13].

Basic Chemical reaction is given by:

$$F + H_2 \rightarrow HF^* + H + 32kcal/mole$$

$$HF^* \rightarrow HF + H + Laser$$

The arc plasma generator or arc heater is an attractive tool for obtaining the high temperature necessary for dissociation of SF_6 (>2000K). The energy from N_2 arc plasma is utilized to dissociate SF_6 in plenum so as desired number of fluorine atoms are generated for initiating the subsequent lasing reaction in the cavity [14]. For a kW level HF arc-driven chemical Laser system, $1 gs^{-1}$ flow rate of SF_6 is required in plenum to generate desired quantity of fluorine atoms and subsequently $1 gs^{-1}$ of H_2 is added at the nozzle exit plane to initiate the chemical reaction essential for lasing action. A 50 kW arc heater (input power) is sufficient to create N_2 plasma and to carry out the parametric variations of different gases (viz. SF_6, N_2, O_2 etc) in plenum to have desired lasing composition for kW laser output.

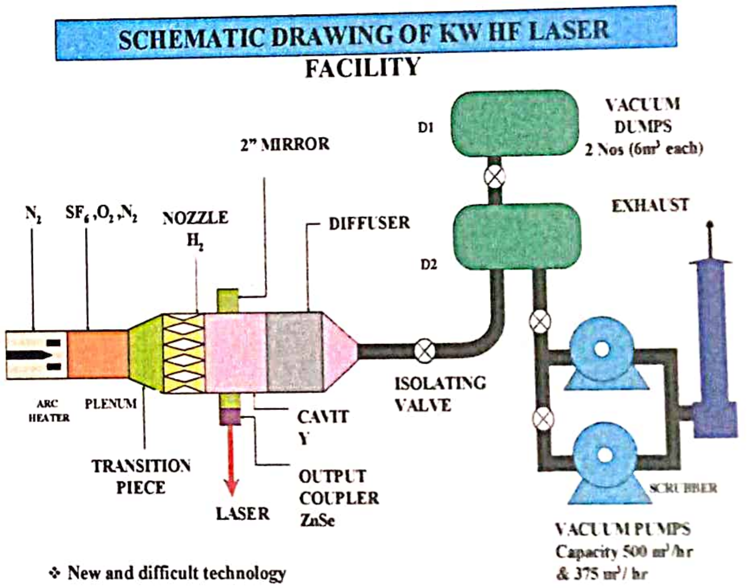
SCHEMATIC DRAWING OF KW HF LASER FACILITY

Fig. 3: Arrangement of key components of the laser tunnel

3. PERFORMANCE EVALUATION OF ARC HEATER

An ordinary electric arc without forced convection has definite intrinsic properties. However, mass flow of gas through the arc chamber represents a new, independent parameter not present in ordinary arcs with natural convection. Typical voltage-current characteristics for a cylindrical configuration with thoriated tungsten cathode are shown in fig 4 for Nitrogen in 50kW Arc Heater. The arc is negative resistance load, so special power source with drooping characteristics is needed for stable operation. Also it has been observed that at fixed mass flow rate, the arc voltage is relatively insensitive to arc currents. However, with increasing mass flow rates the voltage demand and input power increases proportionally.

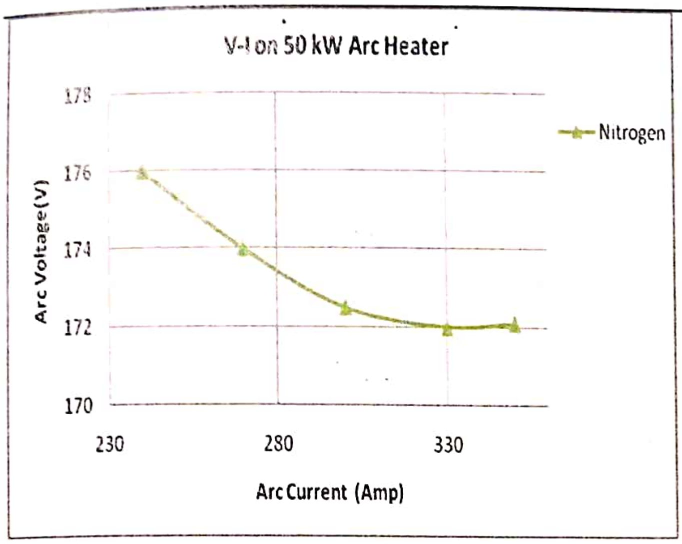

Fig 4: Variation of arc voltage with arc current

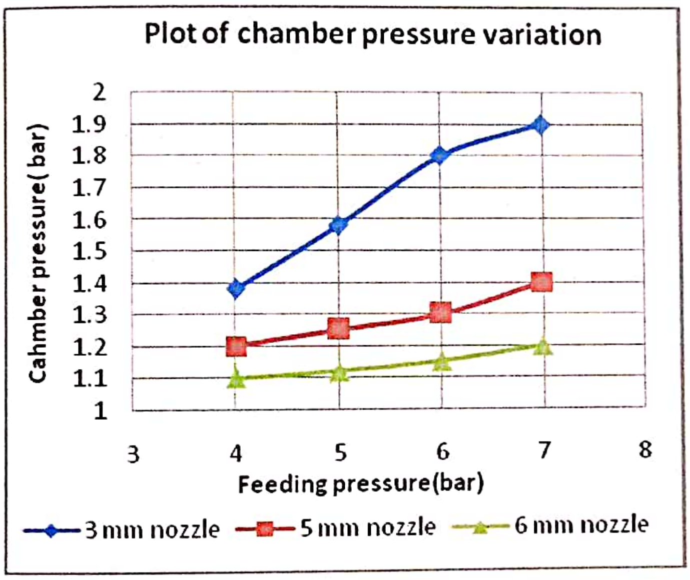

Fig. 5: Variation of chamber pressure for various nozzle combinations

The chamber pressure variations [refer fig (5)] were studied with three different nozzles i.e. 3mm, 5mm and 6mm. It is apparent that the smallest nozzle shows the highest chamber pressure.

Arc heater efficiency is defined as ratio of the power to the gas divided by the gross arc power fed into the arc heater;

$$\eta = 100\left(1 - \frac{PC + PA}{PG}\right)\%$$

PC = Cathode losses in kW
PA = Anode losses in kW
PG = Gross power in kW

The results [refer fig (6)] show that thermal efficiency of the arc heater ranges from 42 to 45 in 50kW arc heater, which means that more than half of the total power input taken away by the cathode and anode cooling water.

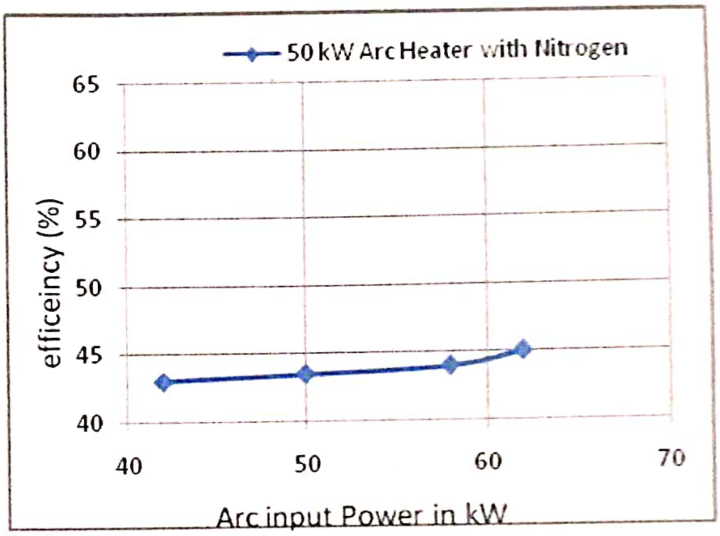

Fig. 6: Efficiency as a function of arc input power

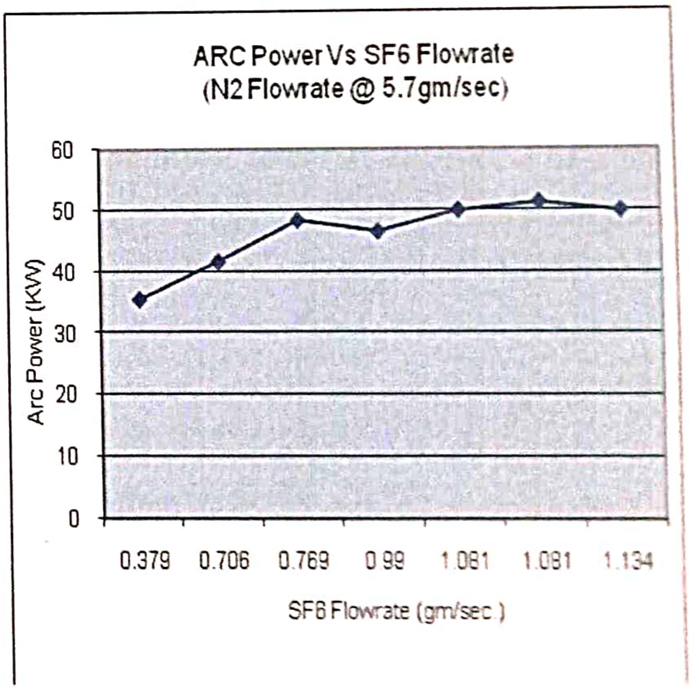

Fig. 7: Variation of arc power with SF_6 flow

4. EXPERIMENTAL RESULTS ON 50KW ARC TUNNEL

The experimental parametric analysis for the developed arc plasma tunnel is highly time intensive where the final aim is to employ it for laser applications. Experiments were carried out to establish the lasing parameters in 50 kW arc tunnel. The results achieved are in compliance with the theoretical values for lasing gas mixture in 50 kW arc tunnel [14]. The desired Mach No in gas mixture is achieved with special supersonic converging/ diverging nozzle attached to plenum of the tunnel. The variation of arc power with variation in SF_6 and H_2 flows is shown in fig (7) and (8) respectively.

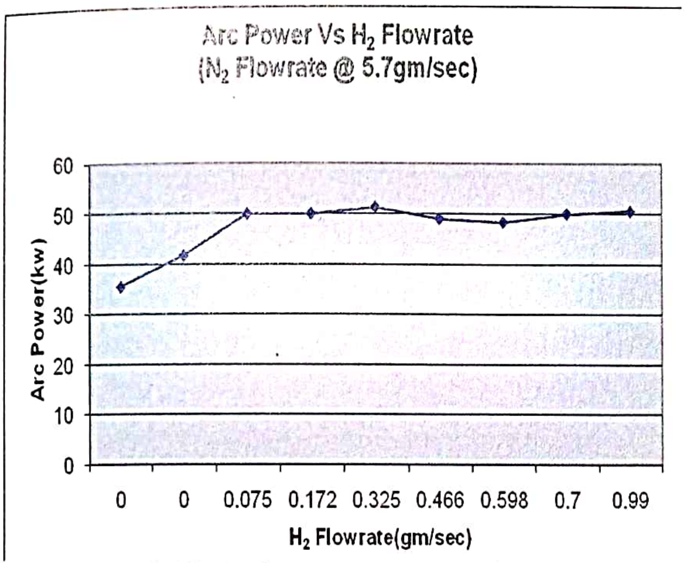

Fig. 8: Variation of arc power with H_2 flow

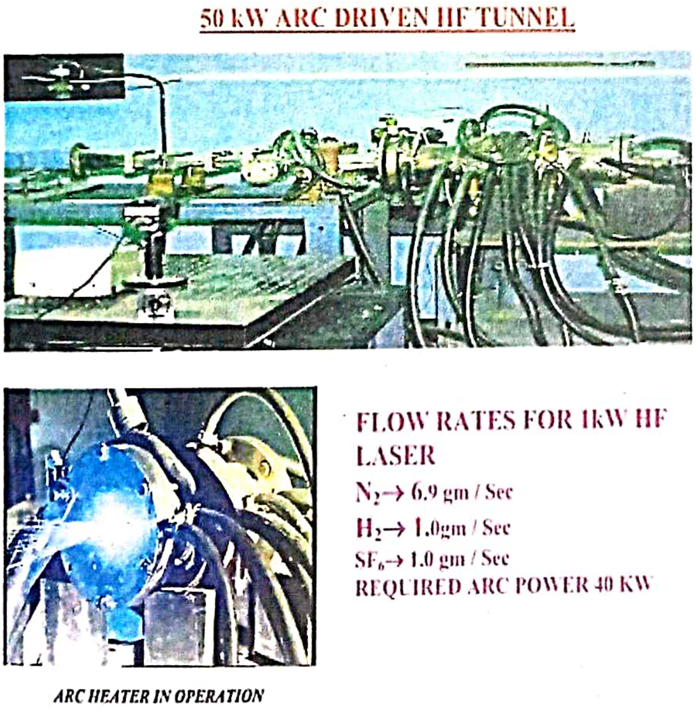

Fig 9: Developed hardware and arc heater in operation

5. CONCLUSION

In this paper an attempt has been made to present the developmental work on DAS using commercially available data cards of Adventech make for hostile arc environment. Experiments were conducted on 50 kW arc heater tunnel for basic arc behavior and for optimizing lasing parameters. The quantitative variation is attributed to the different geometry being employed specific to intended laser application. The experimental results of effect of variation of arc parameters on laser performance are also reported here. The calculated results for different operating conditions show that with an increasing mass flow rates in arc heater, there is increase in the arc voltage demand and result in better thermal efficiencies. Also with increases of arc current, we get the results in shorter arc & lower thermal efficiency. From the analysis of power input distribution it can be concluded that a major part of the electrical power input is consumed by anode cooling water (more than 50% of total power input) and only a small part of total energy is lost due to cathode cooling.

6. ACKNOWLEDGMENT

The authors are highly obliged to Dr A.K.Maini, Director Laser Science & Technology Centre, Delhi for constant encouragement and permission to publish this work.

7. REFERENCES

[1] DL Carroll, "Overview of high-energy lasers: Past, Present and Future", presented at 42nd AIAA Plasma Dynamics Lasers conference, Honolulu, Hi, *AIAA*- 2011-3102, (2011).

[2] B Selvan, K Ramachandran, KP Sreekumar, TK Thiyagarajan and PV Ananthapadmanabhan, "Numerical and experimental studies on DC plasma spray torch" Journal of Vacuum, **84**, 444-452 (2010).

[3] E Gomez, D Amutha Rani, CR. Cheeseman, D Deegan, M Wise, AR Boccaccini, "Thermal plasma technology for the treatment of wastes: A critical review ", Journal of Hazardous Materials, **161**,614-626 (2009).

[4] Andreas Schutze, James Y. Jeong, Steven E. Babayan et al, "The Atmospheric- Plasma Jet: A Review and Comparison to other Plasma Sources", IEEE transactions on plasma science; **Vol.26**, No.6, December, (1998).

[5] D.J.Spencer, H.Mirels et al "Preliminary Performance of a CW Chemical Laser", *Applied Physics Letters*, **16** (6); 235, (1970).

[6] W. Bolton, "Measurement & Instrumentation Systems", Neuunes, Butterworth Heinemann publisher, (1996)

[7] Mainuddin, RK Tyagi, R Rajesh, Gaurav Singhal and AL Dawar, "Real-time data acquisition and control system for a chemical Oxygen-Iodine laser", J of Measurement Science & Technology, Instt. Of Phys publishing, **14** (2003).

[8] H.Edels, "Properties and theory of Electric Arc", IEE Paper No. **3498**; 55, (1961).

[9] Finkelburg and Maecker, "Electric Arcs and Thermal Plasma", Handbook of physics (German); 254, (1956).

[10] S Ghorui, SN Sahasrabudhe, AK Das, "Current transfer in dc non-transferred arc plasma torches", Journal of Applied Physics D, **43**; 245201 (18pp), (2010).

[11] S.J. Davis, D.B. Oakes, M.J. Read, A.H. Gelb,"Atomic Fluorine Source for Chemical Lasers", SPIE paper 4631-29, (2002).

[12] V.D Bulaev et al., "High power repetitively pulsed electric-discharge HF chemical Laser", Russian Journal of Quantum Electronics, volume **40**, No. 7, 40615 (2010).

[13] Evgenii A et al., "Electric-discharge pulsed $F_2 + H_2$ (D_2) chain reaction HF/ DF Laser with 4.2-L active volume" Russian Journal of Quantum Electronics, volume **40**, No. 2, 40103 (2010).

[14] Andre Sontag, Rene Joeckl, "Arc driven supersonic CW HF chemical Laser", SPIE-**1810**, (1992).

KIET IJCE

KIET International Journal of Communications & Electronics

Volume. 1, Issue No. 1, Jan - Feb 2013, ISSN: 2320 - 8996

Comparative Analysis of CMOS based Pseudo Differential Amplifiers

Sunita Rani

Assistant Professor (ECE)
YCOE, Punjabi University, Guru Kashi Campus
Talwandi Sabo(India)
ersunitagoyal@rediffmail.com

Abstract : *This paper presents a comparative analysis of CMOS pseudo differential amplifier and CMOS inverter based class AB pseudo differential amplifier using rail to rail CMFB circuit. In CMOS PDA complimentary CMFB circuit consisting of common mode detector, transimpedance and transconductance amplifier. But CMOS inverter based PDA circuit employs two CMOS inverters and CMFB consisting of current mode common mode detector and transimpedance amplifiers. The circuits have been designed using 0.18µm CMOS technology under 1 Volt supply and simulation results show that in CMOS inverter based PDA the rail to rail output swing is achieved with low common mode gain (-15dB).The output swing of circuit is 0.7V and power dissipation is 96Uw, which is less in comparison to 1V CMOS PDA.*

Keywords: *pseudo differential amplifier; common mode feedback; CMOS inverter*

1. INTRODUCTION

Nowadays, a high performance analog circuit using low voltage becomes essential mainly due to the advance of the large scale integration with complicated circuit systems and the demand for battery-operated portable equipments. However, supply voltage reduction in analog circuit causes several performance degradations and, therefore, new approaches in the design are needed to obtain analog circuits with enough bandwidth, gain and linearity. Operational transconductance amplifier (OTA) is one of the most basic cells as OTA finds many applications in many analog circuits such as operational amplifier, voltage comparators, A-D and D-A converters and high frequency filters. Several approaches have been proposed to design low voltage OTA [1-14] using both fully differential (FD) and pseudo-differential (PD) configurations. FD is typically based on a differential pair with a tail current source while PD is based on two independent inverters without tail current source. It is known that avoiding the voltage drop across the tail current source, in a PD structure, allows wider input and output ranges, and makes the architecture attractive for low power- supply applications. However, PD structure requires an extra common-mode feedback (CMFB) circuit, which serves two purposes: 1) to fix the common-mode voltage at high impedance nodes and 2) to suppress the common-mode signal components. Several approaches have been proposed to achieve CMFB [1-10]. Switched-capacitor circuit was proposed to build a CMFB [1], and the resulting circuit shows small power consumption. However, the CMFB circuits introduces clock-feed through error and load capacitance, [2-3] used simple resistive divider to sense the voltage of two differential nodes. As a result, the voltage swing of the CMFB is not limited. However, not only do these resistors require large silicon area, they load down the output impedances. [4] used MOS resistive network with bulk-driven CMFB technique. However, the circuit has quite low output impedance and high common gain. To solve the problem, methods of employing MOS transistor as CMFB circuit have been proposed [5-6]. The CMFB consists of CM detector and one stage amplifier. As a result, the common-mode gains are quite high and, in addition, the output swings are limited. [7-8] employs transistors with two stage common-mode amplifiers. The resulting common-mode gain is low. The problem with this structure is that the circuit has limited output swing and potential oscillation problem. [9-10] proposed the complementary CMFB, which can achieve both low common- mode gains with good output swings. However, the circuits are complex and show high power consumption. [11-12] proposed positive feedback technique to increase the differential gain. However, the circuit shows quite high common-mode gain (A_{cm} = -6 dB).

2. CIRCUIT DESCRIPTION

The circuit for CMOS pseudo differential amplifier is based on the configuration shown in Fig. 1. As seen, PDA consists of the input transconductor $G_{M(IN)}$ and common mode feedback network (CMFB). When the outputs from $G_{M(IN)}$ are differential signals, the currents through resistors R are of the same value but opposite phase. These currents will flow to each resistor and be mirrored to the Out1A and Out1B. Because these currents are of the same amplitude but opposite in phase, there will be no input current to the transimpedance amplifier and no voltage variation at node C. The current through resistor R are also mirrored and positively feedback to the output of the input transconductor $G_{M(IN)}$. As a result, the output impedance of PD at node V_{o1} and V_{o2} are given by Z_{out}. When the outputs from PD are common mode signals, the common mode current will flow through nodes A and B with the same amplitude and phase. As a result, the summation of these two currents are added and passed to the common mode amplifier (A) which consists of transimpedance amplifier and output transconductor G_{MO}. The output current of G_{MO} is fed back to the output node of input transconductor $G_{M(IN)}$ to eliminate common mode signal. From Fig. 1, it can be easily shown that the common mode output impedance at the output nodes (V_{o1} and V_{o2}) are

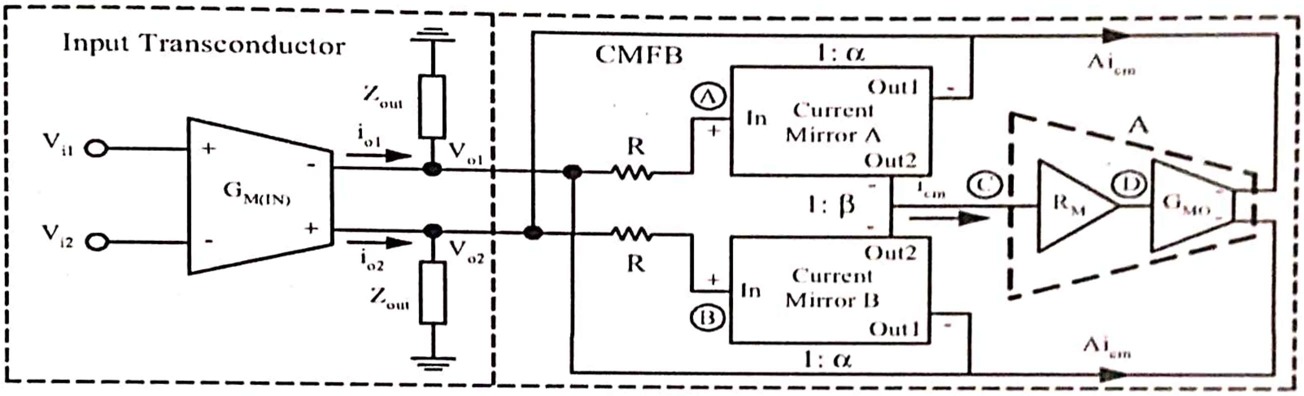

Fig. 1: Block Diagram of the proposed PDA

$$Z_{cm} = \frac{1}{g_{out} + (1 + \alpha + 2A\beta)/R} \tag{1}$$

Where the differential mode output impedance at the output nodes are

$$Z_{dm} = \frac{1}{g_{out} + (1 - \alpha)/R} \tag{2}$$

where A,α,β and g_{out} are the gain of CMFB circuit. From equation 1 & 2 the common mode gain is

$$A_{cm} = G_{M(IN)}\left[\frac{1}{g_{out} + (1 + \alpha + 2A\beta)/R}\right] \tag{3}$$

similarly differential mode gain can be shown as

$$A_{dm} = G_{M(IN)}\left[\frac{1}{g_{out} + (1 - \alpha)/R}\right] \tag{4}$$

From equation (3) and (4) the common mode rejection ratio is

$$CMRR = \frac{A_{dm}}{A_{cm}} = \left[\frac{g_{out} + (1 + \alpha + 2A\beta)/R}{g_{out} + (1 - \alpha)/R}\right] \tag{5}$$

If A is large then CMRR can be increased.

Now, the description for a CMOS inverter based class AB pseudo Differential amplifier has been given below.

A. Conventional Class-AB OTA

A conventional class-AB OTA is shown in Fig. 1 (a). As seen, the circuit is based on CMOS inverter. It is well known that CMOS inverter has high gain and less power consumption. In addition, it contains no internal nodes and, as a result, the performance of the circuit will not be much degraded by the extra parasitic poles at high frequency. The PD structure using CMOS inverter is shown in Fig. 1 (b). It can be easily seen that the differential-mode gain (A_{dm}) is the same as the common-mode gain (A_{cm}), resulting in the unity common-mode rejection ratio (CMRR=A_{dm}/A_{cm}). Since large A_{cm} can lead to large common-mode variation at the output [13], therefore common-mode feedback (CMFB) circuit is required. Large A_{cm} can lead to large common-mode variation at the output [13], therefore common-mode feedback (CMFB) circuit is required.

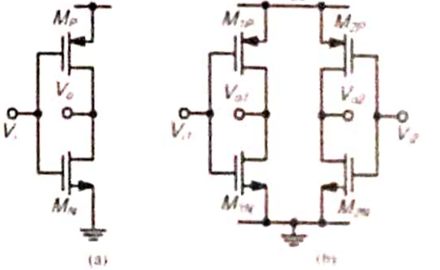

Fig. 1: (a) Inverter based single-ended OTA (b) Pseudo-differential OTA

B. The Proposed PDA Structure

The proposed PDA is based on the configuration shown in Fig. 2(a). As seen, PDA consists of the two independent CMOS inverters ($M_{1N,p}$ - $M_{2N,p}$) and common-mode amplifier (CMA), which serves two purposes: 1) to detect the common- mode signal at the output nodes (V_{o1} and V_{o2}), and 2) to provide positive feedback (see dash line) to enhance the output impedance and differential gain.

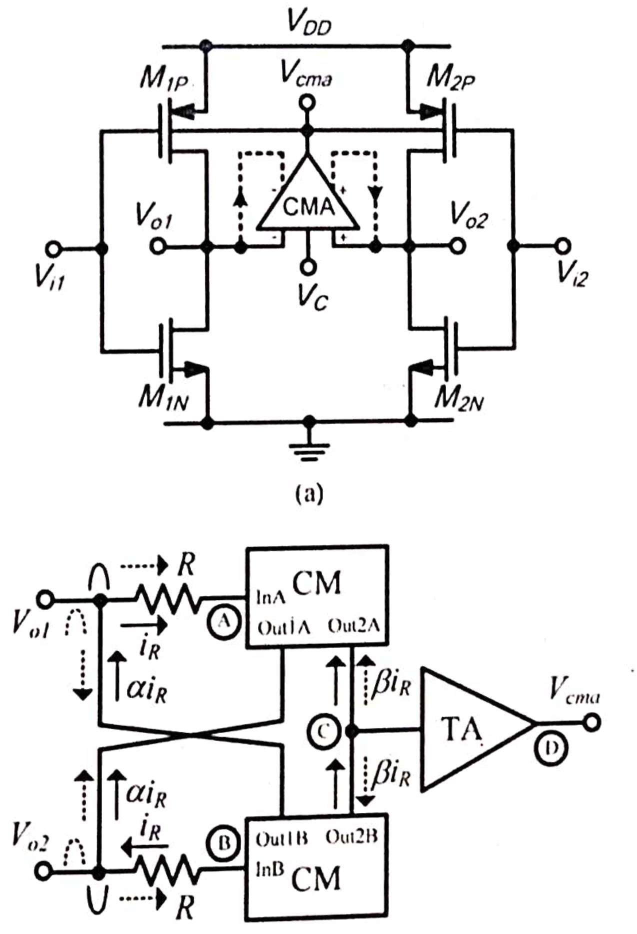

(a)

(b)

Fig. 2: The proposed PDA (a) Circuit configuration (b) Structure of CMA

The operation can be explained as follows. In case of the common-mode output signal ($V_{o1,2}$= V_{oc}), CMA will amplify $V_{o1,2}$ and negatively fed back the result (V_{cma}) to the bulk terminals of $M_{IP,2P}$ such that the common-mode output voltage is suppressed. On the contrary, CMA will not respond to the differential-mode signal (V_{o1}= - V_{o2}), namely, the output of CMA (V_{cma}) stays constant. The DC common-mode voltage is set by V_c. It is noted that the common-mode gain can be further suppressed if V_{cma} is also fed back to the bulk terminals of $M_{IN,2N}$ This can be made possible in the triple-well process. Fig. 2(b) illustrates the architecture of the proposed CMA. As seen, CMA consists of two matched resistors (R), two current mirrors (CM) and transimpedance amplifier (TA). The operation of the CMA can be explained as follows. When the output voltages from PDA are differential signals (see solid signal), these voltages are converted to the currents through resistors R. These currents, which have the same magnitude but opposite phase, flow to each resistor and are mirrored to the Out_{2A} and Out_{2B} terminals (with the current gain of β). Because these currents have the same magnitude but opposite phase, there will be no input current flowing into the transimpedance amplifier (TA) and, thus no voltage variation at node C. In addition, the currents through resistors R are mirrored to the Out_{IA} and Out_{IB} terminals (with the current gain of α), and positively fed back to the output of the PDA, thus enhancing the output impedance (at nodes V_{o1} and V_{o2}) and differential gain of the system. When the outputs from PDA are common-mode signals (see dotted line), the common-mode current flows through nodes A and B with the same amplitude and phase. As a result, the summation of these two currents are added constructively and passed to transimpedance amplifier (TA). The amplified output voltage V_{cma} is negatively fed back to the bulk terminals of $M_{IP,2P}$ to suppress the common-mode voltage, as discussed previously. Straight forward small signal analysis shows that A_{dm} and A_{cm} can be derived and shown as

$$A_{dm} = -G_{M(IN)}\left[\frac{Z_{out}}{1+(1-\alpha)Z_{out}/R}\right] \tag{1}$$

$$A_{cm} = -G_{M(IN)}\left[\frac{Z_{out}}{1+(1+\alpha-2g_{mb}\beta R_F)Z_{out}/R}\right] \tag{2}$$

Where $G_{M(IN)}$ is the transconductance of the CMOS inverter ($G_{M(IN)}$ =$gm_{1N,2N}$ + $gm_{lp,2P}$), Z_{OUT} is the output impedance of the PDA (Zout=$r_{O1N,2N}/r_{O1P,2P}$), α and β are the current gains of the current mirror (CM), g_{mb} is the bulk transconductance of $M_{IP,2P}$, and R_F is the transimpedance gain of the transimpedance amplifier.

From eq (1) & (2), one can find the common mode rejection ratio as

$$CMRR = \frac{A_{dm}}{A_{cm}} = \left[\frac{1+(1+\alpha-2g_{mb}\beta R_F)Z_{out}/R}{1+(1-\alpha)Z_{out}/R}\right] \tag{3}$$

From Eq. (3), one can notice that CMRR can be increased if the transimpedance gain (R_F) is large. In addition, the current gain α and β of current mirrors A and B also play roles in determining the CMRR.

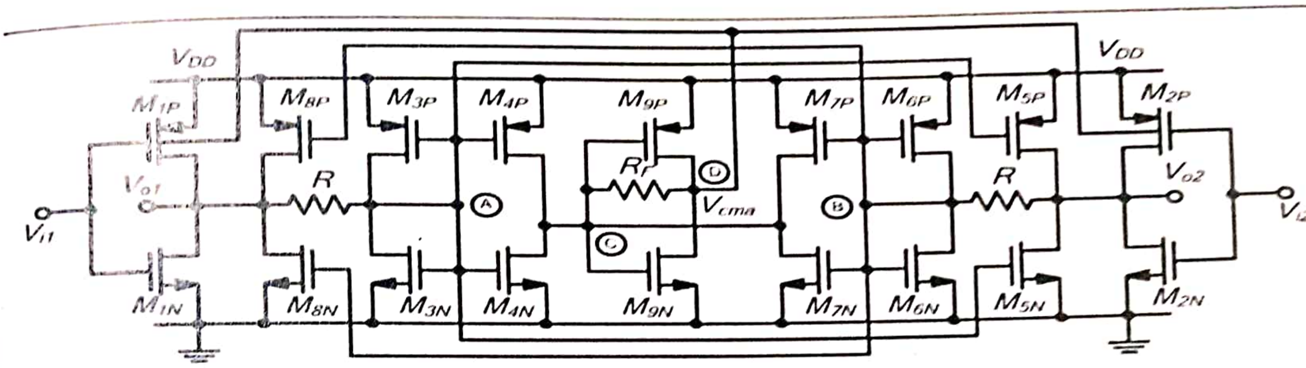

Fig. 3: The proposed class AB pseudo-differential amplifier (PDA)

3. CIRCUIT IMPLEMENTATION

The circuit implementation of Fig.1 for CMOS pseudo differential amplifier is given as in [15].

The circuit implementation of Fig. 2 is illustrated in Fig. 3. $M_{1N,P}$-$M_{2N,P}$ consist to be the input pseudo-differential amplifier, while $M_{3N,P}$-$M_{9N,P}$ consist to be a wide swing CMFB circuit. $M_{3N,P}$-$M_{5N,P}$ form the current mirror A while $M_{6N,P}$- $M_{8N,P}$ are used to form the current mirror B. The current gain with the ratios of α and β can be achieved by adjusting the aspect ratios of $M_{3N,P}$, $M_{5N,P}$ ($M_{6N,P}$, $M_{8N,P}$) and $M_{3N,P}$, $M_{4N,P}$ ($M_{6N,P}$, $M_{7N,P}$), respectively.

It is noted that the choice of α requires precaution. A large value of α can result in a large differential gain. However, large value of α can drive the circuit unstable. In practice, α should be set a little bit larger than one to compensate for the loss, due to the imperfection of the current mirror not being able to perfectly mirror the current from the input to the output. In this work, α is set to 1.3 to enjoy both differential gain and stability. The value of β plays role in determining the common-mode gain, because it is part of the CMFB circuit. As seen in Eq. (2), large value of β results in low common- mode gain. However, it is noted that large β requires large transistors, thus large standby current and parasitic capacitors, which can degrade frequency performance of the system. In this work, β is set to 3.

Transistor $M_{9N,P}$ and R_F consist to be the transimpedance amplifier (TA). The transimpedance gain of the circuit is set by the resistor R_F. The transimpedance amplifier is employed here to enhance the gain of the common-mode amplifier (CMA) and, at the same time, to reduce both input and output impedances (at nodes C and D), so that the time constants associated with these nodes are low. The dc common-mode voltage level (V_c) is equal to the voltages at nodes A and B, which is given by [14]

$$V_C = \frac{V_{DD} - V_{TN(3N,6N)} + V_{TP(3P,6P)}}{1 + \sqrt{\beta_{N(3N,6N)} / \beta_{P(3P,6P)}}} + V_{TN(3N,6N)} \tag{4}$$

where $\beta_{N(3N,6N)}=\mu_n C_{Ox}(W/L)_{3N,6N}$ and $\beta_{p(3p,6p)}=\mu_p C_{ox}(W/L)_{3P,6P}$

For maximum output swing, we have set $\beta_{N(3N,6N)}$ and $\beta_{p(3P,6p)}$ such that V_c is equal to $V_{DD}/2$.

4. SIMULATION RESULTS

To verify the circuit performance, HSPICE is used to simulate the proposed circuit, using a 0.18 µm. CMOS process under the supply voltage of 1 V. In this work, the bias currents of all transistors are chosen to optimize both gain and power dissipation. CMOS pseudo differential amplifier and CMOS inverter based class-AB pseudo differential amplifier show following characteristics.

A. DC transfer characteristic:

Fig. 4(a) and Fig.4(b) show the DC transfer characteristic for CMOS PDA and CMOS inverter based PDA respectively. In both type of PDAs output swing shows rail to rail operation.

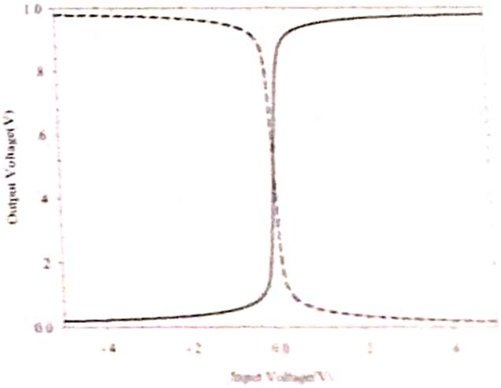

Fig. 4(a): DC transfer characteristics

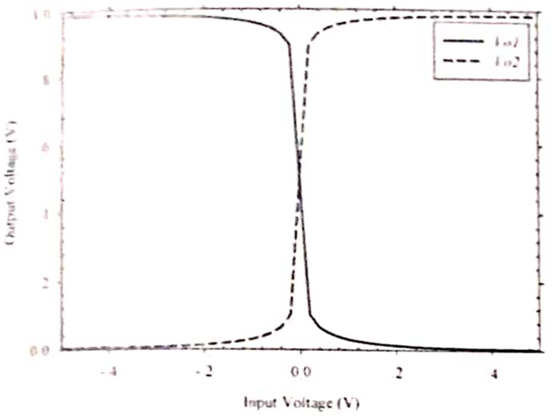

Fig. 4(b): DC transfer characteristics

B. Transient response of output voltage:

Fig.5(a) and Fig.5(b) show differential & common mode voltages. As seen in CMOS PDA differential voltage is ±0.7V & variation in common mode voltage is 0.3mV.But in CMOS inverter based PDA differential and common mode output voltages are 0.7Vp-p & 0.4mVp-p.

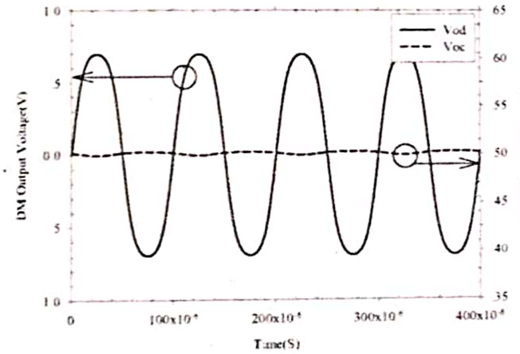

Fig. 5(a): Differential & common mode output voltages

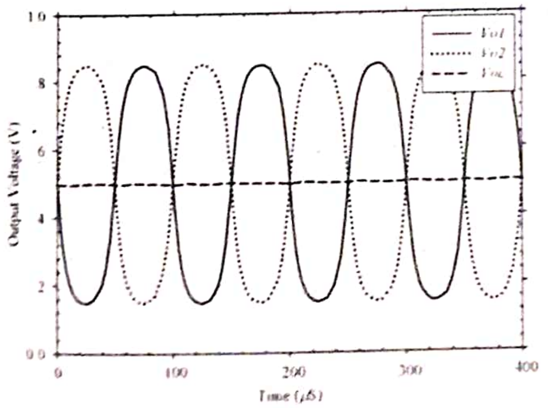

Fig. 5(b): Differential & common mode output voltages

C. Frequency response for DM input signal:

Fig. 6 shows the frequency response in case if differential mode input signal. In Fig.6(a) DC gain is found to be 36dB,while -3dB and unity gain frequency are 14MHZ and 1.25GHZ respectively while phase margin is 87°. As seen in Fig. 6(b) the DC gain is found to be 36 dB, while the -3 dB and unity gain frequency are 8.5 MHz and 800 MHz, respectively. The phase margin is 85°.

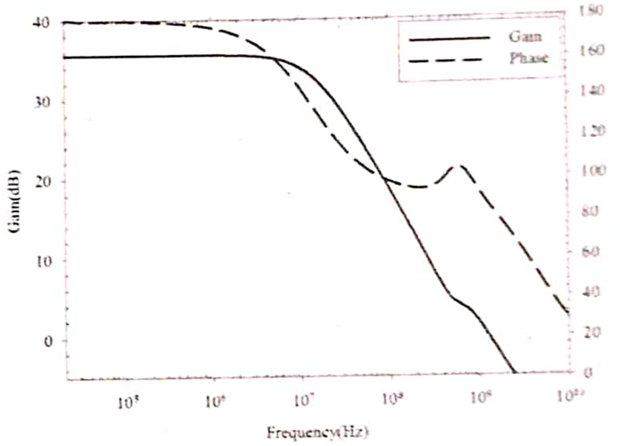

Fig. 6(a): Gain and phase margin of DM

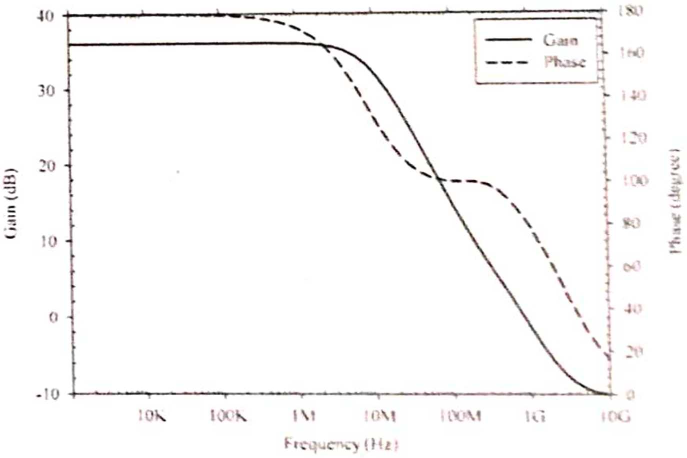

Fig. 6(b): Gain and phase margin of DM

D. Frequency response for CM input signal:

Fig. 7 shows the frequency response of the PDA in case of the common-mode input signal. As seen in Fig. 7(a) common mode gain is -36dB and power dissipation is 0.23mW but Fig. 7(b) shows the common-mode gain is relatively much smaller (-15 dB), while the bandwidth is almost the same as in the differential-mode case. The power dissipation of CMOS inverter based class-AB pseudo differential amplifier is 96 μW.

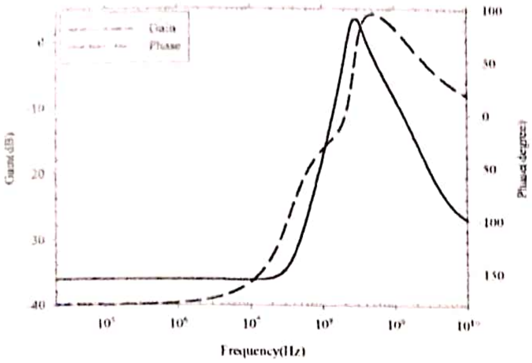

Fig. 7(a): Gain and phase margin of CM

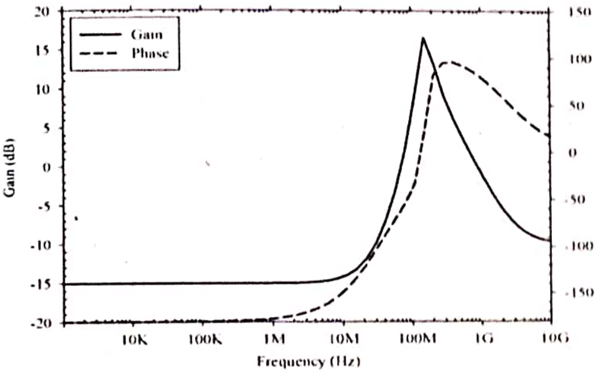

Fig. 7(b): Gain and phase margin of CM

5. CONCLUSION

In this paper a CMOS PDA and CMOS inverter based PDA are used, which operate on low voltage and use CMFB circuit. Simulation results show that in CMOS inverter based PDA common mode gain is -15dB, unity gain frequency is 800MHZ, phase margin is 85° and power dissipation is 96μW which is very small in comparison to 1 volt CMOS pseudo differential amplifier.

6. REFERENCES

[1] O. Choksi and L. R. Carley, "Analysis of switched-capacitor common mode feedback circuit," IEEE Trans. on Circuits Syst. II, vol. 50, pp. 906-917, 2003.

[2] J. N. Babanezhad, "A low-output-impedance fully differential OP Amp with large output swing and continuous-time common-mode feedback," IEEE Solid-State Circuits, vol. 26, pp. 1825-1833, 1991.

[3] G. Ferri, V. Stornelli, A. De Marcellis, and A. Celeste, "A rail-to-rail DC-enhanced adaptive biased fully differential OTA," European Conf. on Circuit Theory and Design (ECCTD), pp. 527 – 530, 2007.

[4] M. Maymandi-Nejad and M. Sachdev, "Continuous time common-mode feedback technique for sub 1V analogue circuits," Electronics Letters, vol. 38, pp. 1408-1409, 2002.

[5] M. M. Zhang and P. J Hurst, "Effect of Nonlinearity in the CMFB circuit that uses the differential-difference amplifier," IEEE Int. Symp. Circuits and Systems (ISCAS), pp. 1390-1393, 2006.

[6] L. Hung-Yi,L. Yen-Tai and K. Chi-Chou, "A simple scheme to extend the linearity of the continuous-time CMFB circuit for fully-differential amplifier,"TENCON'08, pp.1-4, 2008.

[7] L. Lah, J. Choma, and J. Draper, "A Continuous-Time Common-Mode Feedback Circuit (CMFB) for High-Impedance Current-Mode Applications," IEEE Trans. on Circuits Syst. II,vol. 47, pp. 363 – 369, 2000.

[8] F. Schlogl and H. Zimmermann, "1.5 GHz OPAMP in 120nm digital CMOS," European Solid-State Circuits Conference (ESSCIRC), pp.239-242, 2004.

[9] S. Jae-Yoon, L. Cheol-Hee, J. Won-Chang, and P. Hong-June, "Adaptive biasing folded cascade CMOS OP-Amp with continuous-time push-pull CMFB scheme," IEICE Trans. Electron, vol. E80-C, no.9, pp.1203-1210, 1997.

[10] Hua Ma; Yizheng Ye; Minyan Yu; Jinbao Lai; "A novel common-mode sensing circuit with large input swing for Op-AMP with common-mode feedback," ASICON'07, pp. 465 – 468, 2007.

[11] B. Nauta, "A CMOS transconductance-C filter technique for very high frequencies," IEEE Journal of Solid-State Circuits, vol. SC-27, no. 2, pp. 142-153, 1992.

[12] B. Nauta, "A CMOS transconductance-C filter technique for very high frequencies," IEEE Journal of Solid-State Circuits, vol. SC-27, no. 2, pp. 142-153, 1992.

[13] Y. Ro, W.R. Eisenstadt, R.M. Fox, "New 1.4 volt transconductor with superior power supply rejection," IEEE Int. Symp. Circuits and Systems (ISCAS),vol. 2, pp. 644 – 647,1999.

[14] A.N.Mohieldin, E.Sanchez-Sinencio, and ISilva-Martinez, "Nonlinear effects in pseudo differential OTAs with CMFB," IEEE Trans. Circuits Syst. II, Analog and Digital Signal Processing,vol. 50,no. 10, pp.762-770, 2003.

[15] Lee, T.S. and Lu, c.c. 2008. "A 330 MHz 26.4 mW 11 Bit Low Hold Pedestal CMOS Fully Differential Track and Hold Circuit," IEEE Int. Symp. VLSI Design, Automation and Test (VLSI-DAT), pp. 144-147, 2008.

[16] Apirak Saudet and Varakorn Kasemsuwan "A 1Volt CMOS Pseudo Differential Amplifier", IEEE 2006.

KIET IJCE
KIET International Journal of Communications & Electronics
Volume. No. 1, Issue No. 1, Jan - Feb 2013, ISSN: 2320 - 8996

Metamaterial Based Optical Surface Plasmon Resonance Sensor

Archana Yadav[1], Y.K.Prajapati[2], Vivek Singh[3], J.P.Saini[4]

[1]Department of Electronics & Communication Engg., B.I.E.T., Jhansi (U.P), India
archanayadav.ay@gmail.com
[2]Department of Electronics & Communication Engg., B.I.E.T., Jhansi (U.P), India
yogendrapra@gmail.com
[3]Department of Physics, Banaras Hindu University, Varansi (U.P), India
dr_vivek_singh@indiatimes.com
[4]Department of Electronics & Communication Engg., B.I.E.T Jhansi (U.P), India
jps_uptu@rediffmail.com

Abstract: *This paper deals with a comparative study of Surface Plasmon resonance (SPR) sensor using metamaterial and conventional surface Plasmon resonance (SPR) sensor. This comparative study results better understanding of novel property of metamaterials which can be used in the field of sensing. Reflectance is evaluated for the p-polarized light launched in the fiber. Contrary to the conventional case, in which surface polaritions with positive phase velocity appears at a boundary of metallic guide, where as in this case, surface polaritons propagate along the boundary of a metamaterial guide with negative refractive index.*

Indexterms: *Optical fiber, Surface Plasmon resonance (SPR), Reflectance.*

1. INTRODUCTION

The phenomenon of surface Plasmon resonance has been known for a long time and has been used for chemical sensors and remote sensing [1]. It makes use of a prism and a thin metal layer deposited upon the prism. Traditionally, SPR is measured using the Kretschman configuration, with a prism and a thin highly reflecting metal layer (silver or gold) deposited upon the prism base [2]. The reflection spectrum (reflected light intensity versus angle of incidence with respect to the normal of the metal) is measured by coupling transverse magnetically (TM) polarized monochromatic light in to the prism and measuring the reflected light intensity of the ray exciting the prism versus the angle of incidence. Fresnel equations [3] are used to predict reflected and transmitted light intensity from multilayered structures. Resonance condition is established when the frequency of light photons matches the natural frequency of surface electrons oscillating against the restoring force of positive nuclei. This paper explores the use metamaterials to produce the surface Plasmon resonance at microwave frequencies. Metamaterials are materials with negative permittivity and permeability. Metamaterials have attracted considerable attention in recent years [4-8]. These are artificial materials engineered to provide properties which may not be readily available in Nature. These materials usually gain their properties from structure rather than composition, using the inclusion of small inhomogeneties to enact effective macroscopic behavior [9]. Apart from sensing field metamaterial can be used in other applications such as perfect lens, various filter applications, phase shifter, and MRI .By using metamaterial in surface Plasmon resonance (SPR) sensor, it increases refractive index sensitivity by generating the resonance condition at longer wavelength and reduces the value of reflectance.

2. FORMULATIONS FOR A GENERALIZED SURFACE PLASMON RESONANCE SENSOR

Considering the layered structure shown in Fig.1.A Plane wave is incident from the medium 1 with ε_1 and μ_1 on the layer with ε_2 and μ_2 bounded by the medium 3 with ε_3 and μ_3.Here ε and μ are relative permittivity and relative permeability normalized to free space ε_0 and μ_0.The reflection coefficient R is well know [10].

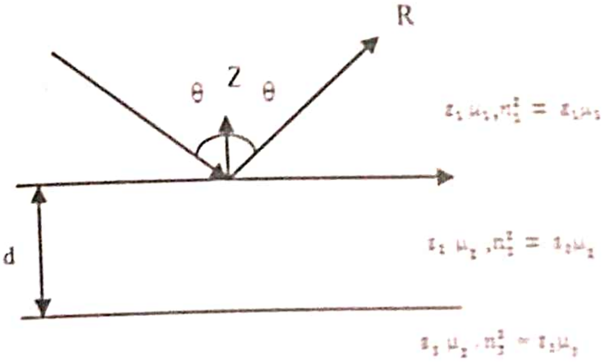

Fig.1 Geometry of three layered Structure

$$R = \frac{A + \frac{B}{Z_3} - Z_1\left(C + \frac{D}{Z_3}\right)}{A + \frac{B}{Z_3} + Z_1\left(C + \frac{D}{Z_3}\right)} \quad (1)$$

Where

$A = D = \mathrm{Cos}k_{z2}d$, $B = jZ_2\mathrm{Sin}k_{z2}d$, $C = \frac{j\mathrm{Sin}k_{z2}d}{Z_2}$

$k_{zi} = \sqrt{k_i^2 - (k_i \mathrm{Sin}\theta_1)^2}$, $i = 1, 2, 3$, $k_i = k_0 n_i$

$k_0 = \frac{\omega}{c}$ is the free space wave number

$$Z_i = \begin{Bmatrix} \frac{k_{zi}}{\omega \varepsilon_0 i} \text{ for p} - \text{polarization } (E_x, E_z, H_y) \\ \frac{\omega \mu_0 \mu_i}{k_{zi}} \text{ for s} - \text{polarization } (H_x, H_z, E_y) \end{Bmatrix}$$

In this formulation, both ε_i and μ_i are complex. However for a passive medium , we require, using exp($j\omega t$) time dependence,

$\mathrm{Im}(\varepsilon_i) < 0$
$\mathrm{Im}(\mu_i) < 0$
$\mathrm{Im}(n_i) < 0$
$\mathrm{Im}(k_{zi}) < 0$
$\mathrm{Re}\sqrt{\frac{\mu_i}{\varepsilon_i}} > 0$

In this paper we examine equation (1) for metamaterials and discuss its physical meanings.

3. CONVENTIONAL SURFACE PLASMON RESONANCE SENSOR

Before we discuss metamaterial surface plasmon resonance sensor, firstly we see the conventional optical sensor making use of the surface Plasmon resonance.

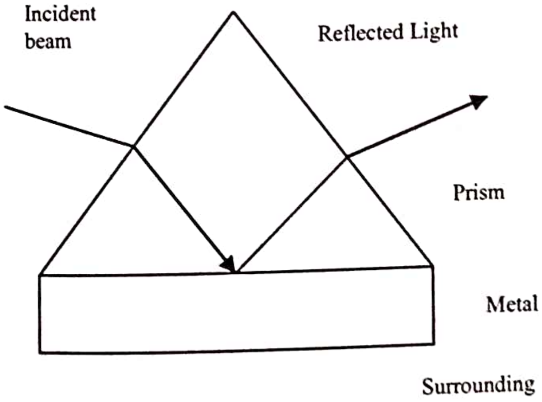

Fig 2.Schematic geometry of the conventional surface plas mon resonance sensor strucuture

Fig. 2 illustrates the model geometry of the three layered surface Plasmon resonance (SPR) presented here. The model structures consist of a high index prism (SF10 with refractive index n = 1.723), Ag metal layer, and a water buffer (n = 1.332) for a p-polarized incident light of 632.8 nm to have sharp resonance curves and minimum reflectivity dips.

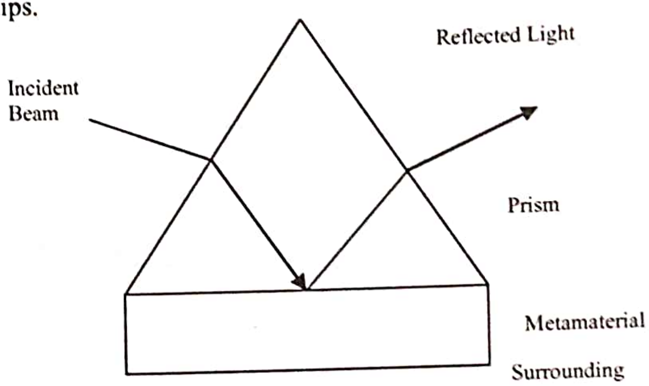

Fig 3.Schematic geometry of the metamaterial based surface plasmon resonance sensor structure

4. SURAFCE PLASMON FOR META MATERIALS

We now generalize the conventional Plasmon sensor discussed in above section to include the metamterials with arbitrary ε and μ.Fig. 3. Illustrates the model geometry of the three layered SPR structure using metamaterial in the place of Ag metal layer in conventional SPR sensor. All considerations are same as made for conventional structure only Ag metal layer is replaced by metamaterial layer. This layer of metamaterial, which is having the value of ε is -0.66-0.001*i and the value of μ is -2.All values of the index for the prism and water buffer layer are kept same as taken for the conventional plasmon resonance sensor .

5. RESULTS AND CONCLUSION

This paper has presented the use of metamaterials for Plasmon resonance sensors (SPR) at microwave frequencies and also deals with the comparison of conventional surface Plasmon resonance sensor using Ag metal layer and surface plasmon resonance sensor using metamaterial. Fig.4 shows the reflectance curve for the conventional surface plasmon resonance sensor as a function of incident angle θ, in the incident medium of the SF10 prism. The optimum thickness of Ag metal layer is determined to be 131 nm. The complex refractive index of Ag used is 0.082 + 4.1563 * i. Fig 5 shows the reflectance curve for the metamaterial based sensor as a function of incident angle θ.Thickness of Metamaterial layer is same as Ag metal layer.

From the above discussion, it can be said that on the same thickness of the layer, metamaterial based surface plasmon resonance sensor gets the lower value of reflectance in comparison to the reflectance of the Ag metal layer (conventional surface plasmon resonance sensor). Numerical values of minimum reflectance of silver- metal layer and metamaterial based surface plasmon resonance sensor are 0.95537 and 0.00090 respectively and incident angles for the silver- metal layer and metamaterial based surface plasmon resonance sensor are 54.74612. and 32.80183 respectively.

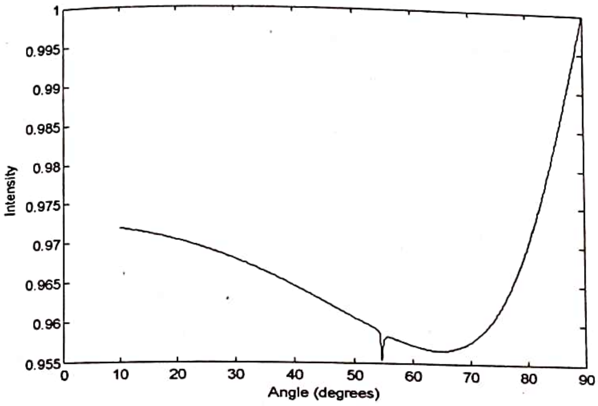

Fig. 4 Reflectance curve for conventional surface plasmon resonance sensor as a function of incident angle.

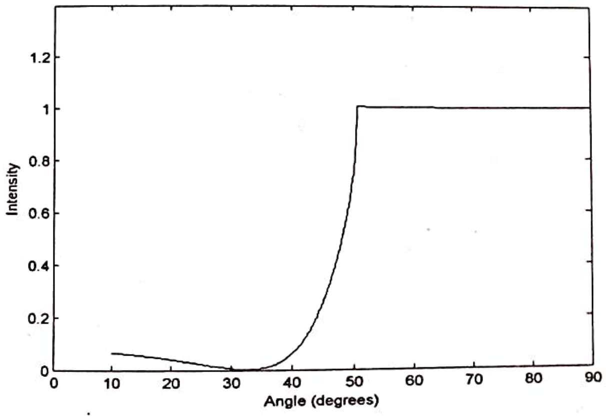

Fig. 5 Reflectance curve for metamaterial based surface plasmon resonance sensor as a function of incident angle.

6. REFERENCES

[1] Jorgenson, R. C. and S. S. Yee, "A fiber-optic chemical sensor based on surface Plasmon resonance" Sensors and Actuators B, Vol. 12, 213–220, 1993.

[2] E.Kretschmann and H.Raether, Radiative decay of non radiativesurface plasmons excited by light, Z. Naturforsch, Teil A,23 (1968) 2135-2136.

[3] E.Hecht, "optics", Addison-Wesley: Massachusetts, 1974.

[4] Veselago, V. G.,"The electrodynamics of substances With simultaneously negative values of ε and μ,"Sov.Phy.Usp., Vol.10,No.4, 509-514,Jan.-Feb.1968.

[5] Pendry, J. B., A .J. Holden, D. J. Robbins, and W.J. Stewart," Magnetism from conductors and enhanced nonlinear phenomena," IEEE Trans. Microwave Theory and Techniques,Vol.47,No.11, 2075-2084,November 1999.

[6] Smith, D. R., W. J. Padilla, D. C. Vier, S. C. Nemat-Nasser, and S. Schultz, "Composite medium with simultaneously negative permeability and permittivity," Phys. Rev. Lett., Vol. 84, No. 18,4184–4187, May 2000.

[7] Pendry, J. B., "Negative refraction makes a perfect lens," Phy.Rev. Lett., Vol. 85, No. 18, 3966–3969, October 2000.

[8] Ziolkowski, R. W. and E. Heyman, "Wave propagation in media having negative permittivity and permeability," Phy. Rev. E, Vol. 64, No. 5, 056625, 2001.

[9] Shridhar E.Mendhe & Yogeshwar Prasad Kosta,"Metamaterial Properties and Applications", International Journal of Information and Technology & Knowledge Management January- June 2011, Volume 4, No1, pp.85-89.

[10] Ishimaru, A., Electromagnetic Wave Propagation, Radiation, and Scattering, Prentice Hall, 1991.

KIET IJCE
KIET International Journal of Communications & Electronics
Volume. No. 1, Issue No. 1, Jan – Feb 2013, ISSN: 2320 - 8996

Optical Detection of Chlorine for Chemical Oxygen Iodine Laser

Mainuddin[1], **Gaurav Singhal**[2], **A. K. Varshney**[3], **R. K. Tyagi**[4], **A. K. Maini**[5]
[1,2,3,4,5]Laser Science and Technology Centre,
Defence Research and Development Organization,
Metcalfe House, Delhi-110054, India

Abstract: *This paper focuses on the implementation of optical technique for measurement of chlorine gas utilization which is one of the critical parameters for Chemical Oxygen Iodine Laser (COIL). COIL employs chlorine as one of the fuel components to generate singlet oxygen molecules after its reaction with Basic Hydrogen Peroxide (BHP) solution. The efficiency of COIL is strongly dependent on utilization of chlorine which in turn maximizes the laser output power. An optical absorption based in-house custom built chlorine detection system has been developed and interfaced with COIL.*

Keywords: *Chlorine; Data acquisition; Chemical laser; Interface electronics; Graphical user interface*

1. INTRODUCTION

COIL is one of the flowing medium infrared gas lasers [1-3] which utilizes various gas effluents and chemicals. It is the only chemical laser based on electronic transition. It has distinct benefits in terms of scalability, efficiency (>20%), shorter wavelength (λ=1.315μm) enabling fibre compatibility for remote operation and also good laser material interaction. Owing to these advantages it is highly sought after laser source for numerous applications. The pumping energy source for this laser is singlet oxygen $O_2(^1\Delta)$, which is an excited form of oxygen molecule with energy level very near to the atomic iodine. This allows possibility of a near resonant energy transfer. Singlet oxygen is required not only for pumping but also for dissociation of iodine molecules. It is produced using chemical method by the reaction between chlorine gas and BHP solution. The production of singlet oxygen is strongly dependent on the amount of chlorine reacted to the BHP solution. There is a need for development of non contact type method for estimation of chlorine utilization so that flow of laser gases does not disturb. An optical absorption based chlorine utilization measurement system has been developed for optimization of COIL.

COIL first demonstrated by McDermott [4] in 1978, is the only chemical laser with electronic transition. A two phase reaction between BHP solution and chlorine gas produces pumping medium, singlet oxygen $O_2(^1\Delta_g)$. This is diluted with sufficient nitrogen buffer gas and mixed with the lasing species i.e. iodine. The total flow is then supersonically expanded into the laser cavity, where laser power at 1.315 μm wavelength is extracted according to equations (1) and (2).

$$O_2(^1\Delta)+I(^2P_{3/2})\Leftrightarrow O_2(^3\Sigma)+I^*(^2P_{1/2}) \tag{1}$$

$$I^*(^2P_{1/2})+nh\upsilon\rightarrow I(^2P_{3/2})+(n+1)h\upsilon \tag{2}$$

The pumping source, $O_2\,(^1\Delta)$ is an excited form of oxygen molecule with energy level very near to the atomic iodine and hence almost a near resonant energy transfer can be achieved. Various methods such as chemical, electrical (RF and Microwave discharges) and optical methods have been used for the generation of these pumping molecules. Amongst these, the chemical method is the only method till date that has been successful for the large-scale production of singlet oxygen with required yield. The chemical method is based on the reactions between chlorine gas (Cl_2) and BHP solution as,

$$2KOH+H_2O_2+Cl_2\rightarrow 2KCl+2H_2O+O_2(^1\Delta_g) \tag{3}$$

The lasing medium (iodine atoms) is injected into the pumping medium in the gaseous form. In typical COIL operation, commercially available iodine crystals are converted into vapor form in an evaporator and supplied with the aid of heated nitrogen gas. Fig. 1 shows the functional block diagram of COIL, which exhibits interconnections of all subsystems.

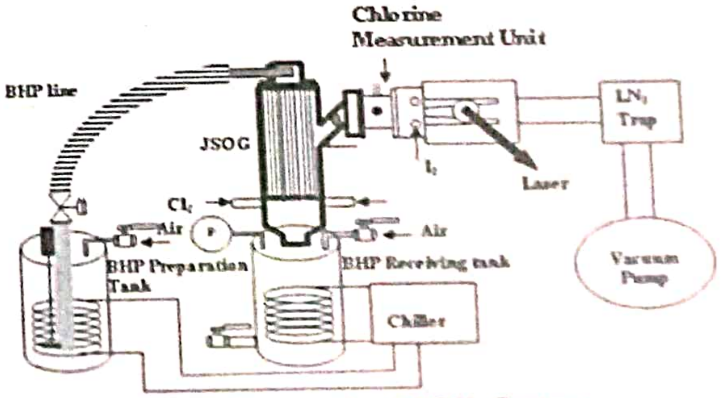

Fig. 1: Schematic of COIL System

The BHP solution is prepared in a separate storage tank and is supplied to singlet oxygen generator (SOG) reaction chamber in the form of jets. The chlorine is supplied to SOG reaction chamber from the bottom side so that it reacts with the surface of the liquid jets to produce singlet oxygen molecules. The supplied BHP through SOG is collected in receiving tank attached at the bottom of the SOG reaction chamber. The temperature of BHP solution has to be maintained at a temperature of -20° C from the safety and operational performance point of view. Thus, a cooling system attachment for both the BHP preparation and receiving tanks is essential.

SOG is an important subsystem in COIL. The input to SOG is chlorine and BHP solution. The concept of chemical based jet type singlet oxygen generator (JSOG) for the production of singlet oxygen for COIL applications was first demonstrated by Balan *et.al.* [5] and later implemented by Zagidullin [6]. Basically the generator consists of a large number of fine jets of BHP flowing through an atmosphere of chlorine.

The chemical generation of singlet oxygen involves a liquid–gas phase interaction and hence involves many fluid dynamic aspects. The parameters associated with the reaction i.e. chlorine utilization, molar flow rate and pressure of chlorine gas line, pressure, temperature and flow rate of BHP inside SOG are required to be controlled and monitored.

In this article, we present the optical absorption based chlorine utilization diagnostic system for COIL.

2. SYSTEM DESCRIPTION

A. Basic principle

The principle behind the estimation of chlorine flow is peak absorption of chlorine at ~ 330 nm [7, 8] with an absorption cross-section (σ) of 2.75×10^{-19} cm^2. In COIL operation, known flow rate of chlorine is passed through SOG and reaction (3) utilizes the chlorine for singlet oxygen generation. Chlorine utilization measurement gives the percentage of chlorine molecules reacted with BHP for generation of laser pumping medium i.e. singlet oxygen.

In order to estimate the utilized chlorine, un-utilized chlorine is measured by applying Beer Lambert law at the exit of SOG. A probe beam (λ ~330 nm) is passed through the optical cell containing measuring medium as shown in Fig. 1. Fig. 2 shows the schematic diagram of chlorine measurement. The intensity of the transmitted beam is given by the Beer Lambert's law:

$$\frac{I_\nu}{I_0} = \exp\left(-\sigma_\nu n L\right) \qquad (4)$$

Where
I_ν- transmitted light intensity at frequency 'ν' (intensity with chlorine)
I_0- incident light intensity (intensity without chlorine)
σ_ν- absorption cross section ((2.75×10^{-19} cm^2)
n- chlorine concentration (molecules cm^{-3})
L- length of the optical cell

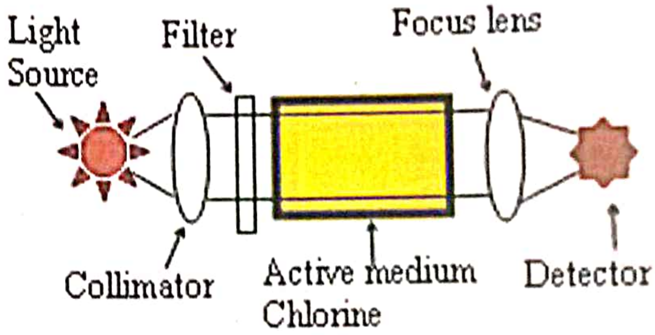

Fig. 2: Optical scheme for measurement of chlorine

From the above relation, the partial pressure of chlorine can be determined as,

$$\left(P_{Cl_2}\right)_{exit} = \left(\frac{kT}{\sigma L}\right) \ln\left(\frac{I_0}{I_\nu}\right) \qquad (5)$$

Where, k is the Boltzmann's constant and T is the temperature of the medium. In case of COIL operation, chlorine is carried to the laser head along with nitrogen and pressure measured in the optical cell is the total pressure of chlorine and nitrogen gas. Thus, unutilized chlorine molar flow rate '$(M_{Cl2})_{exit}$' at exit of SOG can be estimated using Dalton's law,

$$\left(M_{Cl2}\right)_{exit} = \frac{\left(P_{Cl_2} \times M_c\right)}{\left(P_{tot} - P_{Cl_2}\right)} \qquad (6)$$

Where,
P_{tot} - Total pressure at the measuring optical cell
M_c- Molar flow rate of the carrier gas (N_2)

The flow rate of exit chlorine '$(M_{Cl2})_{exit}$' is estimated using relation (6) and chlorine input flow rate '$(M_{Cl2})_{input}$' is known using the principle of orifice under choke flow condition [9]. Hence chlorine utilization 'U_{Cl}' is estimated using the relation (7).

$$U_{Cl} = 1 - \frac{(M_{Cl2})_{exit}}{(M_{Cl2})_{input}} \qquad (7)$$

B. Experimental Setup

The singlet oxygen from generator along with nitrogen is passed through optical cell of 25 cm length and 2.54 cm diameter. The flow medium from the optical cell with traces of chlorine gas is continuously pumped out to liquid nitrogen trap. Ultra Violet mercury lamp is used as a light source along with an interference filter with 330±5 nm. The collimated light is passed through the cell and detected using silicon photodiode (RS component stock no. 303-674). The flow rate of exit chlorine '$(M_{Cl2})_{exit}$' can be estimated using the relation (6) and chlorine input flow rate '$(M_{Cl2})_{input}$' is known using the principle of orifice under choke flow condition. Fig. 3 shows the photograph of developed chlorine measurement system.

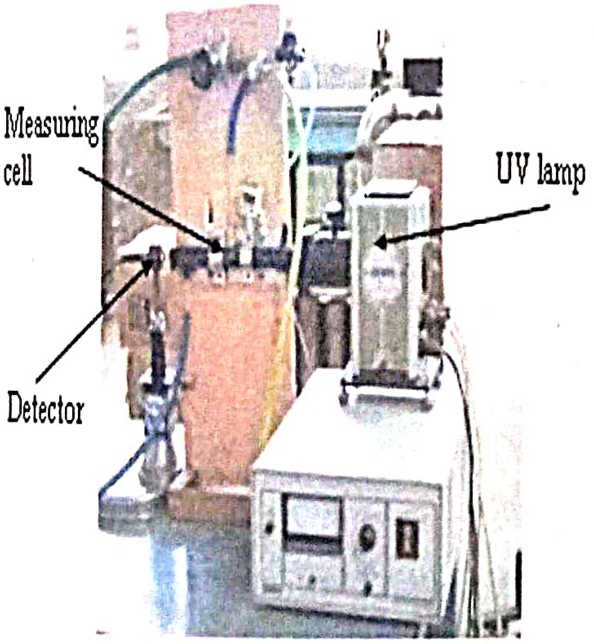

Fig. 3: Photograph of Chlorine measurement system

Initially total pressure in the transport duct (P_{tot}) was measured using a capacitance gauge (M/s Pfeffier make Model No. CMR 262) due to its high accuracy (0.2%), However, these sensors require warm up time of about one hour for achieving accuracies of this order and moreover the water vapor and hazardous gases such as Cl_2 and I_2 adversely affect the performance. Therefore, diaphragm type pressure transmitters from M/s Metran of "Metran-22 series" have been used. These employ metallic diaphragm, which are suitable for corrosive environment as encountered in COIL application.

In these diaphragm type sensors, there is a monocrystalline sapphire plate with silicon film tensoresistors (silicon-on-sapphire-structure), connected fast to diaphragm of tensotransducer. Tensoresistors are connected into bridge circuit. Deformation of measuring diaphragm (deformation of tensotransducer's diaphragm) causes proportional resistance change of tensoresistors and misbalance of bridge circuit. Electrical signal from bridge circuit output is fed to microprocessor based electronic module, where it is transformed into unified current output (4-20 mA). These operate at 24 V supply to produce 4-20 mA output current signal. The current signal is preferred because it is less likely to be affected by noise. The temperature of medium is monitored using resistance temperature detector Pt-100.

The continuous recording of temporal variation of pressure and photodiode signal is carried out using a dedicated PCI bus based data acquisition system (DAS). DAS [10] is not only require for diagnostic parameters estimation but also for real time operational control, acquisition, measurement, monitoring, display, storage and analysis of parameters. Fig. 4 shows the scheme of DAS which has been used for estimation of chlorine utilization as well as for other operational requirements of COIL.

C. Chlorine Safety System

A safety interlock scheme has been implemented to cater for any leakage of Cl_2, and storage of BHP solution. Fig. 5 shows the general safety scheme adopted for safe operation of COIL.

For example, chlorine supply system is operated at sub-atmospheric pressure (500-600 torr) to avoid any leakage from the system. Chlorine leak detection system (Model no Advance 200) has been installed for detection of chlorine leakage. This system has option to set a threshold concentration of 1 and 10 ppm and produces an alarm signal (SS), which is compared with preset reference value (RF). If leakage exceeds this limit, data acquisition system issues a command to shut off the experiment and switch on the safety equipment (air ventilation system installed in the chlorine supply system).

The sensor produces 5 mA current output signal according to the concentration (1ppm or 10 ppm as per settings of threshold value) of chlorine. This current output is fed to a current to voltage converter to get a voltage output signal and is compared with a reference signal (5V) to activate air circulation system & alarm and the scheme is shown in Fig. 6. The ventilator output is passed through a scrubber (charcoal) to absorb the traces of chlorine before it is exhausted out of the chimney into the atmosphere.

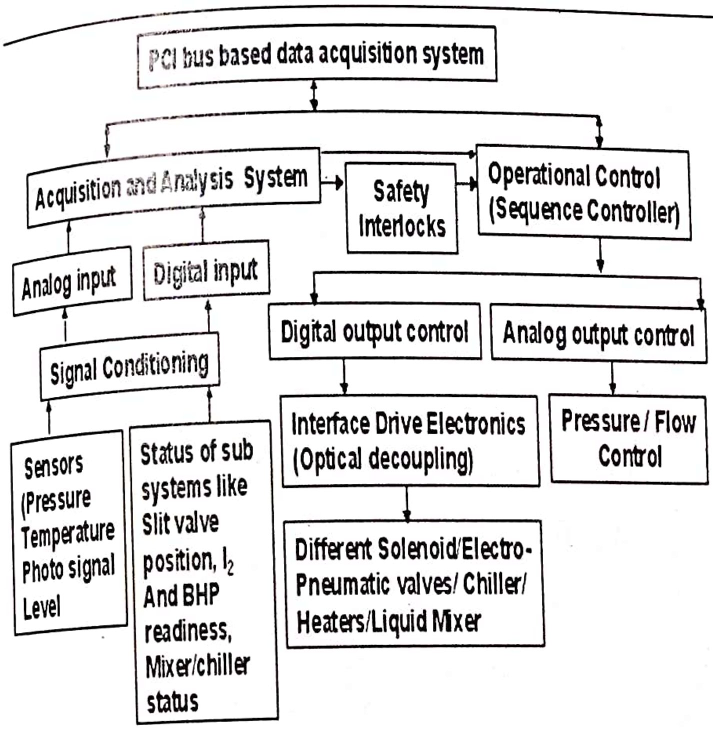

Fig. 4: Schematic of data acquisition system

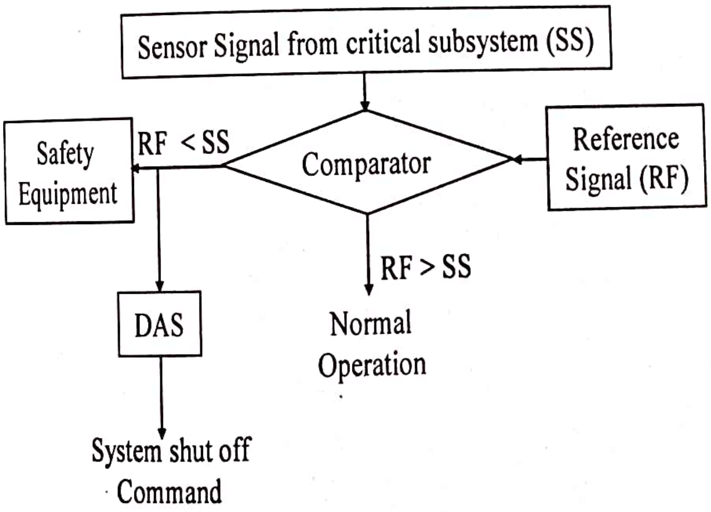

Fig. 5: Scheme for Safety Interlocks

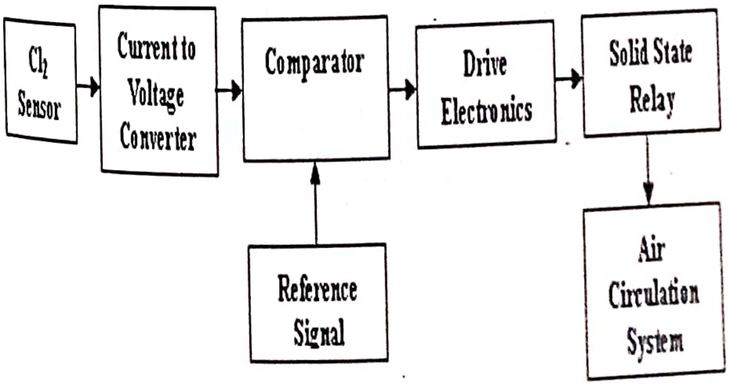

Fig. 6: Automatic control unit for chlorine sensor

D. Data Acquisition System

Chlorine utilization diagnostics system is interfaced with PCI bus based data acquisition system (DAS) which comprises of three modules: (i) acquisition and analysis, (ii) operational and sequence control and (iii) safety interlocks. DAS has been configured using Advantech PCI-1716 multifunction card and application software developed using VC++. Five user's friendly graphical user interfaces (GUI) have been designed for on line parameter acquisition, control and safety interlocks implementation. This card is a 16 bit high resolution multi function card with a sampling rate of 250 kS/s.It includes complete functions for data acquisition and control including A/D conversion, D/A conversion, digital input, digital output and counter/timer. Fig. 7 shows one of the GUI for display of acquired parameters as well as control switching and sequential functions.

The acquisition and analysis system is responsible for the acquisition of analog and digital parameters along with the storage and online estimation of diagnostics parameters in graphical form for analysis of performance of different subsystems. The analog input channels are required for acquiring the signals from transducers like pressure sensor, temperature sensor and photodiode. On the other hand, the digital input channels are used to indicate the status of various subsystems such as the system readiness status for laser firing and on/off status of various electro-pneumatic/solenoid /slit valves.

The operational and sequential control system is responsible for the sequential and switching control of electrical/ electro-pneumatic valves/devices and online control and adjustment of physical parameters like flow rates of gases involved in lasing action. This system also incorporates both analog outputs as well as digital output channels. The analog output channels are required for the flow rate control of different gas feed lines, whereas digital outputs are required for performing switching and sequential operations (on/off control) of various subsystems.

3. RESULTS AND DISCUSSIONS

The developed chlorine diagnostics system has been interfaced with COIL for estimation of chlorine utilization. The experiments have been conducted for large variation in Cl_2 flow rate conditions ranging from few tens of mmols^{-1} to few thousands of mmols^{-1}.

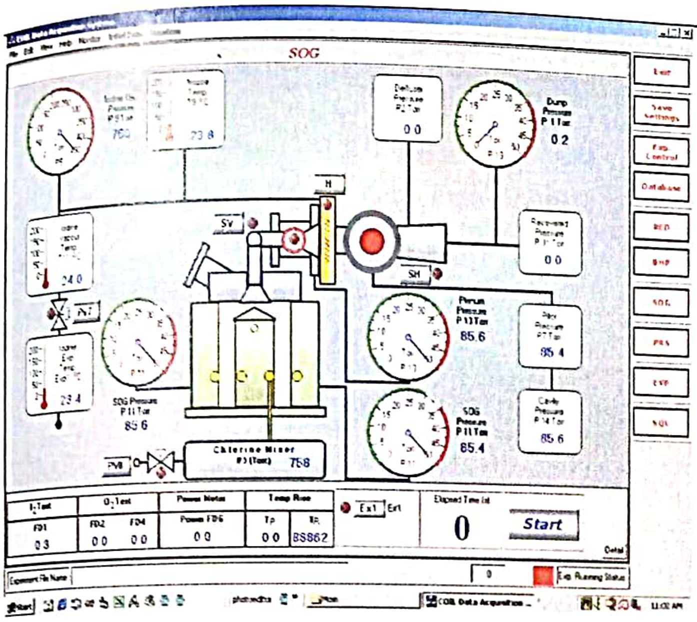

Fig. 7: GUI for display of parameters for COIL operation

The temporal variation of chlorine absorption signal, pressure and temperature signals are acquired by DAS in real time and the corresponding iodine flow rates are estimated and displayed on the PC in real time. The data acquisition card acquires the corresponding data from photo detector, pressure and temperature sensors via different analog input channels of data acquisition card and stored in the different files in the software, which are used for the online estimation of the unutilized chlorine flow rates. Fig. 8 shows typical curve of chlorine absorption signal detected by silicon detector. Initially there is no chlorine and we get a photo signal (I_0) and when chlorine is passed through the measuring cell, there is a dip in the photo signal (I_v) due to absorption of signal by chlorine molecules. This curve determines the partial pressure of chlorine gas using relation (4) and (5). Ultimately chlorine flow rates are estimated using relation (6) which is shown in Fig. 9.

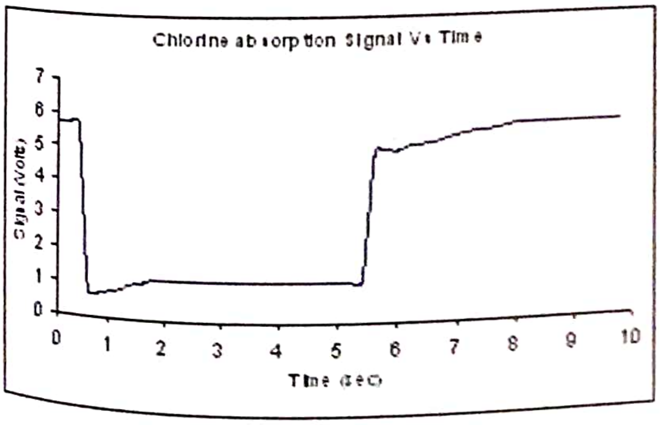

Fig. 8: Typical Chlorine absorption signal acquired by DAS

The observed unutilized chlorine flow rates are ~1.64 $\mathrm{mmols^{-1}}$. The detailed experimentation in the present case corresponding to supplied input chlorine flow rates of ~ 27.5 $\mathrm{mmols^{-1}}$, shows a typical chlorine utilization of nearly 94% using the relation (7).

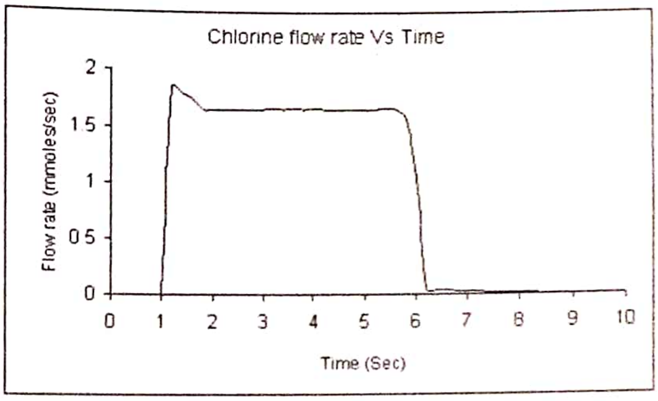

Fig. 9: Typical estimated unutilized Chlorine flow rate

The chlorine utilization is one of the important diagnostics because COIL power is a strong function of chlorine flow rates. Moreover unutilized chlorine can not be sent directly to vacuum pumps (which evacuate the laser chamber) as chlorine is a corrosive gas and affects the life of vacuum system. The unutilized chlorine was therefore trapped and neutralized by standard norms. In our system, we have developed a liquid nitrogen based trap for trapping the unutilized chlorine which is neutralized after experiments.

4. CONCLUSIONS

An on-line optical absorption based chlorine utilization diagnostics system has been developed for real time monitoring of chlorine utilization. The developed diagnostic system has been successfully incorporated with the COIL system and is being routinely used for COIL parametric studies.

5. REFERENCES

[1] D. L. Carroll, "Overview of high energy lasers: Past, Present and Future", *AIAA* paper, 2011-3102, 2011.

[2] I. Rego, K. N. Sato, Y. Miyoshi, T. Ando, K. Goto, M. Sakamoto, S. Kawasaki, "Studies on the characteristics of the gas dynamics laser with low CO_2-concentration medium by a diaphragmless shock tube", *Proc. Of 34th EPS conference on plasma physics*, 31F, 0-4-036, 2007.

[3] W. H. Behrens, P. D. Lohn, "Hydrogen and deuterium fluoride chemical lasers", *CRC Press* (NY), N4, pp 341-367, 2007.

[4] McDermott W. E, Pchelkin N. R, Benard D. J., Bonsek R. R., "An electronic transition Chemical Laser", *Applied Physics Letters*, 32(8), pp469-470, 1978

[5] Balan N.F., Gizadulin R. M., Zagidulin M. V., Kurov A. Yu., Nikolaev V. D., Pichkasov V. M., Svistin M. I., "Investigation of a jet generator of $O_2(^1\Delta_g)$", Sov. J. Quantum. Electron. pp1412, 1989.

[6] Zagidullin M.V., Nikolaev V.D., Svitin M.I., Safonov V.S., Ufimtsev N.I.,(1996), "The study of buffer gas mixing with active gas on chemical oxygen iodine laser performance with jet SOG", SPIE, 2702, pp310, 1996.

[7] Jarmila Kodymova, and Otomar Spalek, "Performance characteristics of jet type generator of singlet oxygen for supersonic chemical oxygen iodine laser" Japanese Journal of Applied Physics, 37, pp117-121, 1998.

[8] R. Rajesh, Gaurav Singhal, Mainuddin, R. K. Tyagi and A. L. Dawar "High throughput jet singlet oxygen generator for multi kilowatt SCOIL", *Optics and Laser Technology*, 42, pp580-585, 2010.

[9] Mainuddin, M. T. Beg, Moinuddin, R. K. Tyagi, R. Rajesh, Gaurav Singhal and A. L. Dawar, "Real time gas flow control and analysis for high power infrared gas lasers", *International Journal of Infrared and Millimeter Waves*, 1, pp91-105, Jan. 2005.

[10] Howard Austerlitz, "Data acquisition techniques using PCs", 2nd edn., Academic Press, *Elsevier Science*(USA), 2003.

Design and Implementation of Low Power CMOS Super-Regenerative Receiver

Ramji Gupta[1], **Dr. D. K. Raghuvanshi**[2]
[1,2]*Department of Electronics & Communication Engineering*
Maulana Azad National Institute of Technology, Bhopal, Bhopal, India
[1]*ramjigupta38@yahoo.com*, [2]*dkraghuvanshi3@gmail.com*

Abstract: *A low power and low-voltage super-regenerative receiver operating at 60 GHz and implemented in 180-nm CMOS technology is described. The receiver includes a low noise amplifier, a super-regenerative oscillator, an envelope detector. The receiver uses the simplicity and power efficiency architecture for short-range communication. The power consumption of super-regenerative receiver is 2.194-mW at supply voltage of 1 V.*

Keywords: *CMOS, Low noise amplifier, Super-regenerative Oscillator, Low power, ON-OFF keying modulation, CADENCE Virtuoso.*

1. INTRODUCTION

Super-regenerative receivers (SRR) have been used for many decades, after invented by Edwin Armstrong in 1922 [1].This type of receiver holds the edge in high gain, simplicity, low cost, low power consumption and small size area. Hence, the SRR architecture has more attractive to short-distance micro-power communications, comparing to classical solutions, such as the super-heterodyne, the low intermediate or direct conversion receivers.

The unlicensed 60 GHz millimeter-wave band has the potential for short-range applications such as the wireless data transfer between hard disks, storage devices, MP3 players and high definition video receivers. In this paper, we demonstrated a high data rate ON-OFF keying (OOK) modulation super-regenerative receiver at 60 GHz using the 180-nm CMOS technology. The 180-nm low power CMOS provides 1P9M process and exhibits a unit current gain frequency of (f_T) 150 GHz and a maximum oscillator frequency (f_{max}) of 150 GHz. The approach is based on the basic SRR configuration while using a half power reduction oscillator as the SRO [5]. This current-reuse LC-VCO was used to get low phase noise and low power consumption. The proposed receiver was a realistic configuration for short-distance communication applications.

Figure 1 depicts the typical block diagram of super-regenerative receiver including super-regenerative oscillator (SRO) and Low noise amplifier (LNA) [2]-[4]. The core of the diagram is the super-regenerative oscillator which is controlled by a low frequency quench oscillator. The quench oscillator is controlling the loop gain of the SRO and then making the closed-loop system alternatively stable and unstable. Therefore, the SRO periodically starts up and shuts off which is called "quenching". The primary function of LNA is reduced the RF leakage of the oscillation signal and provided an input matching network to the antenna. In normal operation, incoming RF signal is amplified by the LNA, and then directly injected onto the oscillatory nodes of the SRO. The presence of LNA can improve overall system performance in terms of noise.

2. BASIC THEORY OF SUPER-REGENERATION

Super-regeneration is best understood by studying the parallel resonant tank which forms the core of a resonant oscillator, as shown if Fig. 2. The resonant tank consist of an inductor *L*, a capacitor *C*, and a shunt conductance G_{-} - G_{-}. Here G_{-} represents the parasitic loss of the resonant circuit while -G_{-} represents the negative conductance provided by active devices. The active devices compensate for loss in the tank, and the overall conductance $G = G_{-} - G_{-}$ can be either positive or negative depending on the energy supplied by the active devices. An injected input signal is modelled by a sinusoidal current source $A\sin(wt)$.

Summing the currents in Fig. 2, we have

$$C\frac{dV}{dt} + GV + \frac{1}{L}\int V\,dt = A\sin(wt)\,. \tag{1}$$

Solving for *V*, the complete solution of the voltage across the tank can be written as

$$V = e^{-\propto t}\left(K_1 e^{jw_d t} + K_2 e^{-jw_d t}\right) + \frac{A\sin(wt - \theta)}{\sqrt{G^2 + (wC - 1/wL)^2}} \tag{2}$$

Where the damping factor, $\propto = G/2C$, is directly proportional to the conductance *G* and the damping frequency,

$$w_d = \sqrt{\left(\frac{1}{LC}\right) - \left(\frac{G}{2C}\right)^2} = \sqrt{(w_0^2 - \propto^2}$$

The first term in (2) is a transient oscillation at frequency w_d with the damping factor $\propto$, representing the free response, and does not depend on the injected signal. If G is positive, the active device does not provide enough energy to compensate for all the loss in the tank so that the free oscillation dies out and only for second term, which represents the forced response to the injected signal, remains. On the other hand, if G is negative, the active device provides more energy than is dissipated in the resonant circuit, building up a free oscillation from an initial voltage. This special case is termed *super-regeneration*.

In order to detect the injected signal, we first make the conductance G positive, letting the free oscillation die out, and then change the conductance G from positive to negative. Thus, the initial voltage, at the moment that the total conductance turns negative, is solely determined by the forced response (i.e., the second term of (2)), which is proportional to the strength of the injected signal. Since the free oscillation begins from an initial voltage and its amplitude tends to grow towards infinity, this is a very effective way to achieve amplification. Once a free oscillation starts, the oscillation amplitude tends to grow regardless of the injected signal, and therefore to amplify and detect any subsequent input samples, it is necessary to reset any oscillation by periodically alternating the total conductance from negative to positive. Since an LC tank always has a certain positive conductance due to loss (i.e.,G_+), we only have to control the negative conductance $-G_-$ to vary the sign and value of the overall conductance. The value of the negative conductance is controlled by the quench signal. The rate at which we alternate the total conductance is called the *quench frequency.*

From the above discussion, we can draw the following conclusions.

1) Amplification is achieved through the reinforcement of the free oscillation and this growth in oscillation amplitude requires time to build up. In order to achieve a larger gain, (represented by $e^{-\propto t}$ in (2)), we either have to spend more time operating in super-regeneration or increase by increasing the absolute value of the negative conductance.
2) The initial voltage of the free oscillation is proportional to the strength of the injected signal. Thus, it is straightforward to use super-regeneration to detect amplitude modulated (AM) signals.
3) The system does not continuously respond to the injected signal; it only responds as the conductance turns negative. Therefore, a super-regenerative receiver is a sampling system that samples the incoming RF signal with a sampling frequency equal to the quench frequency.

One major limitation of the super-regenerative technique is poor frequency selectivity, since an injected signal at any frequency might cause a free oscillation. However, since the free oscillation in super-regeneration starts with an amplitude determined by the forced response, which has a band-pass characteristic (second term in (2)), the system can inherently provide a band-pass frequency response. Without active devices, the quality factor of the resonant tank is

$$Q = \frac{1}{G_-}\frac{1}{\sqrt{L/C}} \qquad (3)$$

An on-chip LC tank normally has a quality factor of 10 or less and, therefore, offers poor frequency selectivity. However, we can significantly improve frequency selectivity through Q -enhancement. As shown in Fig. 3, Q -enhancement is achieved by using the negative conductance G_- to cancel some of the positive conductance G_+ , while keeping the overall conductance G positive. The resulting enhanced Q can be expressed as [6]

$$Q_{en} = \frac{1}{G_- - G_-}\frac{1}{\sqrt{L/C}} \qquad (4)$$

In summary, we first operate the circuit as a Q-enhanced band-pass filter to select the band of interest. Next, we increase the negative conductance to achieve super-regeneration and amplify the selected signal. The initial condition for super-regeneration is set at the moment when the overall conductance turns negative. Therefore, by periodically controlling the negative conductance, operating the circuit first in the Q-enhanced mode and then in the super-regenerative mode, we detect the signal sampled at the quench frequency.

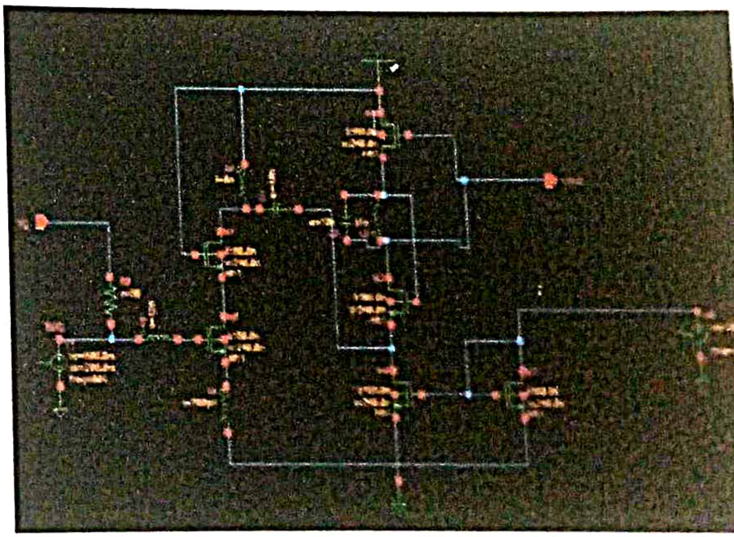

Fig. 1: Super-regenerative receiver block diagram and receiver circuit schematic [1].

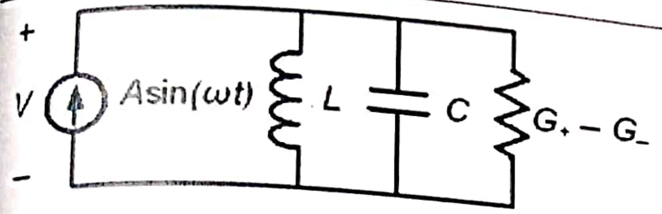

Fig. 2: Parallel resonant circuit representing an SRO [3]

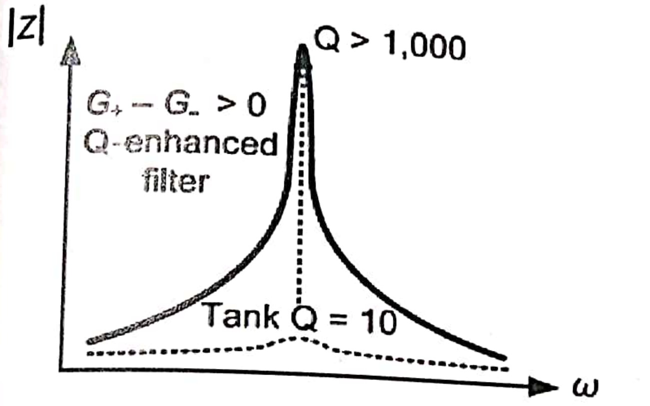

Fig. 3 Plot of impedance versus frequency with and without Q-enhancement [3].

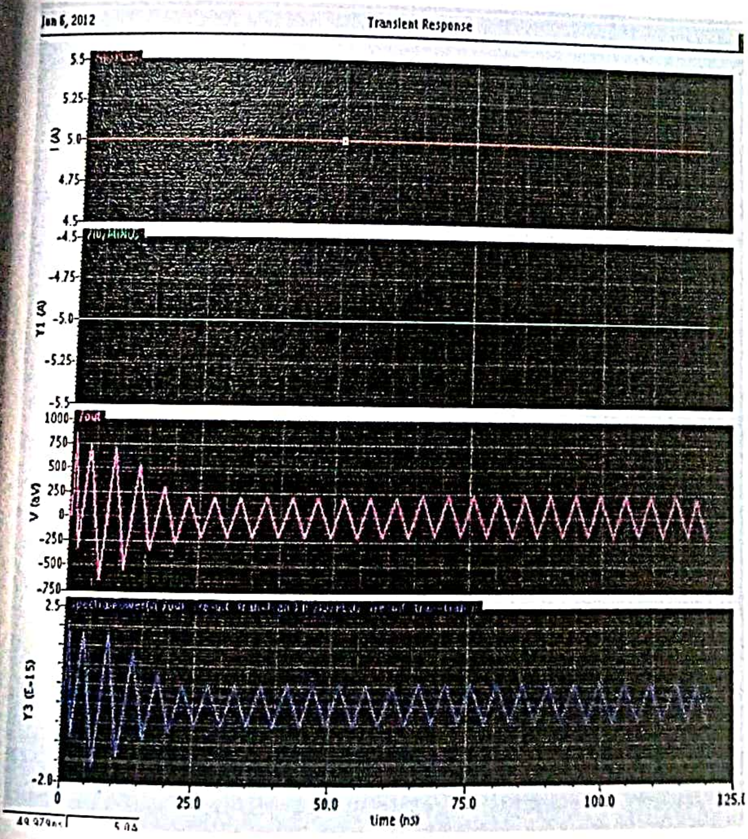

Fig. 4 Simulated Transient response and spectral power wave of SRO

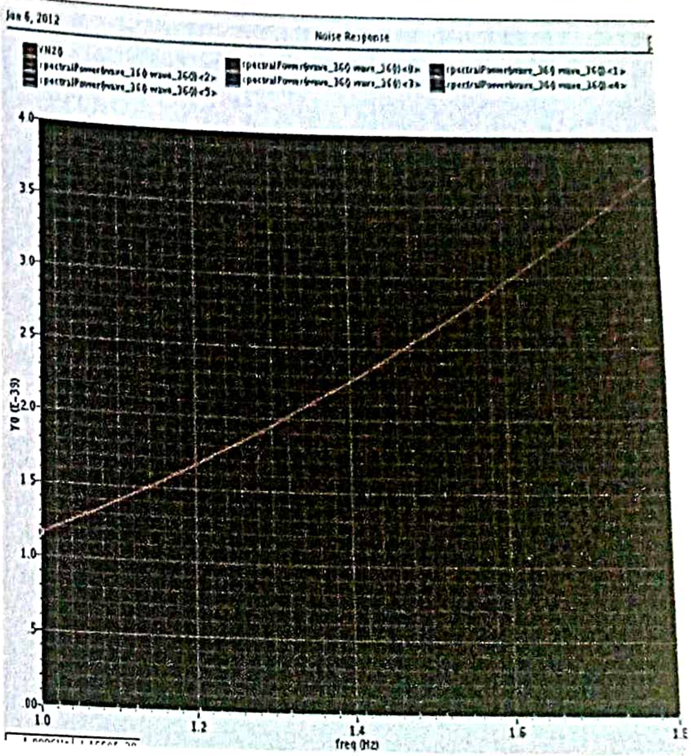

Fig. 5 Simulated Noise response of SRO

3. RECEIVER ARCHITECTURE

A. Super-regenerative Oscillator

The proposed SRO is based on the current-reuse differential LC oscillator which is first published in [5]. Figure 1 shows the circuit topology including an LC tank and two transistors M3 and M5. A 0.21 nH inductance and 9 fF capacitance are used in the tank and gate width of cross coupled pair are 180 μm and 240μm, respectively. Unlike the conventional VCO where the cross-coupled pairs switch alternatively, the transistors M3 and M5 switch on and off at the same time without common-source node. Therefore, this VCO is inherently immune to phase noise degradation causing by second harmonic terms. Moreover, the PMOS transistor M5 in the cross-connected pair helps to reduce the phase noise due to lower flicker noise and hot carrier effects [6]. Here, we used this topology and added a current source (consists of M4 an M2) which is modulated by the quench signal. The dc bias is 0.2 V while providing a 0.4 V peak-to-peak sinusoidal ac signal. Since threshold voltage of M2 is 405.5 mV, the tail current is directly modulated by the quench signals. The damping rate of the resonator is equal to the quench frequency. From the simulation results, the current source can be modulated up to 1 GHz. However, the describing 500 MHz data rate is a compromise between sensitivity and low current consumption.

B. Low Noise Amplifier

A cascode with source degenerated configuration is used in the LNA as shown in Figure 1. The LNA serves as a buffer between the antenna and oscillator. The input matching network is used to convert the impedance from antenna. In this case, we assumed a 50 ohms load at the input and the lumped elements L_g, L_s provide matching for optimum noise figure and impedance matching. Since the LNA is directly connected to oscillator, the output network (L_D and C_1) is a conjugate matching of the impedance looking into the oscillator. Moreover, the cascode configuration presents a high impedance to the oscillator preventing the load effect of the current source. Figure 6 shows the proposed test-bench of LNA,

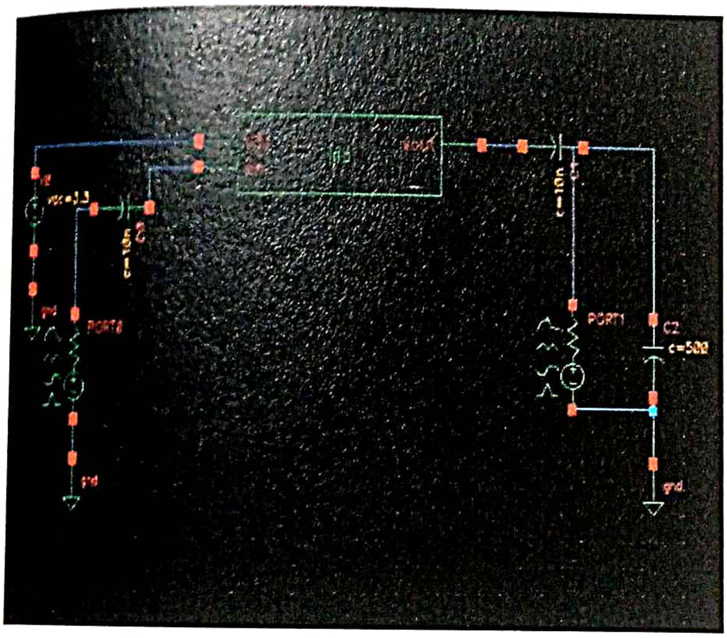

Fig. 6 Test-bench of LNA

It describe simulated parameter which are important in design and verification of LNA,s

Low-noise amplifier (LNA) is an electronic amplifier used to amplify possibly very weak signals (for example, captured by an antenna). It is usually located very close to the detection device to reduce losses in the feed-line. This active antenna arrangement is frequently used in microwave systems like GPS, because coaxial cable feed-line is very lossy at microwave frequencies, e.g. a loss of 10% coming from few meters of cable would cause a 10% degradation of the signal-to-noise ratio (SNR).

An LNA is a key component which is placed at the front-end of a radio receiver circuit. Per Friis' formula, the overall noise figure (NF) of the receiver's front-end is dominated by the first few stages (or even the first stage only).

Using an LNA, the effect of noise from subsequent stages of the receive chain is reduced by the gain of the LNA, while the noise of the LNA itself is injected directly into the received signal. Thus, it is necessary for an LNA to boost the desired signal power while adding as little noise and distortion as possible, so that the retrieval of this signal is possible in the later stages in the system. A good LNA has a low NF (like 1dB), a large enough gain (like 20dB) and should have large enough inter-modulation and compression point (IP3 and P1dB). Further criteria are operating bandwidth, gain flatness, stability and input and output voltage standing wave ratio (VSWR).

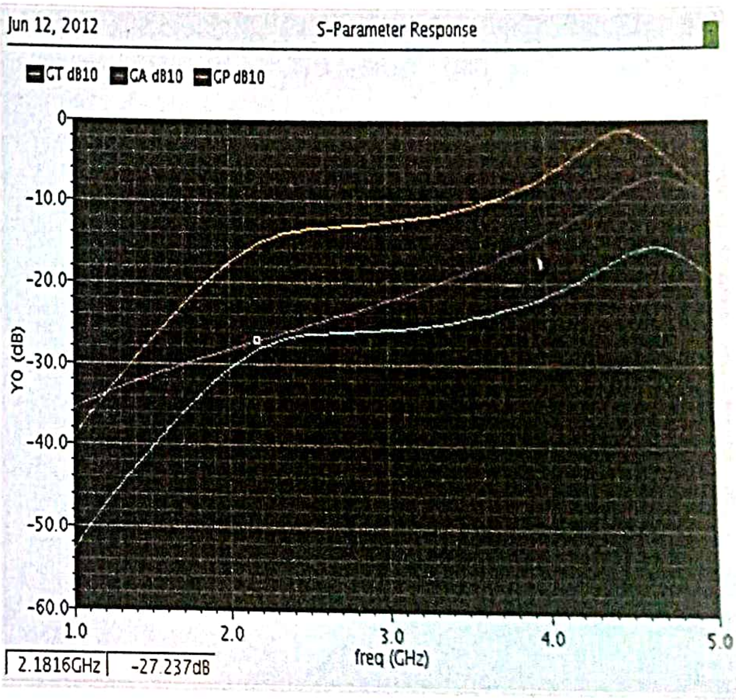

Fig. 7: Simulated LNA small-signal gain

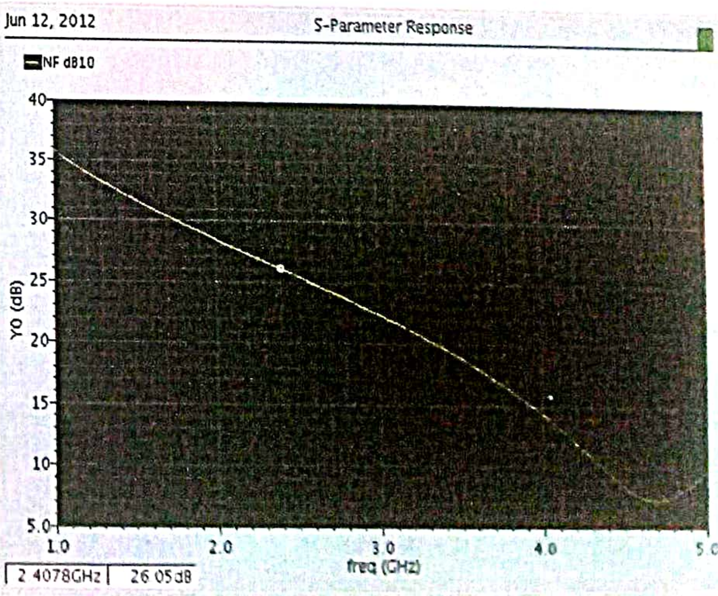

Fig. 8: LNA noise figure simulation result

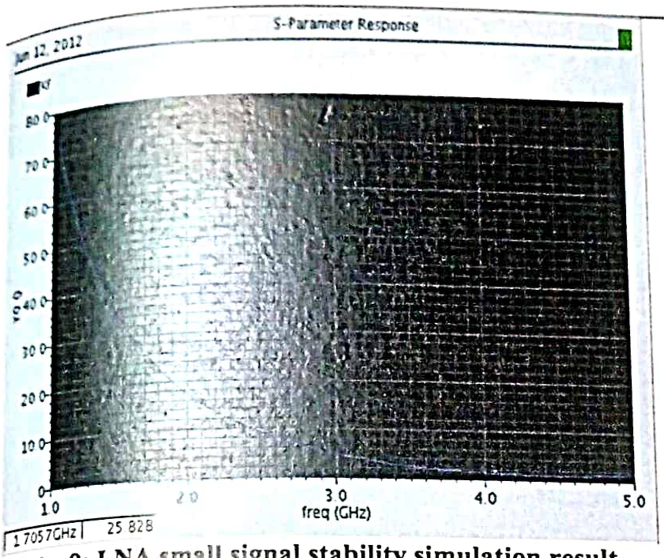

Fig. 9: LNA small signal stability simulation result.

Table I
Performance Comparison [1]

Reference	Technology (nm)	Frequency	DC Power (mW)
Tanomura [7]	CMOS 90	2.4 GHz	206
Sasaki [8]	CMOS 180	UBW	11
Zheng [9]	CMOS 180	UWB	137
Lee [10]	CMOS 90	UWB	35.8
This work	CMOS 180	60 GHz	2.194

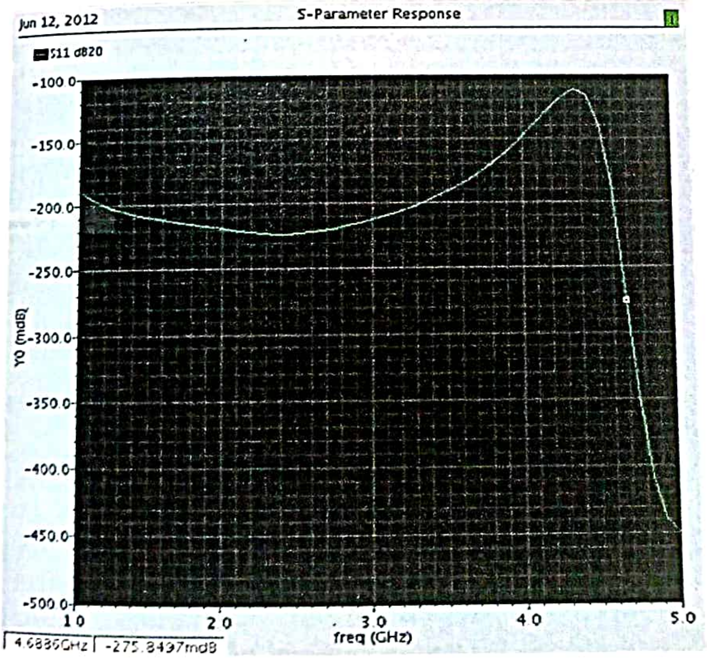

Fig. 10: LNA input port reflection coefficient simulation result.

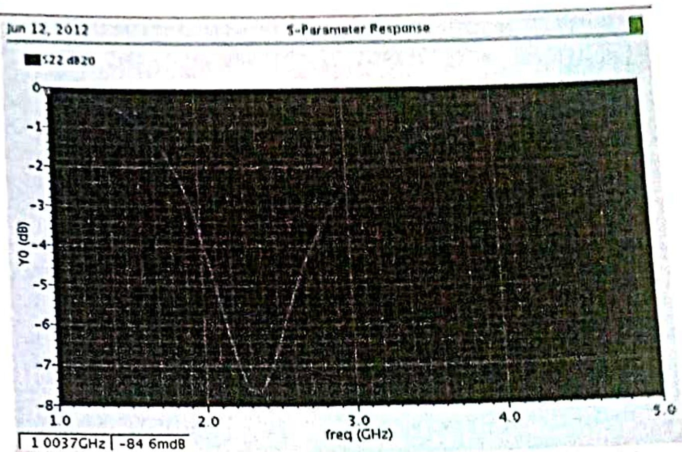

Fig. 11: LNA outport reflection coefficient simulation result

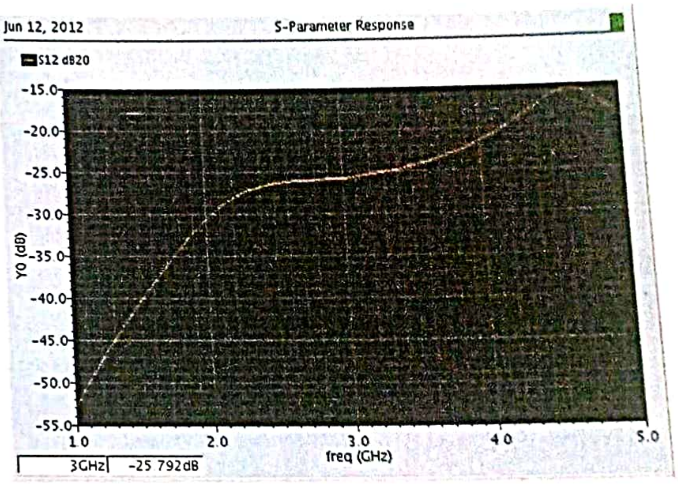

Fig. 12: LNA Reverse power gain simulation result

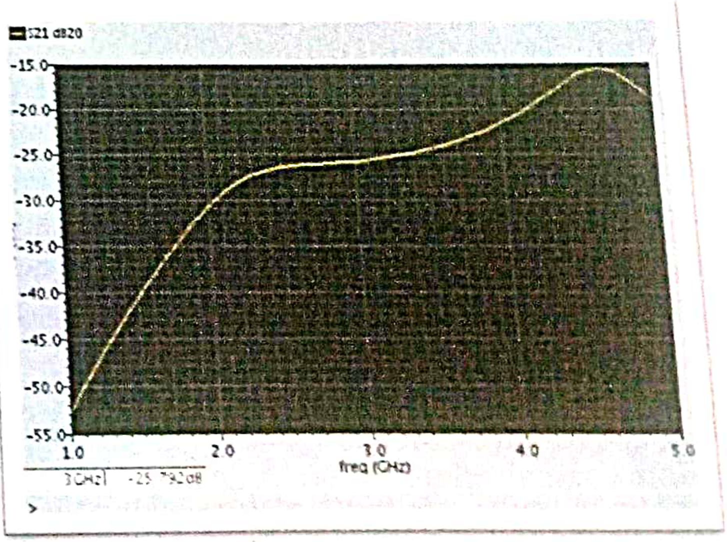

Fig. 13: LNA Forward power gain simulation result

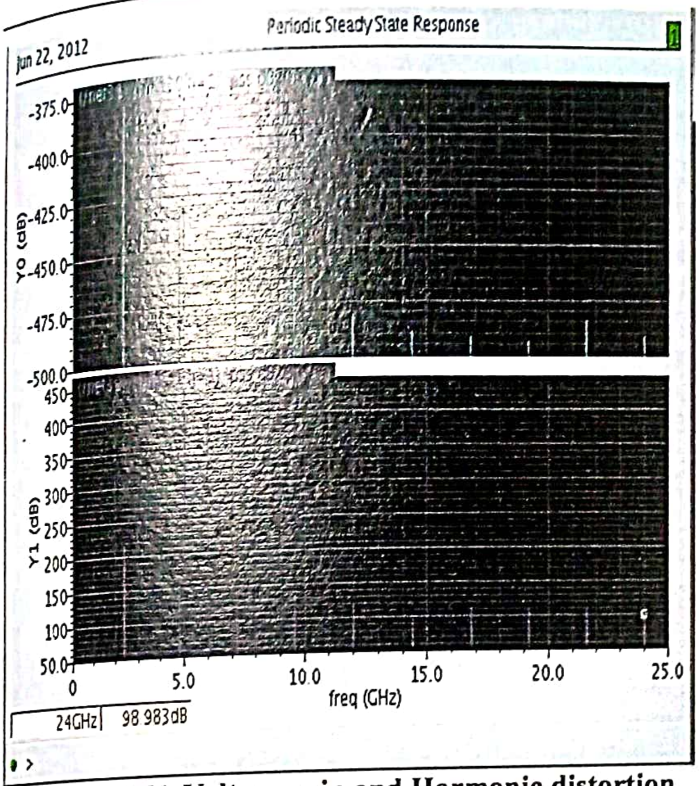

Fig. 14: LNA Voltage gain and Harmonic distortion simulation result

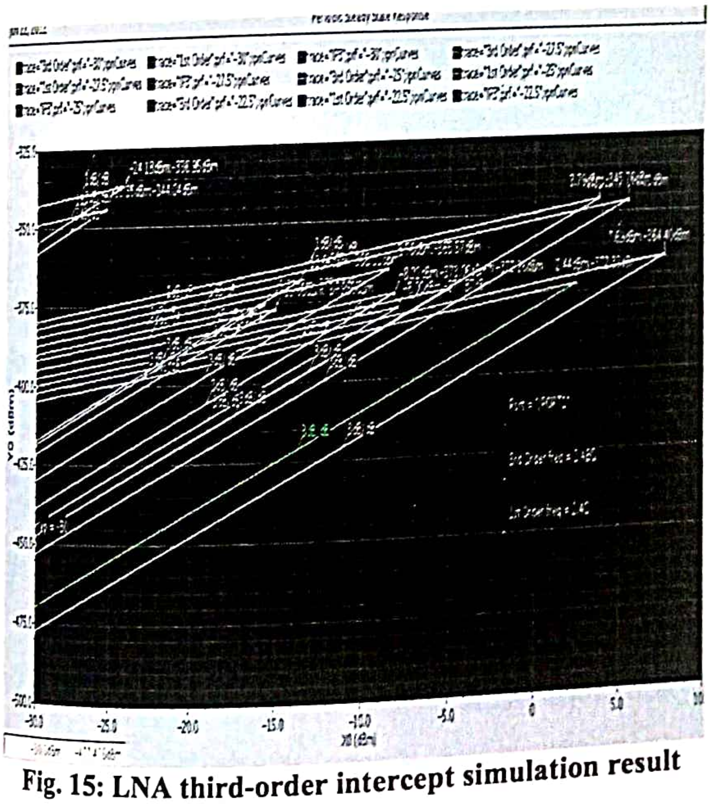

Fig. 15: LNA third-order intercept simulation result

Fig. 7 shows simulated LNA small-signal gain , there are three power gain are commonly used in LNA design. GT, Transducer power gain which is the ratio between the power delivered to the load and the power available from the source.

$$G_T = |S_{21}|^2 \tag{5}$$

Second one is operating power gain, Gp is the ratio between the power delivered to the load and the power input to the network.

$$G_P = \frac{1}{1-|S_{11}|^2}|S_{21}|^2 \tag{6}$$

And third one is available power gain, GA is the ratio between the power available from the network and the power from the source.

$$G_A = |S_{21}|^2\frac{1}{1-|S_{22}|^2} \tag{7}$$

Fig. 8 shows the LNA noise figure simulation result which is 7 dB at 4.7 GHz. Fig. 9 shows LNA small signal stability simulation result, Fig.10 and 11 shows LNA input and output port reflection coefficient simulation result respectively.

4. RECEIVER SIMULATION RESULTS

The simulated setup environment is according to the prototype receiver showing in Figure 1.

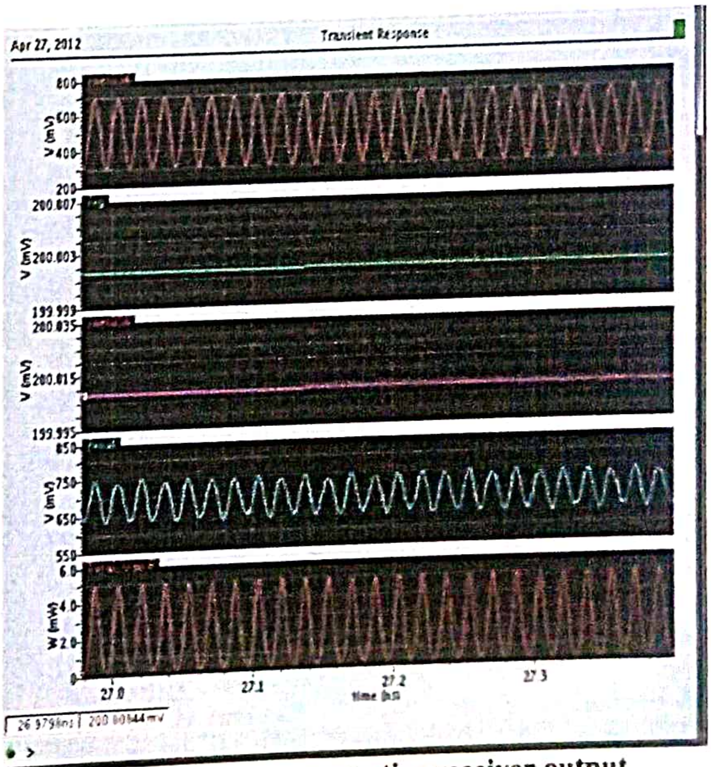

Fig. 16: Super-regenerative receiver output

Since the proposed receiver is an open loop architecture, the manual signal align is used for achieving higher data rate. Figure 15 illustrated the transient response of the super-regenerative receiver. The first waveform is a 12 MHz input signals with a 60 GHz carry frequency. The SOR was operated in a critical region as a detector. While SRO detects the sequent input signals then starts to damping. The second last is output waveform for baseband processor. After detecting from SRO, an ideal envelope detector is proposed to demodulate the data to the baseband.

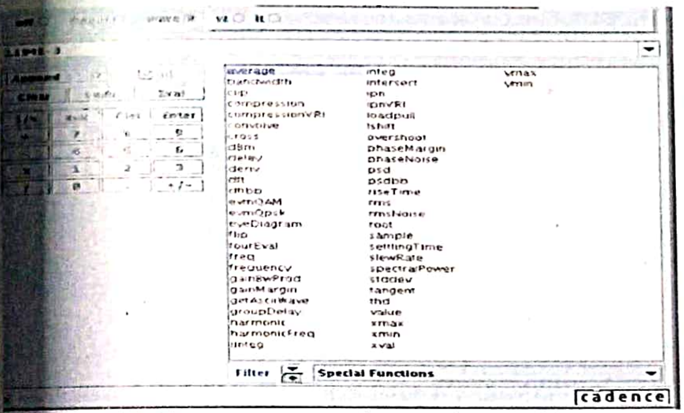

Fig. 17: Super-regenerative receiver DC Power simulation result

Figure 15 shows the DC Power of the super-regenerative receiver. Note that, in order to obtain a synchronous receiver providing the manual time delay (i.e 3.4 nano seconds) in simulation is need. However, the close loop receiver architecture is a general solution for achieving synchronous [3]- [4].The core of super-regenerative receiver is the SRO and SRO is a sensitive and a critical operation circuit. Therefore, the topology selection and operation knowledge of SRO are the key points in the super-regenerative receiver design. Table I summarizes the main features of the receiver [1].

5. CONCLSION

A high data rate low power CMOS super-regenerative receiver was proposed in this paper. The simple architecture was suitable for low-cost, low power and short-range wireless communication. In this work, we demonstrated a compatible low-power performance. The proposed receiver architecture can be operated at higher data rates in the simulation results. However, noise figure increases progressively 12 dBm due to the hangover limitations. The current design successfully simulated an unlicensed 60 GHz super-regenerative receiver with an excellent tradeoff between sensitivity, data rate and power consumption [1]. The receiver can be further realized in the future works.

6. REFERENCES

[1] Kunng-Hao Liang, Luis Chen, and C. Patrick Yue, " 200-Mb/s 10-mW Super-regenerative Receiver at 60 GHz," *IEEE 2009.*

[2] A. Vouilloz, M.Declercq, and C. Dehollain, "A Low-power CMOS Super-regenerative at 1GHz," *IEEE J. Solid State Circuits, vol.36, pp. 440-451, Mar., 2001.*

[3] J. Y. Chen, M. P. Flynn and J. P. Hayes, "A Fully Integrated Auto-Calibrated Super-Regenerative Receiver in 0.13-µm CMOS," *IEEE J. Solid State Circuits, vol. 42,* no. 9, pp. 1976-1985, Sep.,2007.

[4] F.X. Moncunill-Geniz, P. Pala-Schonwalder, C. Dehollain, N. Joehl, and M. Declercq, "An 11-Mb/s 2.1- mW Synchronous Superregenerative Receiver at 2.4 GHz," *IEEE Trans. Microwave Theory Tech,* vol.55, no.6, pp.1355-1362, June 2007.

[5] S. J. Yun, S. B. Shin, H. C. Choi and S. G. Lee, "A 1 mW Current-Reuse CMOS Differential LC-VCO with Low Phase Noise," *ISSCC Dig. Tech. Papers*, pp. 540-541, Feb. 2005.

[6] C. Hung and K.K.O, "Fully Integrated 5.35-GHz CMOS VCOs and Preselers," IEEE Trans. Microwave Theory Tech, vol. 49 no. 1, pp. 1355-1362, Jan. 2001.

[7] M. Tanomura, Y. Hamada, S. Kishimoto, M. Ito, N. Orihashi, K. Maruhashi and H. Shimawaki, "TX and RX Front-Ends for 60GHz Band in 90nm Standard Bulk CMOS," *ISSCC Dig. Tech. Papers*, pp.558-635, Feb. 2008.

[8] Sasaki, "A 12-mW 500-Mb/s 0.18-µm CMOS Pulsed UWB Transceiver Suitable for Sub-meter Short-range Wirelss Communication," in *Proc. IEEE Radio* Frequency Integrated Circuits (RFIC) Symp., June 2008.

[9] Yuanjin Zheng, King-Wah Wong, M. Annamalai Asaru, Dan Shen, Wen Hu Zhao, Yen Juthe, P. Andrew, Fujiang Lin, Wooi Gan Yeoh, and R. Singh, "A 0.18 µm CMOS Dual-Band UWB Transceiver," *ISSCC Dig. Tech. Papers*, pp.114-590, Feb. 2007.

[10] F.S. Lee, and A. P. Chandrakasan, "A 2.5nJ/b 0.65V 3-to-5 GHz Subbanded UWB Receiver in 90nm CMOS," *ISSCC Dig. Tech. Papers*, pp.116-590, Feb. 2007.

[11] S. Sarkar, and J. Laskar, "A Single-Chip 25pJ/bit Multi- Gigabit 60GHz Receiver Module," *Microwave Symposium, 2007. IEEE/MTT-S International*, pp.475-478, June 2007.

[12] D. C. Daly, and A. P. Chandrakasan, "An Energy-Efficient OOK Transceiver for Wireless Sensor Networks," *IEEE J. Solid State Circuits,*, vol.42, no.5, pp.1003-1011, May 2007.

[13] Jia-Yi Chen, M.P. Flynn, and J.P. Hayes, "A Fully Integrated Auto-Calibrated Super-Regenerative Receiver," *ISSCC Dig. Tech. Papers*, pp. 1490-1499, Feb. 2006.

[14] B. Otis, Y.H. Chee, and Y. Rabaey, "A 400 µW-RX, 1.6 mW-TX super-regenerative transceiver for wireless sensor networks," *ISSCC Dig. Tech. Papers*, pp.396-397, Feb. 2005.

[15] F.X. Moncunill-Geniz, P. Pala-Schonwalder, and O. Mas- Casals, "A generic approach to the theory of super-regenerative reception" IEEE Trans. Circuits Syst. I, *Reg. Papers*, vol.52, no.1, pp.54-70, Jan. 2005.

KIET IJCE

KIET International Journal of Communications & Electronics
Volume. No. 1, Issue No. 1, Jan - Feb 2013, ISSN: 2320 - 8996

Quantitatave Estimation of Symmetrical Radiation Beam with Suspended Rectangular Microstrip Antenna

J. K. Sah[1], S. Chatterjee[2], P. Bharati[3], A. Anand[4], S. K. Ghosh[5], S. Chattopadhyay[6], A. Ghosh[7]
[12,3,4,5,6]*Department of ECE, Siliguri Institute of Technology,*
P.O-Sukna, Darjeeling 734009, WB, India
piyalirekha@yahoo.com
[7]*Department of ECE, Mizoram University, Aizawl- 796004, Mizoram, India*

Abstract: *A novel suspended rectangular microstrip antenna for symmetrical radiation beam performance is theoretically investigated. The conventional patch antenna on common substrates always produces broader E plane pattern compared to its H plane. In the present investigation, the same microstrip antenna is suspended over its ground plane and may be thought of as it is on air substrate, which shows an excellent radiation pattern with symmetrical 3 dB beam widths at its both E and H plane. The present antenna has been compared with the conventional structure and is presented in the paper. The complete quantitative analysis to explore such radiation beam characteristics for the proposed structure is also presented in this paper. The proposed idea has been verified through a commercial software package for X band.*

Keywords: *Conventional Antenna, Suspended Rectangular Microstrip Antenna, Symmetrical Beam widths.*

1. INTRODUCTION

The rectangular microstrip antenna is the most common and popular antenna for its well known striking features, such as low profile, light weight, and compatibility with monolithic microwave integrated circuits and thus it finds growing number of new applications day by day [1]. This microstrip antenna is etched on conventional substrates with dielectric constant ε_r = 2.2 to 10.2 [2]. But that microstrip antenna is suspended over ground plane is a least investigated configuration in any open literature, though it shows some interesting features particularly in its radiation characteristics. Rectangular microstrip normally radiates linearly polarized wave with about 4-5 dBi gain. These patches radiate along the broadside direction with broader E-plane pattern than H-plane [1]. As the microstrip antenna is inherently a low gain antenna, larger gain is always a positive requirement and can be achieved by increasing its width-to-length ratio as is reported in [3]. But, as soon as the conventional substrate is replaced by air, *i.e* the antenna becomes a suspended rectangular patch, gain of the antenna increases satisfactorily. Some researchers had employed different configurations like, wedge-shaped air dielectric [4] or air cavities within the substrate [5] for different applications. Improved gain for microstrip antenna is always desirable but along with this symmetrical or uniform radiation beam pattern in both the E and H plane is also requisite to cover a wide area, particularly for wireless communications.

This can be achieved using the proposed suspended rectangular microstrip antenna and is presented in comparison with the conventional structure. One very recently reported article [6] shows an antenna fabricated on dielectric strips with appreciable gain and symmetrical beam pattern. But still it suffers from complex manufacturing process and there is no quantitative guide lines reported in [6] in support of their results. But here, the feature of high gain and symmetrical beam radiation is obtained from simpler structure and hence this proposed antenna do not suffers from the disadvantage of complex manufacturing process. A concrete quantitative analysis is presented to explain such behavior of the antenna. An easy and handful relationship between the length of patch antenna and its fringing length for the proposed antenna is established following the aperture antenna concept as reported in [7]. The theory is successfully utilized to evaluate the causes for uniform 3 dB beam widths which is verified using [8] and close agreement is revealed.

2. ANTENNA STRUCTURE

A rectangular microstrip antenna with length L= 11.8 mm and width W= 17.56 mm is shown in Fig. 1 (top-view of the patch and side view of whole antenna structure). A dielectric substrate of thickness h =1.58 mm of relative permittivity of ε_r = 2.33 is sandwiched between the patch and ground plane to develop the conventional patch antenna. On the other hand, the copper plate (patch) of same dimension is simply suspended over the ground plane keeping the finite gap of h =1.575 mm between ground plane and the copper plate (patch) for our proposed structure. For both the cases, the dimensions of ground plane are kept 1.6 λ_0 X 1.6 λ_0.

3. RESULTS AND DISCUSSIONS

Simulated results obtained using [8] for suspended rectangular microstrip antenna and the same with conventional substrate operating around X band is presented.

Fig. 2 shows the complete return loss profile of the proposed antenna which shows that the proper excitation has been achieved by accurately choosing the feed point. The proposed antenna resonates at 10.2 GHz with an impedance bandwidth of nearly 6%.

The next step is to examine the radiation pattern for two identical antennas; one with conventional PTFE substrate and the other with suspended rectangular microstrip antenna. Hence, the radiation patterns are compared between the antennas separately at E and H plane as shown in Fig. 3.

It is revealed that, 3dB beam width in E plane is quite broader than H plane beam width for conventional antenna while, those for proposed antenna show no changes in beam widths between its E and H planes. Commonly available literature shows that the beam width of any antenna in a particular plane typically depends on its dimension at that plane. In fact, the air below the patch modifies the fringing lengths and widths in such a way that the effective length and width acquire particular values such that beam widths remain same in each plane. The case is different when the region below the patch is filled up with conventional dielectric material which results unequal beam widths in different planes. It may also be noted that along with the symmetrical radiation beam, the gain of this present antenna is greater than conventional structure as also evident from Fig. 3. This may be due to the loosely bound electric fields below the patch, which contributes for the radiation fields for the present antenna. This is expected because the dielectric constant of the material below the patch is smaller *i.e* 1 compared to that (2.33) at conventional patch. The total results are summarized in Table-I.

TABLE I: Gain and Beam width of Rectangular Microstrip Antennas (conventional and proposed one)
Parameters as in Fig. 2

Antenna configuration	Peak Gain (dBi)	3 dB Beam width (degree)	
		E Plane	*H Plane*
Conventional antenna	6.0	77	40
Proposed antenna	8.2	56	56

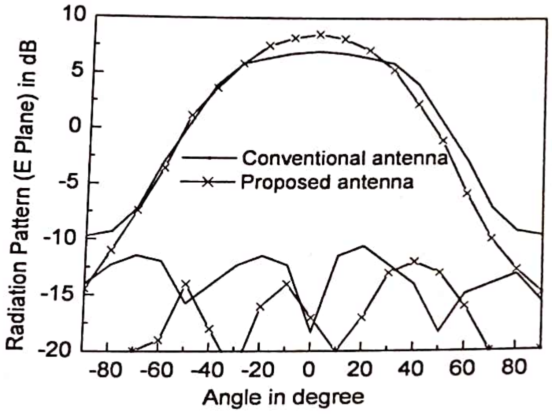

Fig. 2. Return loss characteristics of a suspended rectangular patch antenna. $L = 11.8$ mm, $W = 17.56$ mm, $h = 1.58$ mm, $\rho = 2.6$ mm; Substrate: uniform air: $\varepsilon_r = 1$.

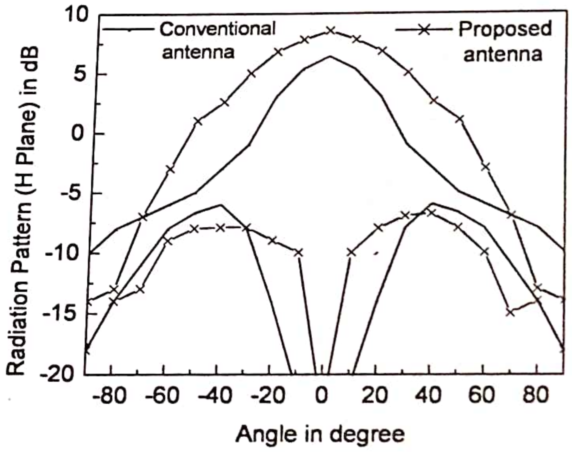

Fig 3. Radiation pattern of present antenna operating at 10.35 GHz compared with a conventional antenna using a PTFE (ε_r=2.33) substrate operating at 7.9 GHz.

4. QUANTITATIVE ANALYSIS

Any rectangular patch antenna radiates along its broadside direction and its field patterns at both E and H planes are given by [3]. This is equally valid for our proposed antenna as this suspended rectangular microstrip antenna may be thought of as it is on air substrate. Now if we follow the concept developed in [7] by one of the present authors, where the radiation from the patch has been considered as the radiation from rectangular aperture then following [10],[11] we may write the 3 dB E plane and H plane beam widths as

$$\theta_E = \frac{51^0}{{L+2\Delta L}/{\lambda}} \tag{1}$$

and

$$\theta_H = \frac{67^0}{{W+2\Delta W}/{\lambda}} \tag{2}$$

Now for beam widths to be equal in both the planes,

$$\theta_E = \theta_H \tag{3}$$

$$\frac{51^0}{{L+2\Delta L}/{\lambda}} = \frac{67^0}{{W+2\Delta W}/{\lambda}} \tag{4}$$

Thus,

$$\frac{{W+2\Delta W}/{\lambda}}{{L+2\Delta L}/{\lambda}} = \frac{67^0}{51^0} = 1.31 \tag{5}$$

$$\Rightarrow W + 2\Delta W = 1.31L + 2.62\Delta L \tag{6}$$

Again for most commonly used aspect ratio W/L=1.5; following [9] we may write,

$$\Delta W = \Delta L\left(1.5 - {W}/{2L}\right) = 0.75\Delta L \tag{7}$$

Thus equation (6) may be rewritten as

$$1.5L + 1.5\Delta L = 1.31L + 2.62\Delta L \tag{8}$$

Hence

$$L \cong 5.9\Delta L \tag{9}$$

Following the design guidelines [8]; the fringing lengths and widths (ΔL and ΔW), have been calculated and it is seen that, fringing length ΔL for the present antenna is 1.99 mm, where as that for antenna with conventional substrate is only 1.27 mm. Again if we keep our eyes on the length of the antenna it is 11.8 mm, which confirms that equation (9) is satisfied and this result in fact creates a theoretical background for such symmetrical 3 dB beam width characteristics for proposed suspended rectangular microstrip antenna.

5. CONCLUSIONS

A simple suspended rectangular microstrip antenna has been proposed for symmetrical 3 dB beam width characteristics and the proposed idea has been verified thoroughly using quantitative analysis in the perspective of half power beam widths of rectangular aperture antenna. A simple handful relationship between the length of patch antenna and its fringing length is established. The proposed antenna is very helpful for the researchers and in search of such low profile antenna with symmetrical beam radiation pattern.

6. REFERENCES

[1] R.Garg, P.Bhartia, I.Bahl, and A. Ittipiboon, Microstrip Antenna Design Handbook, Artech House, Norwood, USA, 2001.

[2] M. T. Islam, M. N. Shakib, N. Misran, T. S. Sun, “Broadband microstrip patch antenna,” *European Journal of Scientific Research*, Vol. 27, pp.174-180, 2009.

[3] S.M. Danish Abbas, S. Paul, J. Sen, P. R. Gupta, K. Malakar, S. Chattopadhyay, S. Banerjee, “Aspect Ratio: A Major Controlling Factor of Radiation Characteristics of Microstrip Antenna,” *Journal of Electromagnetic Analysis and Applications*, Vol. 3, No. 11, pp. 452-457, 2011.

[4] F. W. Yao, S. S. Zhong, and X. L. Liang, “Ultra-broadband patch antenna using a wedge-shaped air substrate,” *Proc. Asia-Pacific Microwave Conference*, Vol.4, 2005.

[5] K. Malakar, J. Nandi, S. Mitra, P. K. Gorai, S. Chattopadhyay, S. Banerjee, “Rectangular Microstrip Antenna with Air Cavity for High Gain and Improved Front to Back Ratio,” *Journal of Electromagnetic Analysis and Applications*, Vol. 3, No. 9, pp. 368-372, 2011.

[6] K. Malakar, S.M. Danish Abbas, S. Chattopadhyay, “Suspended Plate Antenna with Dielectric Strips for Improved Gain Symmetrical 3-D Beam Width,” *International Journal of Electronics Engineering*, Vol. 3, No. 1, pp. 17-19, 2011.

[7] D. Guha, S. Chattopadhyay and J. Y. Siddiqui, “Estimation of gain enhancement replacing PTFE by air substrate in a microstrip patch antenna,” *IEEE Antennas and Propagation Magazine*, vol. 52, no.3, pp. 92-95, 2010.

[8] High Frequency Structure Simulator, HFSS *v10*, Ansoft Corp.

[9] S. Chattopadhyay, M. Biswas, J. Y. Siddiqui, and D. Guha, “Rectangular microstrip with variable air gap and varying aspect Ratio: Improved formulations and experiments,” *Microwave Opt. Technol. Lett.*, Vol. 51, pp. 169-173, 2009.

[10] C.A. Balanis, Antenna Theory: Analysis and Design, 2nd Ed., John Wiley & Sons, Inc., 2001.

[11] J. D. Kraus, R. J. Marhefka, Antennas: for all Applications, 3rd Ed., Mc. Graw Hill, 2003.

KIET IJCE
KIET International Journal of Communications & Electronics
Volume. No. 1, Issue No. 1, Jan - Feb 2013, ISSN: 2320 - 8996.

Advance Process Control of Binary Distillation Column

Madhu Pandey[1], **Vijendra Singh**[2]
[1,2]*ICE Division, Netaji Subhas Institute of Technology, New Delhi, India-110078*

Abstract: *Distillation columns are important unit operations in chemical process plants. This paper reviews advance control techniques of modeling and simulation of distillation columns. The aim of this paper is the advance control design of the distillation column for separation of binary mixture. Advance control strategy is effective for systems that have large time constants and disturbances and advance control strategy is fit for a system that lacks an accurate model. It aims at providing simple recommendations to assist the engineer in designing control systems for distillation columns. The standard LV-configuration for level control combined with a fast temperature loop is recommended for most columns. The response to change in feed composition has larger gain than the response to change in feed flow rate. The paper also compares the simulation results with some of other works.*

Keywords: *Binary Distillation Column, Fundamental Modeling, Simulation.*

1. INTRODUCTION

A Distributed Control System (DCS) is an enabling technology that provides a platform for further improvement to realize greater benefits from the Unit. It also serves to facilitate further process and operational improvement that is otherwise limited by the nonavailability of technology that is mature and easy to use.

With Advanced Process Control, the DCS is able to push the process to a higher level of productivity, and is able to deliver bottom line improvement. Currently gaining popularity in the process industry is Multi-Variable Model Predictive Control Technology. Experts unanimously agree that APC is able to deliver sustainable measurable benefits simply by stabilizing the plant to yield consistent quality products. The logic for this is that control strategies should be developed with an understanding of the process and its nuances; the control system on which the APC would sit; the need for integration with wider plant objectives, as well as a knowledge of base layer control loops. It is also important to consistently translate economic objectives into operating objectives. APC allows for companies to operate its facilities with greater safety, cost effectiveness, reliability, and compliance with environmental factors. When jointly used with other unit-operation optimization technologies, APC can prove to be extremely beneficial. Optimization is not a one-time event, it has to be a continuous effort to enhance operating performance in ever-changing conditions. The attraction of adopting a model based approach to controller development is illustrated in the block diagram shown in Figure 1.

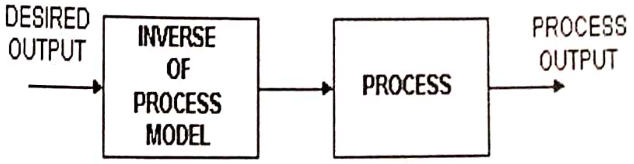

Fig. 1: Ideal Model Based Control

By implementing advanced control, benefits ranging from 2% to 6% of operating costs have been quoted [Anderson, 1992].These benefits are clearly enormous and are achieved by reducing process variability, hence allowing plants to be operated to their designed capacity. Advanced control comes into play from the level of basic control through that of process optimization. Instead of having the operators manually adjust control units for specific variables, advanced systems provide generalized models that automate regulatory and constraint control as well as process optimization. In regulatory control single loop feedback improvements such as feed forward, cascade control can be used to supplement PID algorithms. Time delay compensation techniques can also be applied to compensate for long delays permitting tighter control. At the level of constraint control, multivariable techniques can be used.

Advanced control technology is therefore a combination of:

- Advanced hardware (on line sensors, pneumatic or electronic analog with digital systems, computer hardware and digital control units)
- Advanced control algorithms at the regulatory, constrained and optimization levels.

In order to control a distillation column, the first step is to develop a model of the column. By modeling we can understand the behaviour of the column, predict future reaction and therefore devise a control structure for the column. This paper reviews some important techniques in distillation column modeling and then describes a model for a lab-scale binary continuous distillation column.

The paper is organized as follows. A review of advance process control in part I, modeling of continuous distillations is presented in part II, the modeling of our distillation column is detailed in part III, the simulation results are shown in part IV, and the conclusion and future work are presented in part V of this paper.

2. THE DISTILLATION COLUMN

Distillation column is considered one of the most important unit operations in chemical engineering, and also the most studied unit operations in terms of control. A distillation column is used to separate a mixture into its components by the application and removal of heat. It consumes a huge amount of energy in both heating and cooling operations. There are many types of distillation columns based on different classifications such as: batch, continuous, binary, multiproduct, tray, packed. In this paper we focus on continuous binary distillation columns since continuous columns are dominant in industry and binary columns are usually referred to as a foundation by the researchers when they examine other types of distillation columns.

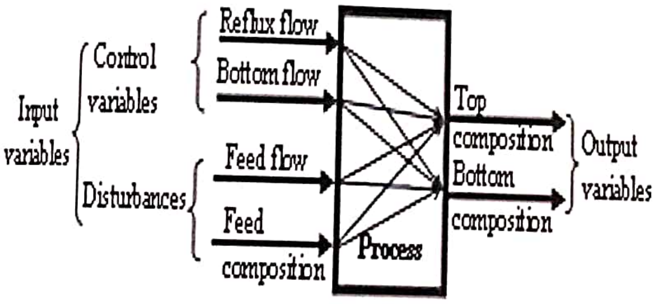

Fig. 2. Distillation process input and output variables.

A simple two-product continuous distillation column is shown in Fig .3 .The column has N stages on which the vapour-liquid equilibriums occur. The feed enters the column on the stage N_F. This stage divides the column into a rectifying section and a stripping section. Near the bottom of the column is a reboiler which provides energy to the column. The mixture is heated to form a flow of vapour rising up inside the column. In the stripping section, the less volatile component is enriched while in the rectifying section the more volatile component is enriched. The top product is condensed by the condenser from which there is a reflux flow back to the top of the column to enhance the purity of the product.

The difficulties in controlling distillation columns lie in their highly nonlinear characteristics; their multiple inputs multiple outputs (MIMO) structure and the presence of severe disturbances during operation. The nonlinearity of distillation columns is well known. It has been shown that the purer the products get, the more nonlinear the system becomes. A distillation column is also a typical example for an MIMO system in which there are strong interactions between the variables. The interactions occurring between the inputs and the outputs are difficult to identify. The disturbances to a distillation column can come from many sources. They can come from the feed (feed flow rate, feed composition), from the pressure inside the column, from the cooling water etc. These difficulties pose numerous challenging control problems and also attract a large number of researchers from different disciplines.

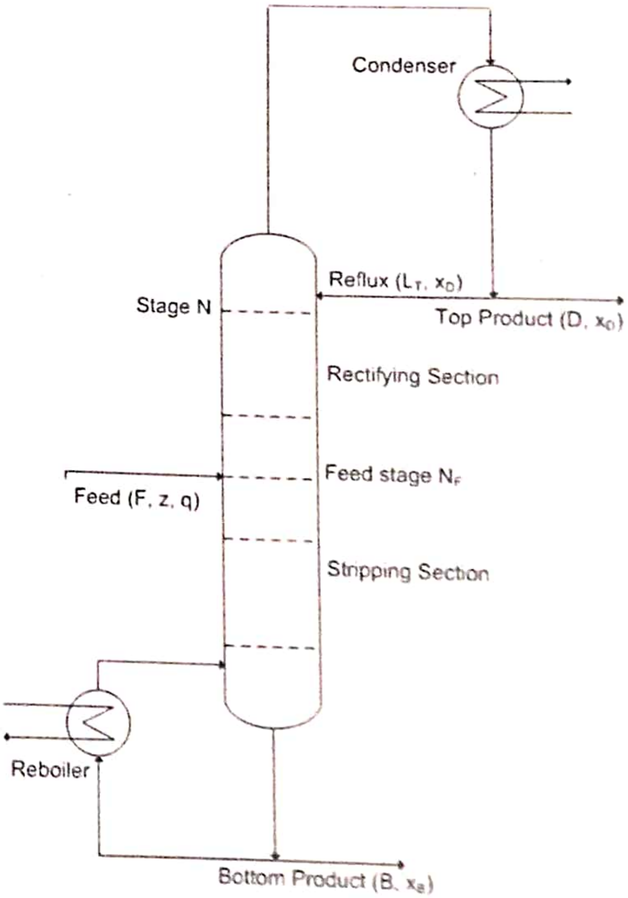

Fig. 3: A Two-product Distillation Column

3. MODELING OF CONTINUOUS DISTILLATION COLUMNS

Modeling of distillation columns is often classified into three groups: fundamental modeling, empirical modeling and hybrid modeling. In fundamental modeling, the model is constructed based on the physical properties of the system, such as the preservation of mass, energy and momentum. And depending on the levels of accuracy of the assumptions we will have different models ranging from simple to rigorous models. This method of modeling has the advantage of global validity, accuracy and it gives more complete process understanding. However, this method is quite complex for controller design with huge amount of computation and simplifications are often needed. The empirical modeling (sometimes called the black-box modeling) utilizes the input and output data from the operation of the column to build the relationship between the input and the output. With this method we do not need to understand the inner dynamics of the column, and the computation can be reduced. But in using this method we have to carry out experiments on the real column, and the results may not be applied for other column, even the results from one column can be different if the column's conditions are different between the experiment and the actual operation of the column. The hybrid modeling (or the 'grey-box' model) combines the fundamental modeling and the empirical modeling. This method utilizes the advantages of the other two, but in order to do that we need a well-structured model in which we have to decide which part of the model to use fundamental technique and which part to use empirical data. In our project we will focus mainly on the fundamental modeling, even though the empirical model is dominantly used in the industry. The reason is that we want to understand the dynamics of the distillation columns, and since the black-box model "may not be used to predict the behaviour of the system at other operating conditions".

The paper summarized the simplifications of the rigorous model since no references had been found on solving all the equations of the rigorous model. The simplifications are aimed to the vapour dynamics, to the energy balance and to the liquid flow dynamics. The paper recommends not neglecting liquid dynamics (i.e. not assuming constant liquid holdups) due to the fact that the initial response, an important factor in feedback control, is largely affected by the liquid holdups.

Abdulla *et al.* have done a quite complete review on the recent nonlinear modeling applications in continuous distillation column. The summary states that the empirical modeling has been preferred in industry because of its simplicity compared to the fundamental model; and the current development focuses on hybrid models, which can exploit the advantages of both fundamental model and empirical model; and that the neural network method is used the most to combine with the fundamental model in empirical modeling.In the case of fundamental modeling, the model is often simulated to understand the column's dynamic behaviour. The development of distillation column's simulation has been going along with the growth of computing capacity. As of 1930s and 1940s only graphical methods and simple short-cut models were used to get insights of the steady-state behaviour of the distillation columns. The fast-growing of computing power has allowed the use of more complex and rigorous models. Computer programming and the numerical methods to solve the differential equations play an important role.

4. MODELING OF THE APC

The APC (Advanced Process Control) column is a pilot distillation column that has 15 trays and equipped with a DCS control system. The feed is positioned at tray 7. The model is developed based on a model. In the model the following assumptions are made:

1. Binary mixture, the feed contains only two components
2. The pressure inside the column is fixed by controlling the cooling water
3. Constant relative volatility, $\alpha = 1.5$
4. Constant molar flows
5. No vapour holdup, the vapour holdup on each tray is negligible
6. Linear liquid dynamics
7. Equilibrium on all stages
8. Total condenser, there is no vapour holdup in the condenser

The total material balance equation on stage *i* is:

$$\frac{d}{dt} M_i = L_{i+1} - L_i + V_{i-1} - V_i \tag{1}$$

where M_i is the liquid holdup on tray i, L_i and V_i are the liquid flow rate and vapor flow rate that come towards tray i.

The material balance for the light component on tray *i* is:

$$\frac{d}{dt}(M_i x_i) = L_{i+1}x_{i+1} - L_i x_i + V_{i-1} y_{i-1} - V_i y_i \tag{2}$$

where x_i and y_i is the composition of the light component and heavy component on tray *i* respectively.

At the feed stage (*NF*=7) we have:

$$\frac{d}{dt} M_{NF} = L_{NF+1} - L_{NF} + V_{NF-1} - V_{NF} + F \tag{3}$$

and

$$\frac{d}{dt}(M_{NF} x_{NF}) = L_{NF+1} x_{NF+1} - L_{NF} x_{NF} + V_{NF-1} y_{NF} - (4)$$

$- {}^{y}NF\, {}^{y}NF - 1 \; {}^{+\,Fz}F$

in which F is the feed flow rate and z_F is the concentration of the light component in the feed.

The reboiler is also an equilibrium stage with i=1:

$$\frac{d}{dx} M_1 = L_2 - V_1 - B \tag{5}$$

$$\frac{d}{dx} M_1 x_1 = L_2 x_2 - V_1 y_1 - B x_1 \tag{6}$$

At the condenser we have $i = NT = 16$ and

$$\frac{d}{dx} M_{NT} = V_{NT-1} - L_{NT} - D \tag{7}$$

$\frac{d}{dx} M_{NT} x_{NT} = V_{NT-1} y_{NT-1} - L_{NT} x_{NT} - D x_{NT}$ (8) Where B is the bottom product flow rate and D is the distillate product flow rate. The composition of the heavy component is related to the composition of the light component via the relative volatility formula:

$$y_i = \frac{\alpha x_i}{1+(\alpha-1)x_i} \tag{9}$$

The liquid flow dynamics is considered due to its important effect on the initial response of the column. The formulas for the liquid holdup are:

$$L_i = L_{ob} + \frac{M_i - M_{0i}}{\tau} + (V_{i-1} - V_0)\lambda \tag{10}$$

$$L_i = L_o + \frac{M_i - M_{0i}}{\tau} + (V_{i-1} - V_{ot})\lambda \tag{11}$$

For i from NF+1 to NT-1.
where L_0 is the nominal reflux flow and M_{0i} is the nominal reboiler holdup (kmol) on stage i. These values are achieved after we do steady state simulation (see Table 1). τ is the time constant for liquid dynamics, in this model it is chosen to be 0.063 (min), and λ represents the effect of vapor flow on liquid flow. In the simulation we ignore this effect by setting $\lambda = 0$. L_{0b} is the nominal liquid flow below feed, given by the formula:

$$L_{ob} = L_o + q_{FO} F_o \tag{12}$$

in which F_0 = 1(kmol/min) is the nominal feed rate, q_{F0} = 1 is the nominal fraction of liquid in the feed.

5. SIMULATION RESULTS AND DISCUSSION

Because the distillation process is a nonlinear one it is wise to use a model based control structure, which can take account of the process nonlinearities by changing the process model according to the operating point. The process is a nonlinear one, but represented as a reunion of linear models one for each channel and operating point. At each simulation initialization step the bottom and top composition, the feed flow and composition are sent from the process to the control structure, in MATLAB. Here, using these data the model parameters (time constants and gain) are determined and loaded in controller. Using these model parameters, the two controlled variables (reflux flow and bottom product flow) are computed and sent at each sampling instant to the process.

The dynamic system behaviour analysis consisted of modifying the compositions set point, the disturbances and the controllers tuning parameters. (figures 4 to 7)

For top composition advance controller has the following default simulation parameters:

- prediction horizon – is variable, and it is calculated using the process model time constant T1.
- control variable time horizon – 30 sampling times;
- output weight (minimum value: 0, maximum value: 1);
- control variable weight – 0.2 (minimum value: 0, maximum value: 1).

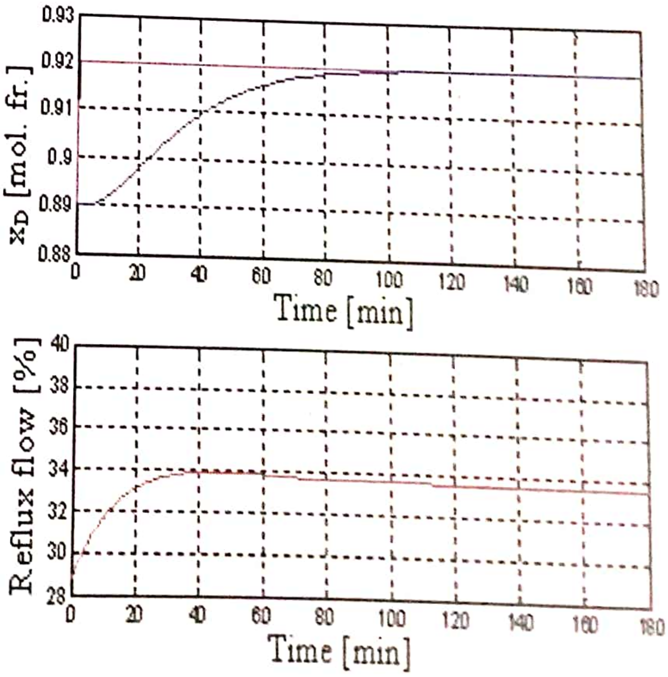

Fig. 4: Top composition trend when the controller setpoint increases from 0.89 mol. fr. to 0.92 mol. fr.

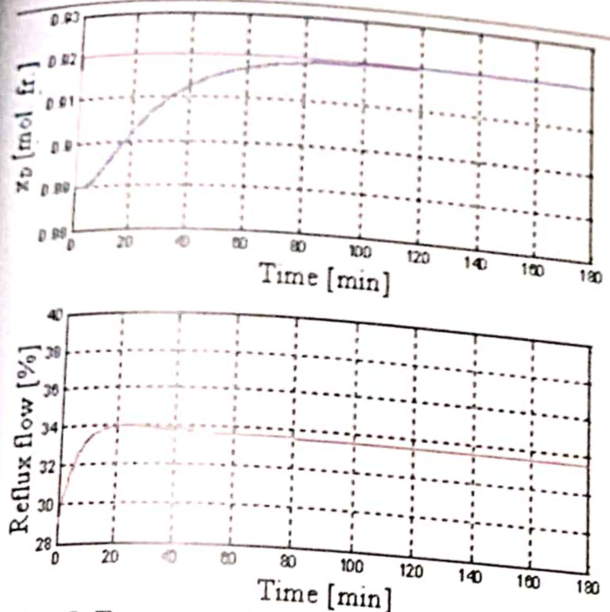

Fig.5: Top composition trend when the controller setpoint increases from 0.89 mol. fr. to 0.92, control variable time horizon is 25.

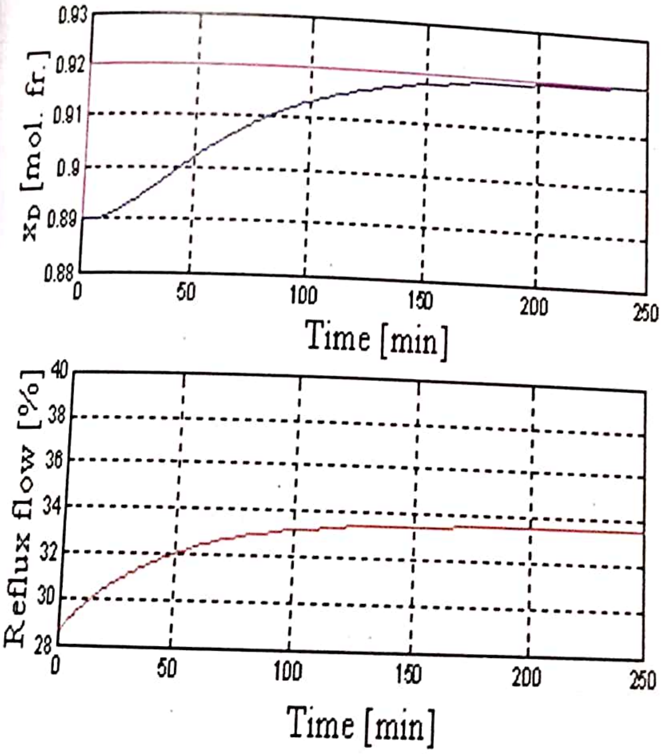

Fig.6: Top composition trend when the controller setpoint increases from 0.89 mol. fr. to 0.92, control variable weight is 0.7.

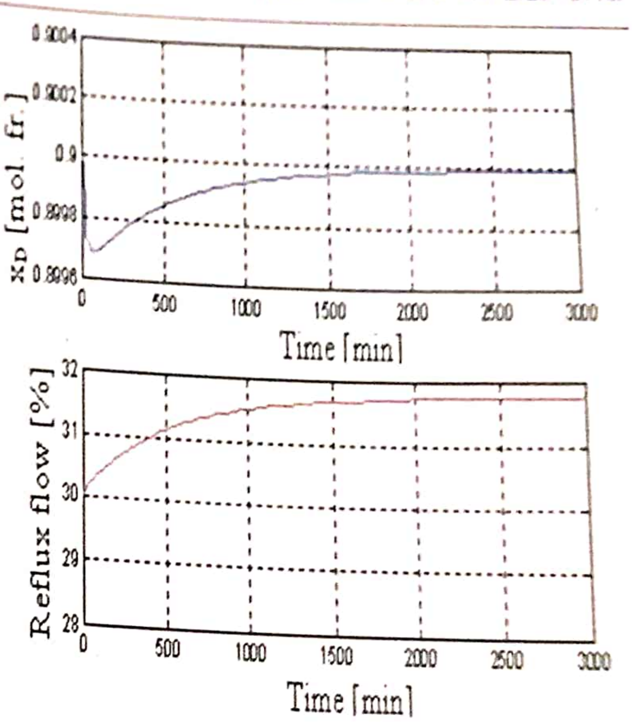

Fig.7: Top composition trend when the feed flow increases from 241.5 kmol/h to 246.5 kmol/h.

6. CONCLUSION AND FUTURE DIRECTIONS

This paper presented the advance process control design of a binary distillation column under disturbance. Control of the top and bottom compositions of the column is a difficult task due to presence of the control loop interactions and nonlinearities. The structure allows taking into account dynamic variations of the process and adapting the controller parameters to this various conditions. Advance controllers achieved a accurate performance in controlling the top and bottom compositions and also in controlling the feed rate, top and bottom rates. As can be seen from the presented trends, the behaviour of the process with the control system was studied for different values of the tuning parameters, observing that a decreasing of the control variable horizon or a decreasing of the control variable weight, from the default values, can lead to an increasing of the transient time. Also we can observe that the process output value reaches the set point value with the best dynamic performances for the default values of the tuning parameters. The control system has a robust behaviour when a disturbance appears in the process.

7. REFERENCES

[1] Z. Abdullah, N. Aziz and Z. Ahmad.(2007) “Nonlinear Modelling Application in Distillation Column”. *Chemical Product and Process Modelling*: Vol. 2:Iss. 3, Artical 12. Available at: http://www.bepress.com/cppm/vol2/iss3/12

[2] Warren.L McCabe, Julian C.Smith, Peter Harriot, “Unit Operation of Chemical Engineering”, 1993

[3] W. L. Luyben. “Derivation of Transfer Functions for Highly Nonlinear Distillation Columns”. *Ind. Eng. Chem. Res*. 1987, 26, 2490-2495

[4] S. Skogestad. “Modelling and Dynamic Simulation for Process Control: Issues in dynamic modeling using distillation as an example”. Lecture notes at seminar on “Modelling and Optimization of Chemical Processes” NTH, Trondheim, 26-28 August 1991.

[5] B. Wittgens and S. Skogestad. “Evaluation of Dynamic Models of Distillation Columns with Emphasis on the Initial Response”. *Modelling, Identification and Control*, 2000, vol. 21, no. 2, 83-103

[6] E. W. Jacobsen. “Studies on Dynamics and Control of Distillation Columns”. Ph.D. dissertation. Uni. of Trondheim, Trondheim, Norway. Dec. 1991.

[7] Yager R.R, Filev D.P “Essentials of advance Modelling and Control”, John Wiley, New York, 1994

C. Fuentes and W. L. Luyben. “Control of high-purity Distillation Columns”. *Ind. Eng. Chem. Process. Des. Dev*. 361, 1983.

KIET IJCE

KIET International Journal of Communications & Electronics
Volume. No. 1, Issue No. 1, Jan - Feb 2013, ISSN: 2320 - 8996.

Adaptive Column Strip Burst Mapping Algorithm for IEEE 802.16 WiMAX Networks

Ahmed M Husein Shabani[1], **Prof. M.T.Beg**[2], **Ammar Abdul-Hamed Khader**[3]

[1,2,3]*Dept. of Electronics & Communication Engineering, Jamia Millia Islamia New Delhi, India*
[1]*ahm_eced@yahoo.com*, [2]*mtbegjamia@yahoo.co.in*, [3]*ammar_hameed_eng@yahoo.com*

Abstract: *Worldwide Interoperability for Microwave Access (WiMAX) is a Broadband Wireless Access technology based on IEEE 802.16 standard which utilize orthogonal frequency division multiple access (OFDMA) as its multiple access technique. OFDMA gives flexibility in resources allocation to accommodate maximum possible users supporting several services classes with quality of service (QoS). One of the most key performance factors of OFDMA resource allocation is downlink data mapping mechanism where the data is allocated to the users in rectangular regions, called burst. This paper proposes Adaptive Column Strip Burst Mapping Algorithm for IEEE802.16 WiMAX. The proposed algorithm is compared with eOCSA (enhanced One Column Striping with nonincreasing Area first mapping) algorithm and the result shows the proposed algorithm achieve higher efficiency.*

Keywords: *component; formatting; WiMAX; OFDMA; Burst Mapping.*

1. INTRODUCTION

WiMAX is a wireless broadband solution that offers a rich set of features with a lot of flexibility in terms of deployment options and potential service offerings [1]. IEEE802.16d, IEEE802.16e and IEEE802.16m are standards for Wireless Metropolitan Area Network (WMAN) [2, 3, 4]. In parallel, the WiMAX forum releases several technical specification profiles [5]. WiMAX is one of the most promising technologies for broadband wireless access solution, as well as a 4G candidate. The important futures of WiMAX are scalable OFDMA, multiple input multiple output (MIMO) antenna, beam forming and adaptive modulation and coding (AMC), support time division duplexing (TDD) and frequency division duplexing (FDD), space time coding, strong security and multiple QoS classes [6].

The frame structure in TDD WiMAX is divided into downlink sub frame followed by an uplink sub frame separated by a small gap as shown in Figure.1. Farther the downlink sub frame and uplink sup frame are divided into symbols in time domain and orthogonal subcarrier in frequency domain. The sub carriers are grouped into logical subchannel using distributed permutation mode such as partial use of subcarriers (PUSC) and full use of subcarriers (FUSC) or adjacent permutation mode like adaptive modulation and coding (AMC). The subchannels are modulated with several modulation schemes adaptively based on SNR Quality to improve overall channel efficiency. In a frame, minimum data allocation unit is a slot which consists of one subchannel over one or more symbol based on used permutation mode. DL-MAP & UL-MAP messages are used by BS to control access to the air frame. These messages contain the informational elements (IEs) that specify the burst profile.

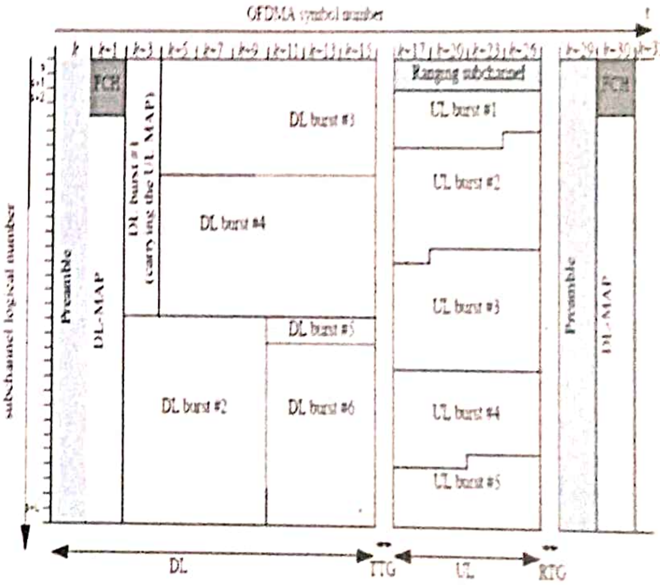

Fig. 1: OFDMA TDD frame structure

In WiMAX system, base station (BS) controls the allocation of the resources in both uplink and downlink direction. The downlink resource allocation involves three main steps. First step is Call admission control where the BS decides whether to accept or reject new connections based on the available resource and QoS requirements. Second step is scheduling where the scheduler select data packet to be sent in the current frame for each subscriber station (SS) from the queued traffic flows. It also decides size of the selected data packets in slots based on the available slots and quality of services without any shape constrain. Third step is mapping or allocating the selected data packets (known as "burst") into downlink subframe and this is main focus of this paper. Since, the standard specifies that mapping data burst has to be in rectangular form into downlink sub frame. This constrain make the mapping as two-dimensional rectangle mapping problem. Shaping the selected data bursts in rectangles may require allocation of extra slots and fit those rectangles into big rectangle may leave some unutilized slots. Thus these unutilized slots affect the efficiency of mapping algorithm and WiMAX system performance. Also there are many consideration with two-dimensional rectangle burst mapping problem like: (i) minimize the number of burst time symbols to reduce SS active time and power consummation such as the work proposed in [7], (ii) minimize the number of burst subchannels to efficiently utilize the subchannel such as the work proposed in [8, 9] and (iii) reduce number of bursts to reduce DL-MAP overhead size such as the work proposed in [10].

The two-dimensional rectangle burst mapping problem is considered to be NP-complete problem [11]. The complexity of the solution grows exponentially with the number of objects [14]. Recently many heuristic algorithms have been proposed to solve this problem and we will discuss some of proposed algorithms which are more related to our work in related work section.

Most of the proposed mapping algorithms are non sequential where the scheduler select all the bursts to be packed in the current frame. Then mapping algorithm starts packing of those bursts. Also the first step of packing algorithm is sorting. This gives us information like, number of bursts to be packed, maximum burst size, smallest burst size and average burst size. This information may be utilized to increase Mapping efficiency. In this paper, we propose Adaptive Column Strips mapping algorithm for downlink IEEE802.16 WiMAX networks. In addition, we compare efficiency of our algorithm with eOCSA algorithm. The result shows our algorithm has higher packing efficiency. To best of our Knowledge this is not discussed elsewhere.

2. RELATED WORK

Recently several algorithms are proposed to address problem of two dimensional burst mapping for IEEE802.16 WiMAX. In this section we briefly discus some of proposed algorithms based on column striping. Ohseki et. al. In [12] propose an algorithm that first prepares a bucket of one time slot with more than one sub channel to construct data from different SSs with the same MCS in combined columns. It starts as one column, and if the buckets grow it expands by filling another column which may not be fully utilized.

One Column Striping with non-increasing Area first mapping (OCSA) proposed by So-In et. al. In [13] and it's enhancement in [14]. The algorithm can be described in three main steps. First step sort the bursts in decreasing order. Second step vertically allocate the large burst with minimum width and maximum height in one column. Third step allocate the left space in the allocated column horizontally. The algorithm minimizes the bursts time symbols which reduce SS active time. But when most bursts sizes are large the left space in third step cannot allocate to any burst this increases the unused space and degrade the algorithm efficiency. For example allocating set of bursts (96, 66, 42, 42, 40, 37, 32, and 5) using eOCSA will result more unused slot. Also the algorithm unable to allocate theses bursts (40 37 32) and the efficiency degrade to 69.72%.

Orientation-Based Burst Packing (OBBP) algorithm present by Eshanta et. al. In [15]. The algorithm is based on burst factorization and pre-arranging them using matrices. This simplifies finding optimal column or rows to minimize the unused slot and avoids padding. The algorithm shows good efficiency at heavy load. When the number of bursts is large and small in size the algorithm required more computation time for factorization and select optimal column. Where similar efficiency can achieved with less computation time using simple best fit without any factorization.

3. ADAPTIVE COLUNM STRIP MAPPING ALGORITHM

Columns strip mapping simplify the two dimension packing problem. The algorithm strips the two dimension area into columns then packs the burst in columns. In this way it is easy for the algorithm to deal with the leftover empty space in the columns and determine the next burst can be packed to minimize the leftover space. There are two main steps in designing of Column striping packing algorithm. The first step is selecting column strip width and the second step is selecting which burst and its dimensions to be packed first in the column.

In our design we consider PUSC with 10 MHz channel and According to WiMAX forum specification the dimensions of downlink frame data are rectangle in size (12 symbols width (w) × 30 subchannel high(sch)) with total area is 360 slots. The number and the sizes of the bursts to be packed in one frame depends on many factors like, either the burst contain the data for single user or it group the data for different users ,Scheduling mechanism and the allowed burst size. In our case, we assume that minimum burst size is 2 and maximum is 150 slots and the number of burst is vary from 5 to 40 bursts with constrain total data size is 360 slots.

A. Selecting column strip width

The rectangle data width is 12 symbols so that the possible stripping columns width are combinations sum of number 12 like, (10,2), (6,4,2), (5,4,3), (4,3,3,2), (3,3,2,2,1,1) and ....(1,1,1,1,1,1,1,1,1,1,1,1).We observe from packing algorithms proposed in [13, 14, 15] that when the bursts packed into DL-subframe, as the sizes of bursts become large i.e. it's number is small then the width of strip column becomes large. But when the sizes of bursts become small i.e. its number is large then the width of strip column becomes small. This gives indication that there is a relation between the number of bursts and the width of strip column. To select the width combination that gives higher packing efficiency based on the number of bursts to be packed, many simulation test for packing different bursts number and sizes with different strip width using the proposed algorithm have been conducted. The simulation result shows that one combination gives higher packing efficiency within specific bursts number range. Table (I) and figure (2) illustrated the mapping efficiency using some strips width combinations which gives higher mapping efficiency within some range. The algorithm will adaptively select these combination based on number of bursts to increase the overall packing efficiency.

Table .I Mapping efficiency using some strips width combinations

No	Width Combination	Best burst number range	Maximum efficiency
1	(5,4,3)	(5 to12)	95%
2	(4,3,3,2)	(12 to 18)	95.72%
3	(3,3,2,2,1,1)	(18 to 24)	96.6%
4	(2,2,2,2,1,1,1,1)	(24 to 30)	97.7%
5	(1,1,1,1,1,1,1,1,1,1,1,1)	(30 to 40)	100%

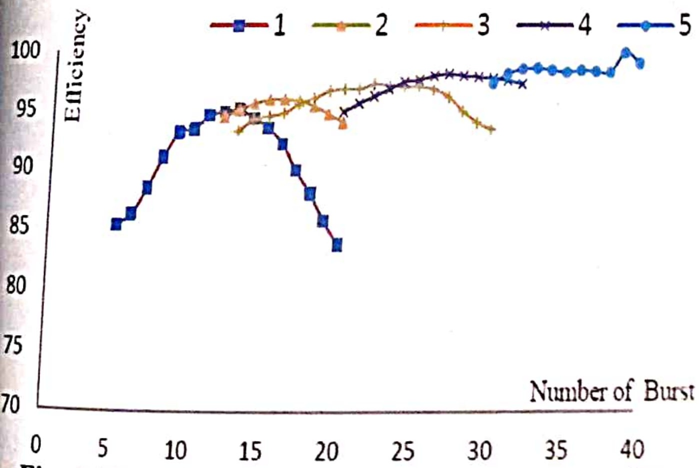

Fig . 2:Mapping efficiency using some strips width combinations

A. Selecting the burst and its dimensions to be packed

After selecting the strips width (W1, W2... Wn) based on the number of bursts. The steps of packing burst as follows:

Step1

Sorting the bursts in decreasing order (B1, B2,.....Bi)

Step2

Divide all bursts by (W1) and return hi as [h1 = int+ (B1/W1), h2 = int+ (B2/W1),......and hi=int+(Bi/W1)] Select Oh such that [(h1+ (Oh)) - sch] is minimum. Where Oh (Optimal height) is summation any of (h2, h3,...hi) and (int+) is closes higher integer . Assume that Oh = (h3+h5) then the bursts that correspond to selected height are (B1, B3, B5).

Step3

Allocate the selected bursts in current column as [(B1→ (W1×h1)), (B3→ (W1×h3)), (B5→ (W1×h5))

Step4

For remaining bursts (B2, B4, Bi) repeat step 2 with divider factor W2. And same steps for the remaining till last Wn or no data burst.

The algorithm select optimal bursts height to minimize the left space also we can minimize both the left space and the extra slot where the extra allocated slots ei = (Wn×hi - Bi) but the complexity may increase. Fig 3 describe Adaptive Column Strip mapping algorithm steps

```
If #burst  = X then select ( w1, w2 ,wn)       //step1
Sort burst =(B1,B2,.....Bi)                    //step2
FOR W= w1, w2,  wn                             // step3
Divide each burst in sorted list by W and return hi= int+
Bi/W
Select[ (h1+any of (h2,h3..,hi)) – sch] is minimum
Allocate the selected bursts  as
 (B1→ (w×h1), B3→ 1( w×h3) ... Bj→ ( w×hj)
Remove the allocated burst from sorted list
END FOR
END
```

Fig 3: Adaptive Column Strips mapping algorithm steps

A. Numerical exampe

In this section, we provide an example that helps explain our algorithm. Once again, the DL subframe is assumed to be 12×30 resulting in 360 slots. The set of bursts to be packed are (84, 42, 63, 14, 50, 70, 34, 3 slots) total data size is 360. The number of bursts are 8 the algorithm will select strips width (5, 4, 3) as in table (I). The packing steps are:-

Step1

Sorting the bursts in decreasing order as (84, 70, 63, 50, 42, 34, 14, 3)

Step2

Divide bursts by (W1=5) as below

Bi/w1	84/5=16.	70/5=14	63/5=12	50/5=10	42/5=8.4	34/5=6	14/5=2.8	3/5=0.6
Int+(	17	14	13	10	9	7	3	1
ei	2	0	2	0	3	1	1	2

Select Oh such that [(h1+ (Oh)) – sch] is minimum where h1=17, Sch=30 then Oh= 13 the corresponding bursts are (84, 63) and its dimension are (5×17), (5×13) without any left space and 3 extra allocated slots

Step3

Repeat step2 with remaining burst (70, 50, 42, 34, 14, 3) using w2= 4

Bi/w2	70/4= 17.5	50/4= 12.5	42/4= 10.5	34/4= 8.5	14/4= 3.5	3/4= 0.75
Int+(hi)	18	13	11	9	4	1
ei	2	2	2	2	2	1

In this step h1= 18, Oh = (11+1) then the corresponding burst are (70, 42, 3) and its dimension are (4×18, 4×11, 4×1) no unused slot and extra slot is 5

Step4

Repeat step2 with remaining burst (50, 34, 14) using W3= 3

Bi/w3	50/3= 16.6	34/3= 11.3	14/3=4.6
Int+(hi)	17	12	5
ei	1	2	1

In this step h1=17, Oh = (12) then the corresponding burst are (50, 34) and its dimension are (3×17, 3×12,) left space = 3 slots and extra slot is 3.

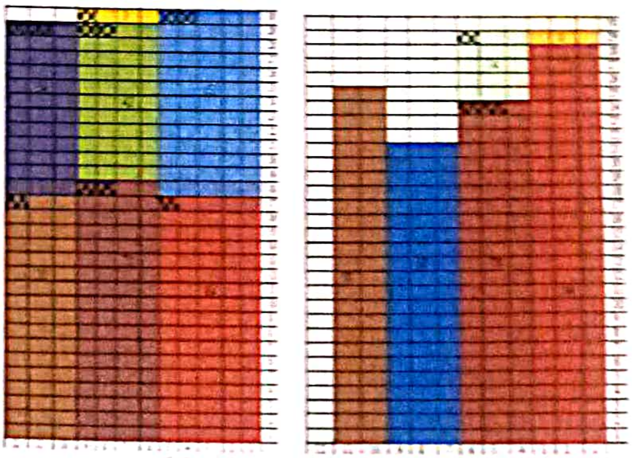
(a) (b)

Fig. 4.: Example of burst mapping using (a) the proposed algorithm and (b) eOCSA algorithm.

The final results obtained from this example are: - total left space = (0+0+3)=3 , total extra slots = (2+1+2+2+1+1+2)=11 ,packing efficiency =360-(3+11)/360 = 96.111 and the burst (14) is failed to allocate . Figure .4 illustrates Example of burst mapping using (a) Adaptive Column Strip mapping algorithm and (b) eOCSA algorithm.

4. PERFORMANCE EVALUATION

In this section, we compare the performance of the proposed algorithms with eOCSA. TABLE-II shows the parameters used in the simulation are as per suggestions of WiMAX forum. The data bursts sizes are generated randomly with the constraint that sum of all bursts is (12×30=360) slots. The number of bursts is chosen from 5 to 40.

TABLE II. :System Simulation Parameters

Parameter	Value
Frame length	5 ms
Channel BW	10 MHz
Permutation scheme	PUSC
Number of subchannels	30
DL subframe	12 slot columns
Total number of slots per DL	30×12 slots
Simulation time	500 frames

Figure. 3 illustrate the average unused slots per DL subframe and the result shows that the average of unused slots for the proposed algorithms is smaller than that for eOCSA. That is because eOCSA left more unused space that cannot accommodate any burst.

Figure. 4 illustrates the average extra allocated slots per DL frame and the result shows that the average extra allocated slots are higher in our algorithm because of height approximation. But our algorithm has total wastage slots smaller than eOCSA.

Figure. 5 illustrate the average packing efficiency and the result shows that the proposed algorithms achieve higher efficiency than eOCSA.

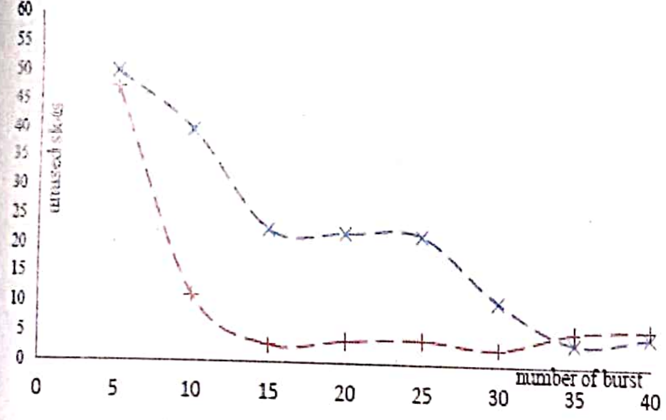

Fig.. 3: average unused slots

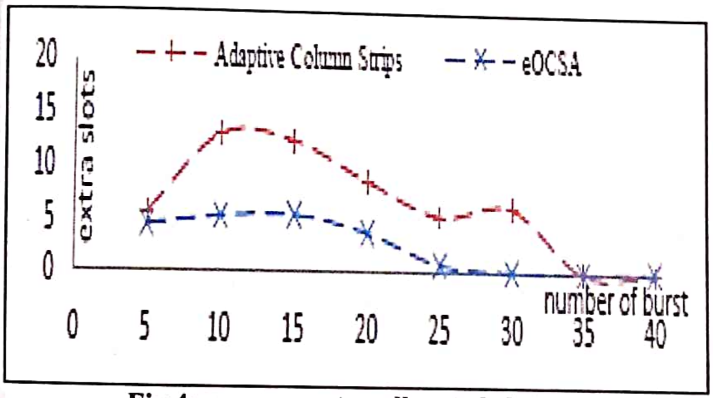

Fig.4: average extra allocated slots

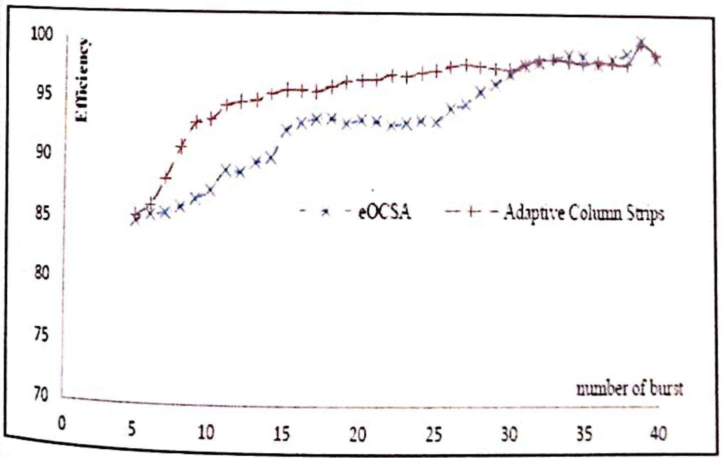

Fig.5: average packing efficiency

5. CONCLUSION

This paper presented adaptive downlink burst allocation algorithm for IEEE 802.16e Mobile WiMAX networks. The proposed algorithm meets the rectangle shape allocation constraint and achieves high throughput by considering mapping for the larger burst first. The algorithm based on column strips and its basic idea is to select the strip columns width adaptively based on number and sizes of the bursts to be packed. Then select the bursts that minimize the left space in the column. The performance of the proposed algorithm is compared with eOCSA. Simulation results show that the proposed algorithm can achieve higher packing efficiency.

6. REFERENCES

[1] J. G. Andrews, A. Ghosh, and R. Muhamed, "Fundamentals of WiMAX Understanding Broadband Wireless Networking", Prentice Hall, 2007.

[2] IEEE Std. 802.16-2004, "IEEE Standard for Local and Metropolitan Area Networks – Part 16: Air Interface for Fixed Broadband Wireless Access Systems," IEEE Computer Society and the IEEE Microwave Theory and Techniques Society Oct. 2004.

[3] IEEE Std 802.16e-2005 "IEEE Standard for Local and Metropolitan Area Networks – Part 16: Air Interface for Fixed and Mobile Broadband Wireless Access Systems.", IEEE Computer Society and the IEEE Microwave Theory and Techniques Society ,28 Feb. 2006.

[4] IEEE Std 802.16m™-2011 "IEEE Standard for Local and metropolitan area networks—Part 16: Air Interface for Broadband Wireless Access Systems" . , IEEE Computer Society and the IEEE Microwave Theory and Techniques Society, 6 May 2011.

[5] WiMAX Forum. "Technical specification release 1, 1.5, 1.6 and 2" at www.wimaxforum.org.

[6] Chakchai So-In, Raj Jain, and Abdel-Karim Tamimi, "Scheduling in IEEE 802.16e Mobile WiMAX Networks: Key Issues and a Survey," IEEE Journal (JSAC), Vol. 27, No. 2, Feb 2009, pp. 156-171.

[7] C. Desset and G. Lenoir, "WiMAX downlink OFDMA burst placement for optimized receiver duty-cycling," IEEE Communication Society, pp. 5149–5154, 2007

[8] Joo-Young Baek, Young-Joo Suh, Member, "Heuristic Burst Construction Algorithm for Improving Downlink Capacity in IEEE 802.16 OFDMA Systems" Journal of Latex Class Files, VOL. 6, NO. 1, November 2010.

[9] Yuan-Cheng Lai and Yen-Hung Chen "Two-dimensional downlink burst construction in IEEE 802.16 networks" EURASIP Journal on Wireless Communications and Networking 2011.

[10] Bacioccola, A., Cicconetti, C., Lenzini, L., Mingozzi, E., &Erta, A., "Downlink data region allocation algorithm for IEEE 802.16e OFDMA.", In 6th IEEE international conference on information communication and signal processing, (pp. 1–5), December 2007.

[11] A. Lodi, S. Martello, and M. Monaci, “Two-dimensional packing problems: A survey,” in European Journal Operational Research, vol. 141, pp. 241-252, Sept. 2002Ohseki, T., Morita, M., & Inoue,T. Burst construction and packet mapping scheme for OFDMA downlinks in IEEE 802.16 systems. , In IEEE Globecom 2007, November 2007 (pp. 4307–4311).

[12] Ohseki, T., Morita, M., & Inoue, T. Burst construction and packet mapping scheme for OFDMA downlinks in IEEE 802.16 systems, In IEEE .Globecom 2007, November 2007 (pp. 4307–4311).

[13] C. So-in, R. Jain, A. Tamimi, "OCSA: An algorithm for Burst Mapping in IEEE 802.16e Mobile," proceedings of the 15th Asia Pacific Conference on Communications (APCC 2009), October 8-10, 2009.

[14] Chakchai So-In, Raj Jain, Abdel Karim Al Tamimi, "eOCSA: An Algorithm for Burst Mapping with Strict QoS Requirements in IEEE 802.16e Mobile WiMAX Networks," Proceedings of the Second IFIP Wireless Days Conference, Paris, France, 14-16 December 2009.

[15] OM Eshanta, M Ismail, K Jumari, OBBP: an efficient burst packing algorithm for IEEE802.16e systems. ISRN Commun Netw article ID 734297 (2011).

KIET IJCE

KIET International Journal of Communications & Electronics
Volume. No. 1, Issue No. 1, Jan – Feb 2013, ISSN: 2320 – 8996.

Trapezoidal Patch with V-shape Slot Microstrip Antenna for Dual Band

Radha Sharma[1], **Rajesh Kumar Vishwakarma**[2]

[1,2]*Jaypee University of engineering and technology Guna, (M.P)*
[1]*radha.pandey31@gmail.com*, [2]*rkv.786@gmail.com*

***Abstract:** In this paper, dual operation trapezoidal patch with V-shaped slot feed by coaxial-probe is presented. The proposed antenna is designed on RT duroid substrate. A (10db) bandwidth of return loss (S11) characteristics for the dual band is 4% and 15.6% respectively. E-planes and H-planes for the dual operation frequencies are satisfactory within the bandwidth. Return loss, VSWR, gain and E-planes and H-planes radiation pattern are simulated by using IE3D simulator.*

***Keywords:** V-shape slot, RT duroid, Dual band, WLAN, WiMAX.*

1. INTRODUCTION

Wireless local area networks (WLAN) are widely used worldwide. The 802.11a standard uses the 5-GHz band which is cleaner to support high-speed WLAN. However, the segment of frequency band used varies from one region of the world to another. Dual frequency microstrip antennas with a single feed are required in various radar and communication systems, such as global positioning system (GPS), WiMAX,WLAN etc.

Microstrip antenna is the ideal choice for such an application due to low profile, light weight, conformal shaping, low cost ,simplicity of manufacturing and easy integration to circuit[1].however, conventional microstrip patch antenna suffers from very narrow bandwidth, typically about 5% bandwidth with respect to the central frequency. there are numerous and well-known method to increase the bandwidth of antennas, including increase of the substrate thickness, the use of a low dielectric substrate, the use of multiple resonators,and the use of slot antenna geometry[2],[3].

Sudhir *et.al*[4] applied a H-shaped slot in a rectangular microstrip antenna to make its broadband structure while improved bandwidth up to 9.5 % .Wong & Hsu[5] applied a U-shaped slot in an equilateral triangular microstrip antenna with improved bandwidth up to 8.67% was recently reported for a circular patch antenna having u-slot[6]. S.W Lee et al. proposed the trapezoidal shape patch antenna embedded with rectangular [7]. M.S *et.al* [8] demonstrates a rectangular patch microstrip antenna with V-slots and corner notches for IEEE802.11.A/HIPERLAN2 applications that enables an impedance bandwidth of 51%. Yogesh Bhomia *et al.* [9] applied V-shape slot on triangular microstrip antenna having impedance bandwidth of 9.2%. A dual slot-loaded microstrip antenna with dual-frequency operation has been reported in [10] and [11], where two parallel narrow slots are etched in the rectangular patch close to its radiation edge. The two slots are chosen to be close to the length of the radiating edge. Other dual-frequency antennas with square-slot and rectangular-slot loading are reported in [12] and [13]. A compact dual-frequency microstrip antenna is proposed in [14], which uses the rectangular microstrip patch loaded with one shorting pin. Some experimental results are also presented in [14].

In this paper, we design a trapezoidal patch with V-shaped antenna which works as a dual frequency. First resonance frequency f1 centered at 3.5 GHz frequency is due to its patch itself. Second resonant frequency f2 is due to V-shape slot, which is centered at 5.0 GHz.

2. ANTENNA STRUCTURE

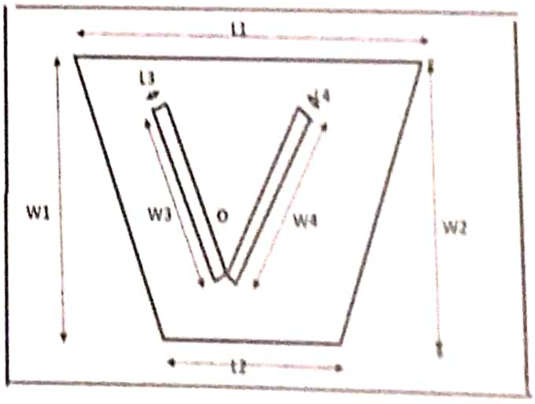

Fig.1: Geometry of proposed antenna

The configuration of proposed antenna is shown in figure 1. The antenna consist of a trapezoidal microstrip patch with V-shaped slot, support on a grounded dielectric sheet of thickness h and dielectric constant ε , The trapezoidal patch has an upper side of length L1, base of trapezoidal patch of length L2 and height of trapezoidal patch of length W1, W2. V-shape slot has a length of L3, L4 and a width of W3, W4 which is loaded on trapezoidal patch. The feed point is located at the central line of the patch, with a distance of $d_{f}(x.y)$ from the bottom edge of trapezoidal patch.The dimension of trapezoidal patch with V-shape slot are tabulated in table 1.

Table 1. Dimension of proposed antenna

S.no	Parameter	Explanation	Value(mm)
1.	L1	Upper side of trapezoidal patch	30
2.	L2	Base of the trapezoidal patch	26
3.	W1,W2	Height of the trapezoidal patch	21.04
4.	L3,L4	Length of the V- shape slot	0.5
5	W3,W4	Width of the V-shape slot	15
6.	ε_r	Dielectric constant	2.2
7	h	Height of dielectric constant	6
8	tanδ	Loss tangent	0.0018
9	(x,y)	Position of probe feed	(13,8)

3. RESULTS AND DISCUSSION

In this section, the simulated results of various parameters like VSWR, Return loss, input impedance and radiation characteristics of proposed antenna are presented and discussed. The simulated results are obtained using IE3D Simulator.

A. Return loss

The simulated result for the return loss less than -10dB is shown in figure 2. From simulated result we get dual band.

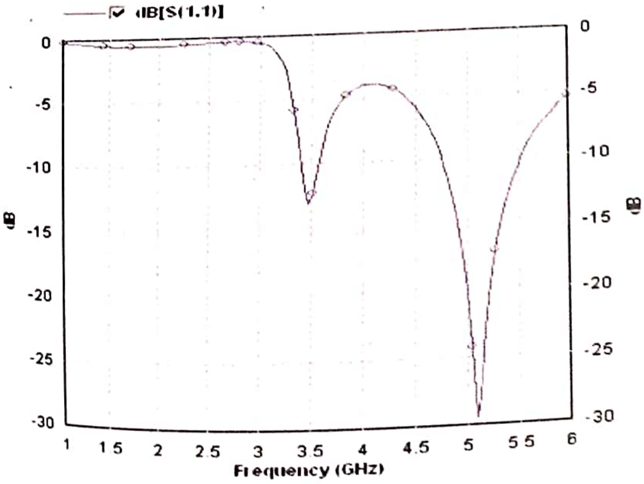

Fig. 2: Return loss

Based on a -10 dB return loss, 4% impedance bandwidth is obtained at first resonant frequencies f1 in the frequency range (3.41-3.57) GHz and 15.6 % impedance bandwidth is obtained at second resonance frequencies in the frequency range of 4.75-5.53 GHz.

B. VSWR

Figure 3. Shows the variation of VSWR with frequency for proposed antenna. It shown that the VSWR occur at first resonant frequency is 1.66 and second resonant frequency is 1.07. This depict that there is good impedance matching between probe-fed microstrip transmission line and the trapezoidal radiating element.

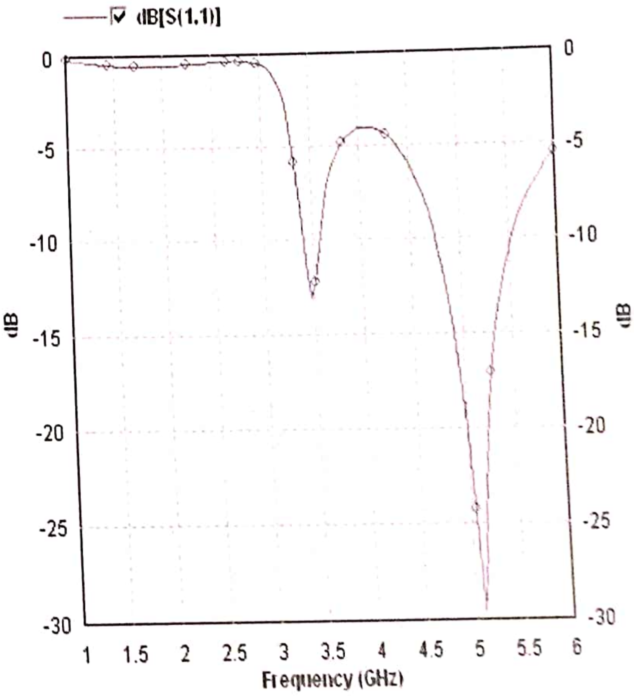

Fig. 3: VSWR

C. Input impedance

The simulated result for the antenna input impedance is plotted in figure 4. It is shown that the real part of the input impedance at first resonant frequency f1 oscillates around 74.83Ω with frequency while the imaginary part of the input impedance at resonant frequency oscillates around 0Ω with frequency.

At second resonant frequency f2, the real part of the input impedance at resonant frequency oscillates around 50Ω with frequency while the imaginary part of the input impedance at resonant frequency oscillates around 0Ω with frequency. Hence, from the graph it is clear that there is proper matching occur at both resonant frequencies.

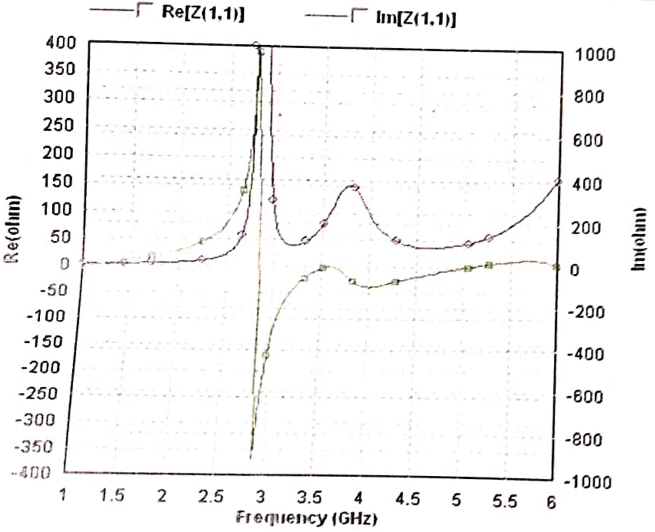

Fig. 4: Real part and imaginery part of input impedance

D. Radiation pattern

From figure 5. Shows the measured radiation pattern at first resonant frequency 3.5 GHz. it can be observed that in the $\phi=0$ plane, the cross polarization is -13 db below the co polarization above the ground plane. In the $\phi=90$ plane, the cross polarization is -19.3 dB below the co polarization level.

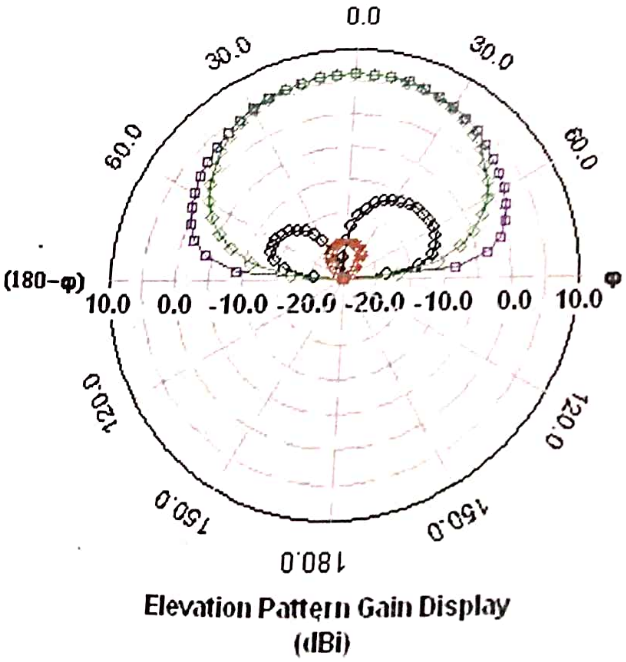

Fig. 5: Radiation pattern at 3.5 GHz

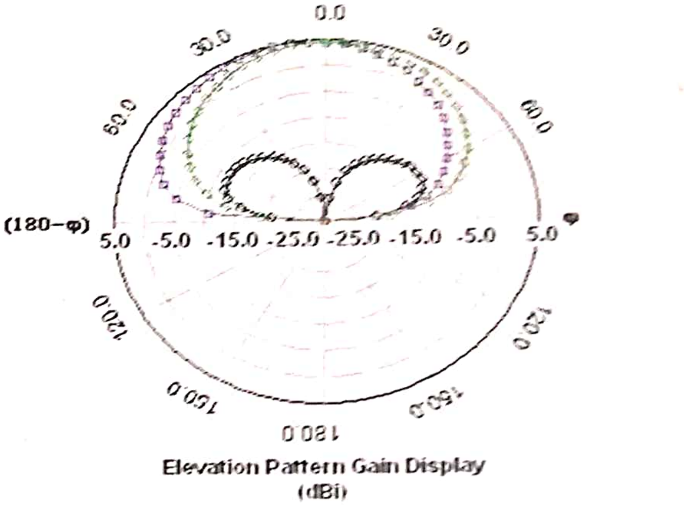

Fig. 6: Radiation pattern at 5 GHz

From figure 6. Shows the measured radiation pattern at second resonant frequency 5 GHz. it can be observed that in the $\phi=0$ plane, the cross polarization is -25.03 db below the co polarization above the ground plane. In the $\phi=90$ plane, the cross polarization is -20 dB below the co polarization level.

E. Gain

The gain of proposed antenna is shown in figure.7 which shows that the maximum achievable gain at first resonant frequency is about5.90 dBi over the entire frequency band of 3.41-357 GHz and 4.14 dBi maximum gains is achieved at second resonant frequency and the gain show stable performance.

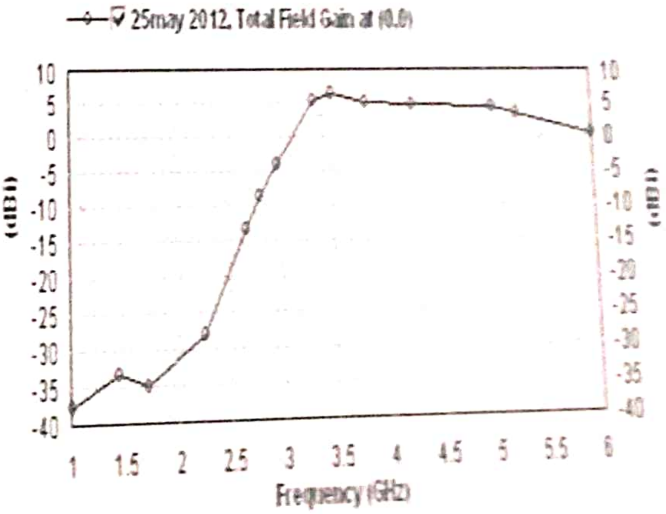

Fig. 7: Gain versus frequency

The simulated results are summarised in table 2.

Table 2. Simulated data

Resonant frequency	F1	F2
Centre frequency	3.5 GHz	5 GHz
bandwidth	4.95	15.6%
Frequency range	(3.41-3.57)GHz	(4.75-5.53)GHz
Return loss	-12.8 dB	-29.37 dB
VSWR	1.66	1.07
Gain	5.9 dBi	4.14 dBi

4. CONCLUSION

The dual frequency and wide-band operation of a trapezoidal patch with V-shaped slot have been studies and simulated. The proposed antenna is compact, occupies small volume and has simple structure compared to other antenna design. The antenna offer a 2:1 VSWR bandwidth of 4% from frequency range (3.41-3.57)GHz at first resonant frequency which cover 3.5 GHz band WiMAX applications. second resonant frequency cover the WLAN(5.15-5.35) band application with impedance bandwidth 0f 15.6%.the simulated return loss, VSWR, radiation pattern and gain showed well performance.

5. REFERENCES

[1] W.He, R.Jin, and J.Gerg, "E-shape patch with wideband & circular polarisation for millimetre wave communication," *IEEE Trans. Antenna Propag.*,vol.56,no.3, pp.893-895,2008.

[2] [2]K.L Lau, K.M. Luk, and K.L.Lee, "Design of a circularly-polarized vertical patch antenna,"*IEEE Trans. Antenna Propag.*,vol.54, no.3, pp.1332-1335,2006.

[3] D.M Pozar & D.H Schauber, "Design of Microstrip antennas and arrays, New York*: IEEE Press*, 1995.

[4] Sudhir Bhaskar & Sachin K. gupta, "Bandwidth improvement of microstrip patch antenna using H-shaped patch", *Publication in the international Journal of engineering Research and application*", vol.2, Issue 1, pp.334-338, Jan-Feb 2012.

[5] Wong KL and Hsu WS, "broadband triangular microstrip antenna with U shape slot" *Electron lett(UK)*,33(1997)2085.

[6] Sharma V, Sharma V K,Bhatnager D, Saini J.S, " Compact dual frequency wide band circular patch antenna with U-slot," *Proc of IEEE International symposium on Antenna and propoagation and USNC/URSI National Radio Science Meeting*, (IEEE,USA),1979,1.

[7] S. W. Lee, S. M. Park, N. Kim, S. W. Park, and S. Y. Rhee, "Design and SAR Measurement of the Trapezoidal Shape Antenna," *Progress In Electromagnetics Research C*, Vol. 26, 127-136, 2008.

[8] M.S.Nishamol, V.P Sarin, D. Tony, C.K Aanandan, " A broadband microstrip antenna for IEEE802.11.A/WIMAX/HIPERLAN2 applications," *Progress In Elecromagnetics Research Letters*,Vol.19,155-161,2010.

[9] Yogesh Bhomia, Ashok Kajila & Dinesh Yadav, "V-slotted triangular microstrip patch antenna,"*International Journal of Electronics engineering*, 2(1), pp.21-23, 2010

[10] S. Maci, G. Avitabile, and G. B. Gentili, "Single-layer dual-frequency patch antenna," *Electron. Lett.*, vol. 29, no. 16, pp. 1441–1443, 1993.

[11] S. Maci, G. B. Gentili, P. Piazzesi, and C. Salvador, "Dual-band slot-loaded patch antenna," *Proc. Inst. Elect. Eng. Microwave Antennas Propagat.*, vol. 142, pp. 225–232, June 1995.

[12] W. S. Chen, "Single-feed dual-frequency rectangular microstrip antenna with square slot," *Electron. Lett.*, vol. 34, no. 3, pp. 231–232, 1998.

[13] S. C. Gao and J. Li, "FDTD analysis of a size-reduced, dual-frequency patch antenna," *Progr. Electromagn. Res.*, vol. PIER 23, pp. 59–77, 1999.

[14] K. L. Wong and W. S. Chen, "Compact microstrip antenna with dual frequency operation," *Electron. Lett.*, vol. 33, no. 8, pp. 646–647, 1997.